Title

Examination of Novel Circuits Linking the Cerebellum and Nucleus Accumbens

Author

D'Ambra, Alexa Fae

Publication Date

2023

Peer reviewed|Thesis/dissertation

Examination of Novel Circuits Linking the Cerebellum and Nucleus Accumbens

By

ALEXA F. D'AMBRA
DISSERTATION

Submitted in partial satisfaction of the requirements for the degree of

DOCTOR OF PHILOSOPHY

in

Neuroscience

in the

OFFICE OF GRADUATE STUDIES

of the

UNIVERSITY OF CALIFORNIA

DAVIS

Approved:

Diasynou Fioravante, Chair

Helen Bateup

Rishidev Chaudhuri

Alex Nord

Jennifer Whistler

Committee in Charge
2023

Abstract

Although the cerebellum is now recognized as part of a long-range brain network that serves limbic functions and motivated behavior, knowledge of cerebello-limbic connectivity is limited, and nearly nothing is known about how the cerebellum connects functionally to the nucleus accumbens (NAc), a region well-known for its role in social, reward, and motivated behaviors. In my first chapter, I report the first electrophysiological evidence that stimulation of cerebellar nuclei in mice of both sexes modulates spiking activity in both NAc core and medial shell. NAc neurons respond with fast excitation and slower, less synchronized inhibition. Fast responses would be well poised to support rapid communication of information critical to the control of motivated behavior, whereas slower responses may be suggestive of a regulatory function, such as gain control. In my second chapter I describe anatomical connections via tracing experiments to chart cerebellar nuclei-NAc pathways identified disynaptic pathways that recruit the ventral tegmental area (VTA) and intralaminar thalamus (Centromedial and Parafascicular nuclei) as intermediary, monosynaptically-connected nodes. Optogenetic activation of cerebellar axons in each of these nodes was sufficient to evoke responses, primarily excitatory, in both NAc core and medial shell. These pathways and the functional connectivity they support could underlie the role of the cerebellum in motivated behavior and further elucidate our growing understanding of the non-motor cerebellum.

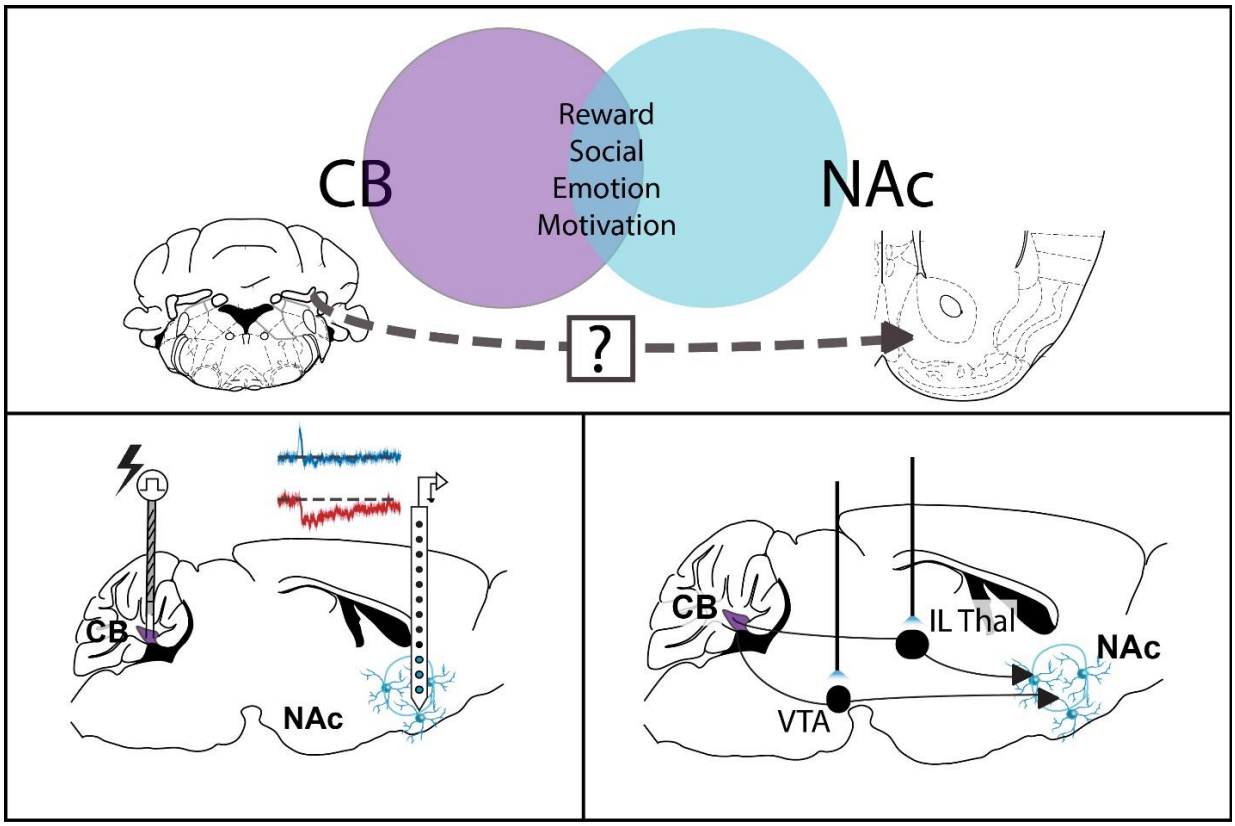

Figure 0.1 Graphical Abstract.

Acknowledgments

To my dissertation committee- Drs. Helen Bateup, Rishidev Chaudhuri, Jochen Ditterich, Diasynou Fioravante, Alex Nord, and Jennifer Whistler- I thank you for your scientific guidance and support. My thesis work has taken many shapes throughout the years, and your expertise helped me to constantly mold the story into one born out of scientific reasoning and academic curiosity. I'd be remiss not to mention Drs. John Gray and Elva Diaz as the endless pools of support I unabashedly dipped into throughout this last year.

To my PI and the Fioravante Lab- I appreciate the numerous "babysitting" offers on long experiment days and the many hours of scientific discussion over many dozens of bagels. I certainly would not be where I am now without you all.

To my fellow neuro-neurds- especially my cohort- thank you for not judging me when I didn't know what a gene was. I am so thankful for your company in which I could commiserate, collaborate, and procrastinate on all things PhD.

To my friends (and more-than) both near and far- you are my biggest cheerleaders and best distractions. Thank you for keeping me humble and reminding me there is a world outside of mice and data.

And to my best friends that I didn't get to choose- my mom, dad, sister, and brother- it's hard to even attempt a thank you that would come close to expressing my gratitude for you all, but I know you'll get it. Your support, along with so many others in our (growing) extended family, kept me on my feet when I felt like I didn't have any to stand on. Not all hurdles are meant to be overcome, but you gave me the tools to face mine courageously. See you in NY!

Table of Contents

Chapter 1: THE NON-MOTOR CEREBELLUM

Insight from humans

In any neuroscience textbook, the cerebellum (CB) can be found under the "movement and motor control" chapter. However, the field of CB research now dedicates a fair share of the spotlight to the structure's non-motor roles. While this shift in focus away from motor learning and coordination only began in the last decade, the CB has long been implicated in higher-order functions such as emotion processing, working memory, and executive functioning (Buckner, 2013; Sokolov et al., 2017; Liang and Carlson, 2019; Hull, 2020). Early knowledge of CB non-motor roles came from behavioral symptoms of injury and stroke patients. Schmahmann and Sherman first described cerebellar cognitive and affective syndrome (CCAS) after recording marked cognitive and behavioral deficits in patients with CB lesions due to stroke (Schmahmann & Sherman, 1998). Imaging studies corroborate these findings, observing CB activation during emotion identification and imitation (Schraa-Tam et al., 2012), during complex linguistics tasks (Peterson et al., 1988), or even while solving puzzles (Kim et al., 1994).

Abundant evidence for the CB's nonmotor role also comes from research on human neuropsychiatric disorders and divergences. One can utilize clinical data on diagnoses commonly associated with altered affect, cognition, and social behavior such as attention deficit hyperactivity disorder (ADHD), autism, and intellectual disability (ID). Studying individuals in these populations could offer insight into the CB's role in the associated symptoms/behavioral manifestations. For example, when comparing brain volume between individuals with and without ADHD, the CB is the most frequently altered structure (Wyciszkiewicz et al., 2017). Volume changes in the CB are typical in individuals with autism, as is reduced CB cortical neuron number (Bauman & Kemper,

2005). Additionally, CB injury at birth is the second highest risk factor for autism diagnosis (Wang et al., 2014). In individuals with autism, CB activation is often reduced during performance of motor and cognitive tasks and CB pathology is extremely common in postmortem tissue (Fatemi et al., 2012; Bauman & Kemper, 2005). GWAS studies have been useful in identifying key genes associated with these diagnoses. This has opened doors for advancements in rodent models, allowing scientists to look at region, or cell-specific contributions to the non-motor behavioral pathologies in these disorders. With this we have entered a new age of directed studies to evaluate the effect of CB perturbation in cognitive performance.

Insight from rodent CB manipulations

CONSERVED CB ORGANIZATION

How valuable is rodent research when it comes to translational applications? Fortunately, for CB research, rodent models are extremely useful. The CB is characterized by a well-described, stereotyped circuit organization. Excitatory inputs into this structure arrive at the Purkinje cells (PCs) in the CB cortex, either directly via climbing fibers or through mossy fiber synapses onto granule cells (GCs) and their parallel fibers (Prestori et al., 2019). The CB cortex contains three key layers: the PC layer, which houses these sole cortical output neurons; the molecular layer, containing PC dendrites and inhibitory molecular layer interneurons; and the GC layer, in which inhibitory Golgi cells synapse onto GCs. All of these cerebellar cells, with the exception of GCs, are inhibitory (Prestori et al., 2019). The cortex can also be divided into 10 major lobules moving from the superior to inferior side of the CB based on the deep fissures that separate them, their cellular makeup, and several functional distinctions

(Kozareva et al., 2021; Guell & Schmahmann, 2019). The PCs in the CB cortex send inhibitory projections to the deep cerebellar nuclei (DCN), which send outputs to the rest of the brain. From lateral to medial, there are three distinct DCN: the dentate nucleus, the interposed nucleus, and the fastigial nucleus. This cellular connectivity, these general lobule divisions, and this DCN organization are all largely conserved between mammals (Sugihara, 2021; Luo et al., 2017), allowing for the use of the rodent CB to model human function in health and disease.

CLINICALLY RELEVANT GENETIC TARGETING

Autism is typically marked by aberrant social behavior, challenges in communication including emotional processing and regulation, and repeated, stereotyped behavior. However, diagnoses are seen in a highly behaviorally and genetically heterogeneous population, so no animal model can clearly encompass or explain observed behavioral differences nor the CB's contribution to them. Additionally, many risk genes that have been identified are associated with multiple disorders or are extremely common in individuals with multiple highly comorbid disorders (Grove et al., 2019; Lee et al., 2019).

The Cadherin 13 (CDH13) gene is highly associated with both autism and ADHD and is highly expressed in certain cells in the CB (Tantra et al., 2018). Deletion of CDH13 in the CB (seen mostly in Golgi and DCN neurons) impairs cognitive flexibility and causes deviations from typical social behavior. Tuberous sclerosis complex (TSC) is a disorder that arises from mutations in the *TSC1* or *TSC2* gene. While symptoms of this disorder include manifestations outside of the brain, TSC is highly comorbid with autism (Redies et al., 2012). *Tsc1* knock out or knockdown exclusively in PCs leads to significantly reduced preference for social novelty and diminished cognitive flexibility in

a reversal learning task (Tsai et al., 2012). Animals with these TSC mutations also have an increase in grooming, suggestive of a repetitive behavioral phenotype.

Another gene highly associated with autism is a gene encoding the chromatin regulator, *Chd8*. *Chd8* mutations are often found in individuals with both autism and ID diagnoses. Our own work has shown that *Chd8* is widely expressed in both the developing and adult cerebellum, and several studies have looked at animal models manipulating this gene both brain-wide and with cerebellar specificity (Gompers et al., 2017; Katayama et al., 2016; Kawamura et al., 2021; Chen et al., 2022). The effects of *Chd8* manipulation are somewhat controversial, with some papers reporting social and repetitive as well as cognitive deficits, and others reporting in-tact social/repetitive behavior, but impaired cognitive performance (Gompers et al., 2017; Katayama et al., 2016). Despite this controversy *Chd8* clearly plays a role in some of the non-motor manifestations of autism. Disruption of *Chd8* in rodent models clearly has an impact on CB development, as shown by volume changes and deficits in foliation (Gompers, 2017; Kawamura et al., 2021). CB-specific *Chd8* manipulation offers insights into the role of the CB in these behavioral differences. Animals lacking *Chd8* specifically in CB granule progenitor neurons show non-motor deficits associated with autism like reduced social preference and heightened anxiety (Chen et al., 2022). Although autism is behaviorally complex and genetically heterogenous, evidence from animal models clearly indicates a role of the CB in sociability, cognitive flexibility, and anxiety.

OTHER GENETIC MANIPULATIONS

Some rodent studies perform manipulations that affect the CB without modeling any particular disorder. For example, some of the first studies looking at CB-specific

mutations used the heterozygous Lurcher mouse line (*Grid2*$^{Lc/+}$*).* This mouse model presents with severe degeneration of the cortical cerebellum, particularly of PCs. Although the main deficit in this transgenic line is ataxia, these animals also perform poorly on spatial learning tasks like the Morris Water Maze (MWM) (Lalonde et al., 1988; Cendelin et al., 2008). These animals also had reduced motivation to explore novel environments (Caston et al., 1998). Another study looked at deletion of *Stat3*, a regulator of synaptic plasticity, in PCs and found that this manipulation caused an enhanced long-term fear memory and fear-potentiated startle responses (Han et al., 2021). Models of CB cortical degradation offer insights into its role in cognition, motivation, and emotion, but they are limited by the time course of the manipulation. Thus, they are incapable of differentiating between having a direct role in the behavior itself and playing a role in the development of behaviorally relevant regions and synapses.

ACUTE MANIPULATIONS AND BEHAVIOR

Lesioning at particular time points of task acquisition can help delineate the CB's role in said task. One study dissected the CB's role in spatial learning and memory by lesioning the CB before or after learning in the MWM. They found that cerebellectomy had a minimal effect when it occurred prior to acquisition but had a profound effect disrupting retention of long-term spatial memory when it was done after learning (Hilber et al., 1998). Consistent with this, local DCN infusion of GABA agonist muscimol shortly after acquisition trials in MWM impairs consolidation of long-term spatial memory (Andre et al., 2019). The CB is not only important for spatial and reward learning, but for some tasks, the CB's role in learning is valence specific. Steinmetz et al. used lesion studies

to determine that DCN are necessary for the learning of an aversive avoidance bar-pressing task, but not for appetitive bar pressing (1992). Reward seeking is a key aspect of motivated behavior. Inactivation of the lateral DCN reduces drive in rats to access an effortful-to-acquire reward (Peterson et al., 2012).

The development of optogenetics allows for temporally specific CB manipulations, further refining experiments and data interpretation. Data from Deverett et al. (2019) show that optogenetic activation of PCs impacted decision making in an evidence-accumulation task. Specifically, manipulation of PCs during sensory evidence accumulation seemed to disrupt working memory necessary to accurately make memory-guided decisions. In addition to cognition, optogenetic manipulation of PCs also impacts social behavior. Jackman et al. (2020) showed that activation of PCs leads to a suppression of aggressive behavior, while inhibition increases aggressive actions and decreases pro-social behaviors. While PC-specific manipulations can tell us a lot about the role of the CB in behavior, the stereotyped circuitry of the CB means that the projections of these cells mostly remain within the CB (i.e., only directly affecting local circuitry). Thus, in order to shed light on how the CB can contribute to such a variety of complex tasks, we must probe CB dynamics and its outputs.

NON-MOTOR CB CIRCUITS

WITHIN CB RECORDINGS IN BEHAVING ANIMALS

Recordings of CB activity in animals performing non-motor tasks on its own has offered some additional insight regarding the cognitive CB. Several studies have shown that activity in the CB corresponds to reward delivery, reward prediction, and violation of reward prediction in various reward learning paradigms (Kostadinov et al., 2019; Larry et

al., 2019; Wagner et al., 2017). Collectively, these studies identified reward-related activity in climbing fibers, GCs, and mossy fibers. One study helped to establish a connection between the CB and aversive associative learning. In this study it was found that fear learning in rats was accompanied by long term changes in CB cortical connectivity (Strata, 2015). Specifically, the excitatory synapses from parallel fibers onto PCs and inhibitory inputs onto PCs experience LTP. These informed not only a connection between the CB and non-motor behaviors, but also described specific cellular contributions within the CB circuit.

Studies like these have offered some additional evidence of behavioral specificity within the CB. Lesions studies (Stoodley and Schmahmann 2010) and functional neuroimaging (Chirino-Perez et al., 2022) data in humans suggest there is a topographic organization of the sensorimotor vs the cognitive CB. These studies largely converge on an anterior-posterior axis in which the cognitive functions are processed mostly in the posterior CB. This functional segregation is a bit more convoluted along the medial-lateral (ML) axis (Timmann et al., 2010). In the stereotyped circuitry of the CB, PC's synapse directly onto cells in the respective DCN depending on their ML location. This feature along with the modular, repetitive circuit structure across the ML axis suggests that the CB must derive its diverse functional repertoire from its varied, distinct inputs and outputs.

MONOSYNAPTIC CIRCUITRY

A recent uptick in research on CB connectivity has increased our knowledge of its projections to (and interactions with) non-motor areas. It is through this circuitry that the

CB takes part in behaviors such as executive function, learning and memory, attention, and emotional learning and regulation.

It is already known that reward, reward expectation, and reward prediction error are all encoded within the CB (see WITHIN CB RECORDINGS IN BEHAVING ANIMALS). Because the CB is thought to act as an instructor for behavioral adaptation, this information is likely passed to other regions to inform reward and aversive conditioning. The VTA, a well-known reward center, receives direct projections from the DCN and influences reward learning (Carta et al., 2019). Additionally, direct projections from the dentate and interposed nuclei to the dorsolateral VTA have been shown to play an important role in the development of depressive symptoms as identified by tasks such as forced swim test and sucrose preference test (Baek et al., 2021).

CB direct projections to several other regions also contribute to depression, affect regulation, and emotional learning. For example, evidence suggests that the CB, likely through the fastigial nucleus, modulates serotonergic neurons in the dorsal raphe that can directly prevent the development of depressive symptoms following chronic unexpected stress (Bambico et al., 2018). The CB's influence over affect also includes anxiety and fear conditioning. The fastigial nucleus is synaptically connected to the ventrolateral periaqueductal grey. The activation or inhibition of these glutamatergic synapses during fear acquisition enhanced or suppressed fear extinction respectively (Frontera et al., 2020).

One region with which CB has direct communication is the thalamus. While much of the DCN projects to motor thalamus to support communication with the motor cortex there are also synapses to non-motor thalamic nuclei. For example, retrograde and

anterograde tracing has shown that the DCN projects to intralaminar thalamic nuclei (ILN)(Judd et al., 2021; Xiao et al., 2018; Hintzen et al., 2017). These regions of the thalamus are thought to contribute to arousal, attention, and learning and memory (Cover & Mathur, 2021; Quiroz-Padilla et al., 2010). When ILN neurons receiving CB input were silenced in rodents, subjects performed worse in a forced alternation paradigm (Xiao et al., 2018). Essentially, animals learn that they must alternate the selected side in a T-maze in sequential trials. When CB-ILN neurons were shut down following learning this paradigm, animals failed to choose the correct side at a rate better than chance, indicating a failure of cognitive flexibility. Kelly et al. (2020) also identified projections from the lateral nucleus of the CB the ventromedial thalamus (VM). Using results from chemogenetic experiments in conjunction with a genetic perturbation, they hypothesized that activation of this circuit likely regulates social behaviors and behavioral flexibility.

Projection regions such as the VTA, dorsal raphe, and thalamus can often be thought of as relay structures that serve to transmit, or transform and transmit, messages from other input structures; and it is only through this polysynaptic connectivity that precise behavioral influence can be effected.

POLYSYNAPTIC CIRCUITRY

Polysynaptic circuitry is key in fine-tuning complex behavior appropriately for particular contexts. For example, cerebello-thalamo-cortical loops are necessary for controlling and updating motor learning (Horne & Butler, 1995; Aumann, 2002). Very little, however, is known regarding long-range CB non-motor connectivity, particularly with sub-cortical structures. Despite this, some tracing studies, as well as much of the

data described above suggest CB connectivity to non-motor regions such as amygdala, cortex, and nucleus accumbens (Fig. 1.1).

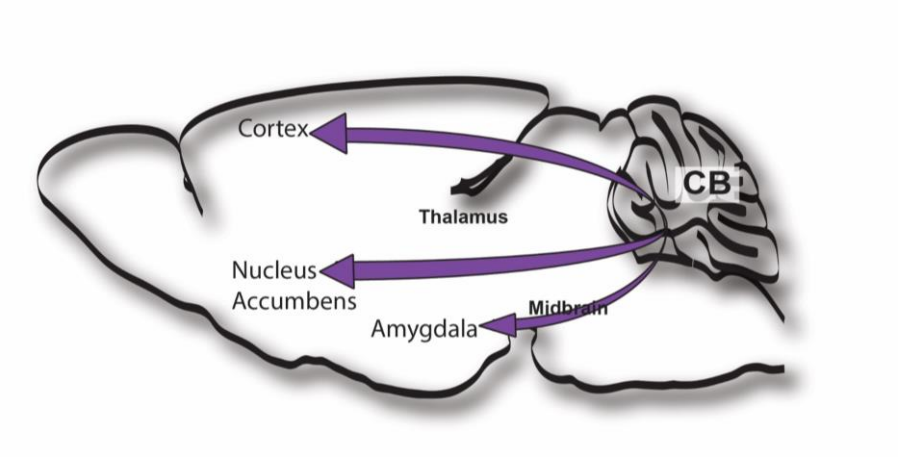

Figure 1.1. Putative polysynaptic, long-range connectivity of the non-motor CB. Schematic depicting regions that are likely involved in CB non-motor circuitry.

It has been shown by our own lab and others, that the CB is disynaptically connected to the amygdala (Jung & Vlasov et al., see appendix ii). Projections from DCN to the parafascicular and centromedial thalamic nuclei continue to the basolateral amygdala. Considering the amygdala's role as the brain's emotional epicenter, it is reasonable to hypothesize that this disynaptic circuit is at least in part responsible for the documented role that CB plays in emotional learning paradigms such as fear conditioning and fear extinction (Frontera et al., 2020; Frontera et al., 2023).

Some disynaptic circuitry from CB to non-motor cortex has been elucidated. In the previously mentioned study by Kelly et al., they showed that neurons in the ventromedial thalamus that receive CB projections also project to the prelimbic cortex (PRL). This disynaptic circuit originates in both medial and lateral nuclei. Evidence from their behavioral experiments using CB transgenic manipulation combined with

optogenetics in the VM-PRL terminals suggests these regions work together to regulate social preference and grooming. The thalamus also acts as an intermediate node in the disynaptic circuit from the DCN to dorsal striatum (Xiao et al., 2018). These two regions communicate via the ILN of the thalamus and explain how the DCN-ILN circuit plays a role in goal-directed behaviors typically associated with the dorsal striatum, such as the forced alternation task involving reward learning.

Though some tasks involving goal-directed learning and motivation are associated with the dorsal striatum, reward learning and motivated behavior, including social behavior, are associated far more heavily with the ventral striatum. Specifically, the two subregions of the nucleus accumbens (NAc), the medial shell (NAc_{Med}) and the core (NAc_{Core}) are key regulators of social, reward, and goal-directed behavior (Floresco, 2014; Shan et al., 2022; Klawonn & Malenka, 2018). While there has been some indirect evidence that the DCN may polysynaptically communicate with the NAc (Holloway et al., 2019) there is no concrete explanation for the overlap of reward- and motivation-related behaviors in which these two regions are involved. Further study is warranted to determine if and how these regions are connected.

There is still much left unknown regarding the CB's involvement in non-motor functions and the anatomy underlying them. In order to shed light on this, we must elucidate the polysynaptic routes through which the CB communicates with non-motor hubs and determine how exactly the CB influences activity in these regions. By continuing to take advantage of new technologies and advances in genetic animal modeling, we can further our understanding of circuits that are important for adaptive behavior in rewarding and social situations. This could have implications for mental

health disorders and neurodivergences that have long stumped our society such as depression, schizophrenia, and autism.

References

Andre, P., M. Zaccaroni, P. Fiorenzani, D. Della Seta, M. Menzocchi, and F. Farabollini. "Offline Consolidation of Spatial Memory: Do the Cerebellar Output Circuits Play a Role? A Study Utilizing a Morris Water Maze Protocol in Male Wistar Rats." *Brain Research* 1718 (September 1, 2019): 148–58. https://doi.org/10.1016/j.brainres.2019.05.010.

Aumann, T. D. "Cerebello-Thalamic Synapses and Motor Adaptation." *Cerebellum (London, England)* 1, no. 1 (2002): 69–77. https://doi.org/10.1080/147342202753203104.

Baek, Soo Ji, Jinsung Park, Jinhyun Kim, Yukio Yamamoto, and Keiko Tanaka-Yamamoto. "VTA-Projecting Cerebellar Neurons Mediate Stress-Dependent Depression-like Behavior." bioRxiv, August 25, 2021. https://doi.org/10.1101/2021.08.25.457606.

Bambico, Francis Rodriguez, Stefano Comai, Mustansir Diwan, S. M. Nageeb Hasan, Joshua Dean Conway, Soroush Darvish-Ghane, Clement Hamani, Gabriella Gobbi, and José N. Nobrega. "High Frequency Stimulation of the Anterior Vermis Modulates Behavioural Response to Chronic Stress: Involvement of the Prefrontal Cortex and Dorsal Raphe?" *Neurobiology of Disease* 116 (August 1, 2018): 166–78. https://doi.org/10.1016/j.nbd.2018.03.011.

Bauman, Margaret L., and Thomas L. Kemper. "Neuroanatomic Observations of the Brain in Autism: A Review and Future Directions." *International Journal of Developmental Neuroscience: The Official Journal of the International Society for Developmental Neuroscience* 23, no. 2–3 (2005): 183–87. https://doi.org/10.1016/j.ijdevneu.2004.09.006.

Carta, Ilaria, Christopher H. Chen, Amanda L. Schott, Schnaude Dorizan, and Kamran Khodakhah. "Cerebellar Modulation of the Reward Circuitry and Social Behavior." *Science* 363, no. 6424 (January 18, 2019): eaav0581. https://doi.org/10.1126/science.aav0581.

Caston, J, C Chianale, N Delhaye-Bouchaud, and J Mariani. "Role of the Cerebellum in Exploration Behavior." *Brain Research* 808, no. 2 (October 19, 1998): 232–37. https://doi.org/10.1016/S0006-8993(98)00847-6.

Cendelín, Jan, Ivana Korelusová, and František Vožeh. "The Effect of Repeated Rotarod Training on Motor Skills and Spatial Learning Ability in Lurcher Mutant Mice." *Behavioural Brain Research* 189, no. 1 (May 16, 2008): 65–74. https://doi.org/10.1016/j.bbr.2007.12.013.

Chen, Xiang, Tong Chen, Chen Dong, Huiyao Chen, Xinran Dong, Lin Yang, Liyuan Hu, et al. “Deletion of CHD8 in Cerebellar Granule Neuron Progenitors Leads to Severe Cerebellar Hypoplasia, Ataxia, and Psychiatric Behavior in Mice.” *Journal of Genetics and Genomics* 49, no. 9 (September 1, 2022): 859–69. https://doi.org/10.1016/j.jgg.2022.02.011.

Chirino-Pérez, Amanda, Oscar René Marrufo-Meléndez, José Ignacio Muñoz-López, Carlos R. Hernandez-Castillo, Gabriel Ramirez-Garcia, Rosalinda Díaz, Lilia Nuñez-Orozco, and Juan Fernandez-Ruiz. “Mapping the Cerebellar Cognitive Affective Syndrome in Patients with Chronic Cerebellar Strokes.” *Cerebellum (London, England)* 21, no. 2 (April 2022): 208–18. https://doi.org/10.1007/s12311-021-01290-3.

Cover, Kara K., and Brian N. Mathur. “Rostral Intralaminar Thalamus Engagement in Cognition and Behavior.” *Frontiers in Behavioral Neuroscience* 15 (2021). https://www.frontiersin.org/articles/10.3389/fnbeh.2021.652764.

Deverett, Ben, Mikhail Kislin, David W. Tank, and Samuel S.-H. Wang. “Cerebellar Disruption Impairs Working Memory during Evidence Accumulation.” *Nature Communications* 10, no. 1 (July 16, 2019): 3128. https://doi.org/10.1038/s41467-019-11050-x.

Fatemi, S. Hossein, Kimberly A. Aldinger, Paul Ashwood, Margaret L. Bauman, Charles D. Blaha, Gene J. Blatt, Abha Chauhan, et al. “Consensus Paper: Pathological Role of the Cerebellum in Autism.” *Cerebellum (London, England)* 11, no. 3 (September 2012): 777–807. https://doi.org/10.1007/s12311-012-0355-9.

Floresco, Stan B. “The Nucleus Accumbens: An Interface Between Cognition, Emotion, and Action.” *Annual Review of Psychology* 66, no. 1 (2015): 25–52. https://doi.org/10.1146/annurev-psych-010213-115159.

Frontera, Jimena L., Romain W. Sala, Ioana A. Georgescu, Hind Baba Aissa, Marion N. d’Almeida, Daniela Popa, and Clément Léna. “The Cerebellum Regulates Fear Extinction through Thalamo-Prefrontal Cortex Interactions in Male Mice.” *Nature Communications* 14, no. 1 (March 17, 2023): 1508. https://doi.org/10.1038/s41467-023-36943-w.

Frontera, Jimena Laura, Hind Baba Aissa, Romain William Sala, Caroline Mailhes-Hamon, Ioana Antoaneta Georgescu, Clément Léna, and Daniela Popa. “Bidirectional Control of Fear Memories by Cerebellar Neurons Projecting to the Ventrolateral Periaqueductal Grey.” *Nature Communications* 11 (October 15, 2020): 5207. https://doi.org/10.1038/s41467-020-18953-0.

Gompers, Andrea L., Linda Su-Feher, Jacob Ellegood, Nycole A. Copping, M. Asrafuzzaman Riyadh, Tyler W. Stradleigh, Michael C. Pride, et al. “Germline Chd8 Haploinsufficiency Alters Brain Development in Mouse.” *Nature Neuroscience* 20, no. 8 (August 2017): 1062–73. https://doi.org/10.1038/nn.4592.

Guell, Xavier, and Jeremy Schmahmann. “Cerebellar Functional Anatomy: A Didactic Summary Based on Human FMRI Evidence.” *The Cerebellum* 19, no. 1 (February 1, 2020): 1–5. https://doi.org/10.1007/s12311-019-01083-9.

Han, Jeong-Kyu, Sun-Ho Kwon, Yong Gyu Kim, Jaeyong Choi, Jong-Il Kim, Yong-Seok Lee, Sang-Kyu Ye, and Sang Jeong Kim. “Ablation of STAT3 in Purkinje Cells Reorganizes Cerebellar Synaptic Plasticity in Long-Term Fear Memory Network.” Edited by Gary L Westbrook, Jennifer L Raymond, Dagmar Timmann, and Keiko Tanaka-Yamamoto. *ELife* 10 (January 18, 2021): e63291. https://doi.org/10.7554/eLife.63291.

Hilber et al., “Differential Roles of Cerebellar Cortex and Deep Cerebellar Nuclei in Learning and Retention of a Spatial Task.”

Hintzen, Andreas, Esther Annegret Pelzer, and Marc Tittgemeyer. “Thalamic Interactions of Cerebellum and Basal Ganglia.” *Brain Structure and Function* 223, no. 2 (March 1, 2018): 569–87. https://doi.org/10.1007/s00429-017-1584-y.

Holloway, Zade R., Nick B. Paige, Josiah F. Comstock, Hunter G. Nolen, Helen J. Sable, and Deranda B. Lester. “Cerebellar Modulation of Mesolimbic Dopamine Transmission Is Functionally Asymmetrical.” *Cerebellum (London, England)* 18, no. 5 (October 2019): 922–31. https://doi.org/10.1007/s12311-019-01074-w.

Horne, M. K., and E. G. Butler. “The Role of the Cerebello-Thalamo-Cortical Pathway in Skilled Movement.” *Progress in Neurobiology* 46, no. 2–3 (June 1995): 199–213.

“Identification of Common Genetic Risk Variants for Autism Spectrum Disorder | Nature Genetics.” Accessed May 17, 2023. https://www.nature.com/articles/s41588-019-0344-8.

Jackman, Skyler L, Christopher H Chen, Heather L Offermann, Iain R Drew, Bailey M Harrison, Anna M Bowman, Katelyn M Flick, Isabella Flaquer, and Wade G Regehr. “Cerebellar Purkinje Cell Activity Modulates Aggressive Behavior.” *ELife* 9 (n.d.): e53229. https://doi.org/10.7554/eLife.53229.

Judd, Elena N, Samantha M Lewis, and Abigail L Person. “Diverse Inhibitory Projections from the Cerebellar Interposed Nucleus.” Edited by Roy V Sillitoe, Ronald L Calabrese, Roy V Sillitoe, Albert I Chen, and Hirofumi Fujita. *ELife* 10 (September 20, 2021): e66231. https://doi.org/10.7554/eLife.66231.

Kawamura, Atsuki, Yuta Katayama, Wataru Kakegawa, Daisuke Ino, Masaaki Nishiyama, Michisuke Yuzaki, and Keiichi I. Nakayama. “The Autism-Associated Protein CHD8 Is Required for Cerebellar Development and Motor Function.” *Cell Reports* 35, no. 1 (April 6, 2021): 108932. https://doi.org/10.1016/j.celrep.2021.108932.

Kelly, Elyza, Fantao Meng, Hirofumi Fujita, Felipe Morgado, Yasaman Kazemi, Laura C. Rice, Chongyu Ren, et al. “Regulation of Autism-Relevant Behaviors by Cerebellar–Prefrontal Cortical Circuits.” *Nature Neuroscience* 23, no. 9 (September 2020): 1102–10. https://doi.org/10.1038/s41593-020-0665-z.

Kim, S. G., K. Uğurbil, and P. L. Strick. “Activation of a Cerebellar Output Nucleus during Cognitive Processing.” *Science (New York, N.Y.)* 265, no. 5174 (August 12, 1994): 949–51. https://doi.org/10.1126/science.8052851.

Klawonn, Anna M., and Robert C. Malenka. “Nucleus Accumbens Modulation in Reward and Aversion.” *Cold Spring Harbor Symposia on Quantitative Biology* 83 (2018): 119–29. https://doi.org/10.1101/sqb.2018.83.037457.

Kostadinov, Dimitar, Maxime Beau, Marta Blanco Pozo, and Michael Häusser. “Predictive and Reactive Reward Signals Conveyed by Climbing Fiber Inputs to Cerebellar Purkinje Cells.” *Nature Neuroscience* 22, no. 6 (June 2019): 950. https://doi.org/10.1038/s41593-019-0381-8.

Kozareva, Velina, Caroline Martin, Tomas Osorno, Stephanie Rudolph, Chong Guo, Charles Vanderburg, Naeem Nadaf, Aviv Regev, Wade G. Regehr, and Evan Macosko. “A Transcriptomic Atlas of Mouse Cerebellar Cortex Comprehensively Defines Cell Types.” *Nature* 598, no. 7879 (October 2021): 214–19. https://doi.org/10.1038/s41586-021-03220-z.

Lalonde, Robert, Yves Lamarre, and Allan M. Smith. “Does the Mutant Mouse Lurcher Have Deficits in Spatially Oriented Behaviours?” *Brain Research* 455, no. 1 (July 5, 1988): 24–30. https://doi.org/10.1016/0006-8993(88)90109-6.

Larry, Noga, Merav Yarkoni, Adi Lixenberg, and Mati Joshua. “Cerebellar Climbing Fibers Encode Expected Reward Size.” *BioRxiv*, January 30, 2019, 533653. https://doi.org/10.1101/533653.

Lee, Phil H., Verneri Anttila, Hyejung Won, Yen-Chen A. Feng, Jacob Rosenthal, Zhaozhong Zhu, Elliot M. Tucker-Drob, et al. “Genomic Relationships, Novel Loci, and Pleiotropic Mechanisms across Eight Psychiatric Disorders.” *Cell* 179, no. 7 (December 12, 2019): 1469-1482.e11. https://doi.org/10.1016/j.cell.2019.11.020.

Luo, Yuanjun, Hirofumi Fujita, Hermina Nedelescu, Mohammad Shahangir Biswas, Chika Sato, Sarah Ying, Mayu Takahashi, et al. “Lobular Homology in Cerebellar Hemispheres of Humans, Non-Human Primates and Rodents: A Structural, Axonal Tracing and Molecular Expression Analysis.” *Brain Structure and Function* 222, no. 6 (August 1, 2017): 2449–72. https://doi.org/10.1007/s00429-017-1436-9.

Petersen, S. E., P. T. Fox, M. I. Posner, M. Mintun, and M. E. Raichle. “Positron Emission Tomographic Studies of the Cortical Anatomy of Single-Word Processing.” *Nature* 331, no. 6157 (February 1988): 585–89. https://doi.org/10.1038/331585a0.

Peterson, Todd C., Lee Villatoro, Tom Arneson, Brittany Ahuja, Stephanie Voss, and Rodney A. Swain. “Behavior Modification after Inactivation of Cerebellar Dentate Nuclei.” *Behavioral Neuroscience* 126 (2012): 551–62. https://doi.org/10.1037/a0028701.

Prestori, Francesca, Lisa Mapelli, and Egidio D'Angelo. "Diverse Neuron Properties and Complex Network Dynamics in the Cerebellar Cortical Inhibitory Circuit." *Frontiers in Molecular Neuroscience* 12 (2019). https://www.frontiersin.org/articles/10.3389/fnmol.2019.00267.

Quiroz-Padilla, María Fernanda, Margarita Martí-Nicolovius, and Gemma Guillazo-Blanch. "Posterior Intralaminar Nuclei of the Thalamus and Cognitive Processes" 51, no. 4 (August 13, 2010): 217–25.

Redies, Christoph, Nicole Hertel, and Christian A. Hübner. "Cadherins and Neuropsychiatric Disorders." *Brain Research* 1470 (August 27, 2012): 130–44. https://doi.org/10.1016/j.brainres.2012.06.020.

Schmahmann, J D, and J C Sherman. "The Cerebellar Cognitive Affective Syndrome." *Brain* 121, no. 4 (April 1, 1998): 561–79. https://doi.org/10.1093/brain/121.4.561.

Schraa-Tam, Caroline K. L., Willem J. R. Rietdijk, Willem J. M. I. Verbeke, Roeland C. Dietvorst, Wouter E. van den Berg, Richard P. Bagozzi, and Chris I. De Zeeuw. "FMRI Activities in the Emotional Cerebellum: A Preference for Negative Stimuli and Goal-Directed Behavior." *Cerebellum (London, England)* 11, no. 1 (March 2012): 233–45. https://doi.org/10.1007/s12311-011-0301-2.

Shan, Qiang, You Hu, Shijie Chen, and Yao Tian. "Nucleus Accumbens Dichotomically Controls Social Dominance in Male Mice." *Neuropsychopharmacology* 47, no. 3 (February 2022): 776–87. https://doi.org/10.1038/s41386-021-01220-1.

Steinmetz, Joseph E., Sheree F. Logue, and Daniel P. Miller. "Using Signaled Barpressing Tasks to Study the Neural Substrates of Appetitive and Aversive Learning in Rats: Behavioral Manipulations and Cerebellar Lesions." *Behavioral Neuroscience* 107, no. 6 (19940801): 941. https://doi.org/10.1037/0735-7044.107.6.941.

Stoodley, Catherine J., and Jeremy D. Schmahmann. "Evidence for Topographic Organization in the Cerebellum of Motor Control versus Cognitive and Affective Processing." *Cortex; a Journal Devoted to the Study of the Nervous System and Behavior* 46, no. 7 (2010): 831–44. https://doi.org/10.1016/j.cortex.2009.11.008.

Strata, Piergiorgio. "The Emotional Cerebellum." *The Cerebellum* 14, no. 5 (October 1, 2015): 570–77. https://doi.org/10.1007/s12311-015-0649-9.

Sugihara, Izumi. "Cerebellar Lobules and Stripes, Viewed from Development, Topographic Axonal Projections, Functional Localization, and Interspecies Homology." In *Cerebellum as a CNS Hub*, edited by Hidehiro Mizusawa and Shinji Kakei, 93–119. Contemporary Clinical Neuroscience. Cham: Springer International Publishing, 2021. https://doi.org/10.1007/978-3-030-75817-2_5.

Tantra, M., L. Guo, J. Kim, N. Zainolabidin, V. Eulenburg, G. J. Augustine, and A. I. Chen. "Conditional Deletion of Cadherin 13 Perturbs Golgi Cells and Disrupts Social and Cognitive Behaviors." *Genes, Brain and Behavior* 17, no. 6 (2018): e12466. https://doi.org/10.1111/gbb.12466.

Timmann, D., J. Drepper, M. Frings, M. Maschke, S. Richter, M. Gerwig, and F. P. Kolb. "The Human Cerebellum Contributes to Motor, Emotional and Cognitive Associative Learning. A Review." *Cortex; a Journal Devoted to the Study of the Nervous System and Behavior* 46, no. 7 (2010): 845–57. https://doi.org/10.1016/j.cortex.2009.06.009.

Tsai, Peter T., Court Hull, YunXiang Chu, Emily Greene-Colozzi, Abbey R. Sadowski, Jarrett M. Leech, Jason Steinberg, Jacqueline N. Crawley, Wade G. Regehr, and Mustafa Sahin. "Autistic-like Behavior and Cerebellar Dysfunction in Purkinje Cell Tsc1 Mutant Mice." *Nature* 488, no. 7413 (August 8, 2012): 647. https://doi.org/10.1038/nature11310.

Wang, Samuel S. -H., Alexander D. Kloth, and Aleksandra Badura. "The Cerebellum, Sensitive Periods, and Autism." *Neuron* 83, no. 3 (August 6, 2014): 518–32. https://doi.org/10.1016/j.neuron.2014.07.016.

Wyciszkiewicz, Aleksandra, Mikolaj A. Pawlak, and Krzysztof Krawiec. "Cerebellar Volume in Children With Attention-Deficit Hyperactivity Disorder (ADHD)." *Journal of Child Neurology* 32, no. 2 (February 2017): 215–21. https://doi.org/10.1177/0883073816678550.

Xiao, Le, Caroline Bornmann, Laetitia Hatstatt-Burklé, and Peter Scheiffele. "Regulation of Striatal Cells and Goal-Directed Behavior by Cerebellar Outputs." *Nature Communications* 9, no. 1 (August 7, 2018): 3133. https://doi.org/10.1038/s41467-018-05565-y.

Chapter 2: Cerebellum activation bidirectionally modulates Nucleus Accumbens activity

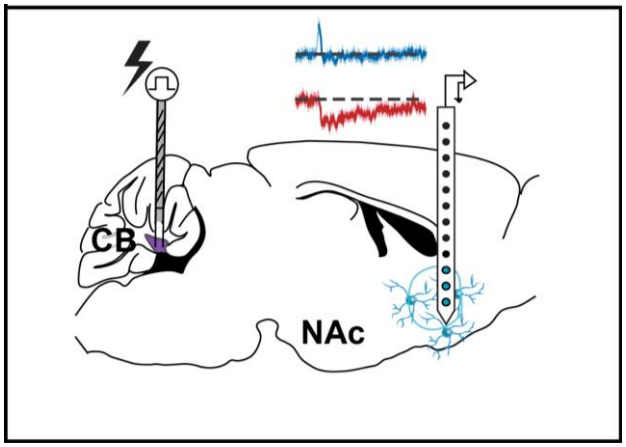

Figure 2.0 Graphical Abstract Depicting Findings Described in Chapter 2

Preface

The following chapter includes data and analyses made available as a preprint in BioRxiv (D'Ambra AF, Vlasov K, Jung SJ, Ganesan S, Anztoulatos EG, Fioravante D (2020). Cerebellar Activation Bidirectonally Regulates Nucleus Accumbens Core and Medial Shell. BioRxiv. Doi: https://doi.org/10.1101/2020.09.28.283952) and in the following manuscript published in *eLife:* D'Ambra AF, Vlasov K, Jung SJ, Ganesan S, Anztoulatos EG, Fioravante D (2023). Cerebellar Activation Bidirectonally Regulates Nucleus Accumbens Core and Medial Shell.DOI: 10.7554/eLife.87252. Author contributions to the work presented in this chapter is as follows: **AFD**: conceptualization, methodology, animal care, investigation, data analysis and visualization, project administration, supervision; **SG**: histological analysis; **EGA**: conceptualization, methodology, data analysis and visualization, resources, project administration, supervision; **DF**: conceptualization, animal care, data analysis and visualization, project administration, supervision, project funding acquisition. Funding: **AFD** was supported by NIH T32 GM007377 and a UC Davis Dean's Distinguished Graduate Fellowship; **EA** was supported by a NARSAD 2018 Young Investigator Grant. This work was supported by a Whitehall fellowship, BRFSG-2017-02, R21MH114178, NSF1754831 and R01MH128744 to **DF**.

Introduction

The NAc is a complex limbic structure that, as a well-known hub of reward learning and social behavior, shares several of the non-motor functions of the CB. Plenty of literature documents this structure's involvement in reward learning, goal-directed task

performance, social behavior, and cognitive flexibility in reward-based tasks (Floresco, 2015; Klawonn and Malenka, 2018; Aquili et al. 2014; others).

These studies and other studies of NAc function separately assess the NAc core (NAc_{Core}) and the NAc medial shell (NAc_{Med}) due to documented differences in their cytoarchitecture, connectivity, and behavioral influence (Groenewegen et al., 1999; Zahm, 1999; Corbit and Balleine, 2011; Ito and Hayen, 2011; Badrinarayan et al., 2012; Li et al., 2018)(Fig. 2.1). In fact, these two subregions can often have opposing roles in social behavior and reward learning (Floresco et al., 2014; Shan et al., 2022). For example, in a behavioral flexibility task in which a reward is devalued due to satiety, only the NAc_{Med} seems to encode the change in reward value (Loriaux et al., 2011). In fact, the Nac_{Med} and Nac_{Core} have been shown to perform distinct roles in several investigations regarding the NAc in behavioral flexibility (Corbit et al., 2001; West & Carelli, 2016). Another point in which NAc_{Core} and NAc_{Med} diverge is in behaviorally-induced dopamine (DA) modulation in each region. It is well-known that DA is a key modulator of NAc activity, particularly during reward/aversive learning; however, this modulation is not always consistent across NAc subregions.

Following cued fear conditioning, the aversive fear cue causes differential changes in DA transmission in the NAc. In NAc_{Core} DA transmission is decreased, whereas in NAc_{Med} there is a slow ramping up of DA (Badrinarayan et al., 2012). Importantly, it is known that CB activation is sufficient to elicit changes in DA release. Together with the functional overlap across CB and NAc, and the demonstrated lack of direct synaptic connection, it is logical to hypothesize that the cerebellum can modulate NAc activity.

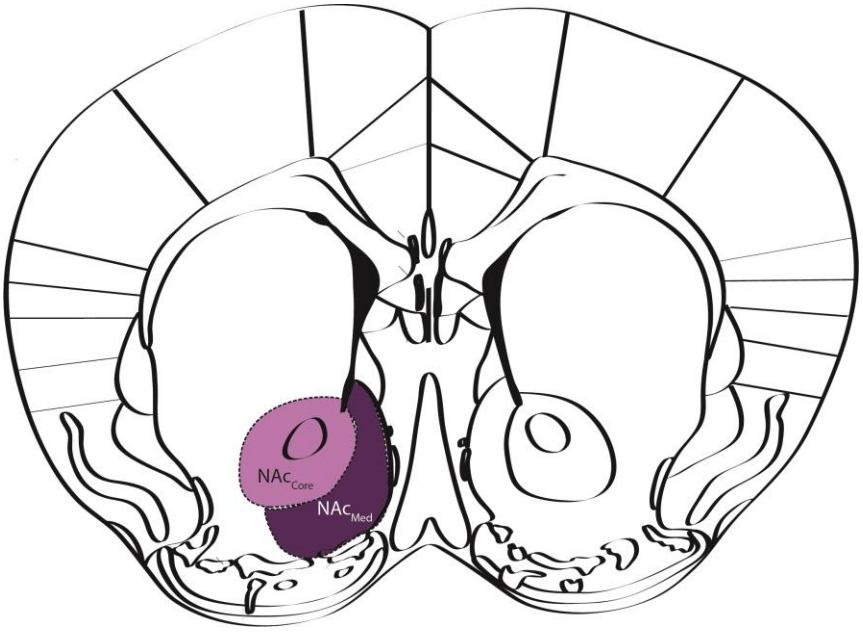

Figure 2.1. Nucleus Accumbens is divided into distinct subregions. Schematic depicting the two key subregions of the NAc: the NAc core, and the NAc shell.

To test this hypothesis, I performed in vivo electrophysiological experiments in which I recorded changes NAc spiking activity in response to CB stimulation. Both multi-unit and single-unit responses were analyzed, revealing potential differences in population versus single neuron behavior following stimulation. Due to the previously shown distinct connectivity of NAc_{Core} and NAc_{Med}, responses were analyzed separately for the two subregions. This work provides the first evidence of an electrophysiological connection between CB and NAc.

Materials and Methods

MICE

C57Bl/6J mice of both sexes were used in accordance with the National Institutes of Health guidelines and the policies of the University of California Davis

Committee for Animal Care. Acute in vivo recordings were performed at postnatal days P43-P91. All animals were maintained on a light/dark cycle (light 7 am - 7 pm), and experiments were performed during the light cycle.

SURGERY

Mice (N = 42 mice of both sexes) were initially anesthetized by brief inhalation of 4-5% isoflurane followed by an intraperitoneal injection of anesthetic cocktail (100 mg/kg ketamine; 10 mg/kg xylazine; 1 mg/kg acepromazine). Anesthetic levels were maintained with periodic injections of the anesthetic cocktail (20-50 mg/kg), as needed. After confirmation of anesthesia depth using a toe pinch response test, mice were placed in a stereotactic frame (Stoelting) on a heating pad. Breathing rate and toe pinch responses were monitored to ensure maintenance of anesthesia. A small craniotomy and durectomy were performed over the DCN (lateral/interposed n.: relative to lambda, in mm: -2.1 to - 2.6 AP; +/-2.1 to +/-2.3 ML). For recordings, craniotomy and durectomy were made over NAc, targeting the medial shell and/or core (relative to bregma: +1.7 to +1.54 AP; +/- 0.4 to +/-1.15 ML).

ELECTRICAL STIMULATION

For local stimulation, a custom stereotrode (~200 µm distance between tips) was lowered 1.95 - 2.45 mm below the brain surface (in DV axis) through the cerebellar craniotomy to reach the DCN. Ten trials of bipolar constant-current electrical microstimulation were delivered at each location at a 15-s inter-trial interval. Each stimulation trial consisted of a 200-Hz burst of two to five 0.5-ms monophasic square-waveform pulses at 100 µA. In a subset of experiments, the stimulation intensity was varied between 30 (N= 14 mice) 100, and 300 (N=40 mice) µA in interleaved blocks of

at least 5 trials per intensity. When stimulation was repeated at different DCN sites in the same experiment, an effort was made to move the stereotrode in a direction perpendicular to the axis of the two poles, so that an at least partly distinct pool of cerebellar neurons could be stimulated.

ACQUISITION OF ELECTROPHYSIOLOGICAL DATA

Recordings were performed with a 12-channel (platinum; 0.2 - 2 MΩ impedance) axial multi-electrode array (FHC; 150 µm distance between channels), dipped in fluorescein dextran (3000 MW) and lowered into the NAc at a depth of 3.75 - 5.25 mm below the brain surface (DV axis). Electrode signals were fed to a digital headstage (RHD 2132, Intan Technologies) for amplification (x20), filtering (0.7 - 7500 Hz) and digitization (30 kS/s with 16-bit resolution), before transfer to an open-source acquisition system (OpenEphys) for display and storage.

HISTOLOGY FOR VERIFICATION OF ELECTRODE PLACEMENT

Positioning of electrodes was initially guided by atlas-based stereotactic coordinates (Paxinos & Franklin) and, upon completion of experiments, histologically verified through electrolytic lesions (single 10-s cathodal pulse of 300 µA) and fluorescence imaging (fluorescein dye track). Coordinates for subsequent animals of the same litter were further adjusted accordingly. At the end of experiments, electrodes were retracted, and animals were perfused with 4% (w/v) paraformaldehyde (PFA) in 0.1 M phosphate buffer (PB). Brains were dissected and post-fixed in 4% PFA, sliced in phosphate buffered saline (PBS) and inspected under a fluorescence stereoscope (Olympus SZX2). Slices containing the dye track from the recording array were identified under 488 nm light; CB slices with electrolytically lesioned tissue were

identified under brightfield illumination. Slices of interest were subsequently stained with DAPI (1:20,000, Thermo Fisher Scientific), mounted on slides, and imaged using a VS120 Olympus slide scanner. Images were manually registered to the Paxinos and Franklin Mouse Brain Atlas and the location of the recording electrode tip and optic fiber were mapped. Only channels along the recording array that were determined to be within NAc_{Core} and/or NAc_{Med} were included in analysis. Experiments with cerebellar electrolytic lesions localized outside the lateral and/or interposed DCN, were excluded from analysis.

QUANTIFICATION AND STATISTICAL ANALYSIS

Electrophysiological data processing and quantification

Custom-written MATLAB scripts (Mathworks) were used for data processing and analysis. Filtering of spikes was achieved through a 4^{th}-order Butterworth high-pass filter (cutoff at 300 Hz). The filtered signal was thresholded at 3-3.5 standard deviations below the average voltage**.** For single-unit analyses, spikes were subsequently sorted in putative single-unit clusters with Plexon Offline Sorter (version 3.3.5) using principal component analysis. Spikes with time differences less than 7ms (10ms for multi-unit) from stimulus artifacts or 1ms (2ms for multi-unit) from the previous spike were discarded. All well-isolated neurons were included in the analyses. Firing rates for multi- and single-unit analyses were computed from spike counts in consecutive 10-ms time bins (peri-stimulus time histogram; PSTH). A cell was excluded from analysis if it had fewer than two trials with spiking during the pre-stimulus baseline.

Quantification of stimulation-induced modulation of NAc spiking activity followed recent studies of cerebellar neurons (Chen et al., 2014; Washburn et al., 2022) and our

own evaluation of the dataset. For multi-unit data, we averaged the PSTH across all trials of the same intensity for any given pair of recording and stimulation sites and normalized to the average pre-stimulus baseline. We considered a change of firing rate to be a response to DCN stimulation only if it (a) took place within the first 500ms following stimulus onset (response window), and (b) exceeded either a positive or negative threshold in standard deviations (σ) for excitatory responses or inhibitory responses respectively. For single-unit analyses, excitatory threshold was 3 σ, and inhibitory threshold was -1 σ. A third criterion was also set for inhibitory responses in which the threshold crossing must persist for a minimum of three time bins (i.e., 30 ms). For single-unit responses that included both excitatory and inhibitory components (mixed responses), we quantified each component individually for amplitude and latency. The same thresholds were employed to identify responses of both NAc subregions and to all stimulation intensities that were tested in this study. For illustration purposes only, all firing rates were convolved with a Gaussian kernel (σ = 16ms). Response onset latency was defined as the first instance at which firing rate changed from baseline as described above, using 1-ms time bins.

Statistics

Statistical analyses were performed in Matlab and GraphPad Prism. Comparisons of the relative frequency distribution of response types were performed with Contingency Table analyses (Chi-square tests). Comparisons of response latencies and firing rates were performed with t-tests and ANOVA. To correct for multiple comparisons, we followed the Benjamini-Hochberg method (Benjamini and Hochberg, 1995) with False Discovery Rate (FDR) set at 10%.

RESULTS

DCN MICROSTIMULATION BIDIRECTIONALLY ALTERS NAc POPULATION SPIKING ACTIVITY

To examine functional connectivity between CB and NAc, we recorded ongoing spiking activity from NAc_{Med} and NAc_{Core} *in vivo* and electrically microstimulated the DCN (Fig. 2.2A). We primarily targeted the lateral DCN, activation of which has been shown to modulate levels of dopamine in NAc (Mittleman et al., 2011). In a subset of experiments, post-hoc analysis localized the bipolar stimulating electrode in the interposed DCN, and these data were included in our analysis. Activation of DCN with five 100-µA current pulses at 200 Hz (total stimulus duration: 25ms) evoked distinct types of responses in multi-unit NAc activity: excitatory (Fig. 2.2B1) and inhibitory (Fig. 2.2B2). The peak firing rate (normalized to baseline) of each excitatory (*blue*) or inhibitory (*red*) response is shown in Fig. 2.2C (average peak response normalized to baseline: excit.: 205.7 % ± 18.4; inh.: 61.2 % ± 2.0). Both types of modulation were robust in terms of amplitude (paired t-test comparing peak average firing rate vs baseline: excit.: t_{119} = -

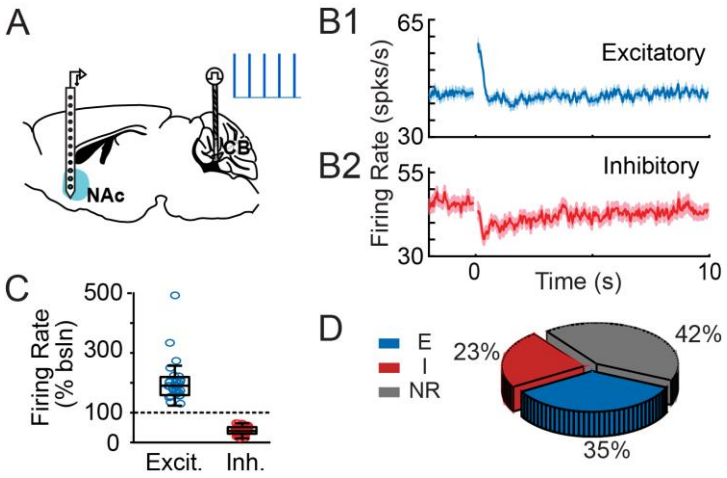

Figure 2.2. Cerebellar stimulation elicits excitatory and inhibitory responses in nucleus accumbens.
A, Schematic diagram of recording setup. NAc: nucleus accumbens; CB: cerebellum. **B,** Average PSTH for excitatory (**B1**) and inhibitory (**B2**) responses in the NAc. Stimulus artifacts have been masked for clarity. **C,** Peak firing rate of all excitatory or inhibitory responses, normalized to baseline. **D,** Distribution of response types elicited by DCN stimulation. *E*: Excitatory, *I*: inhibitory, *NR*: non-responders.

23.9, $p < 0.001$; inh.: $t_{76} = 25.3$, $p < 0.001$). Out of all the recordings performed (n = 94 sites; N = 42 animals), 58% showed effective modulation following CB stimulation. Of these elicited responses, 23% were inhibitory and 35% were excitatory (Fig. 2.2D). We suspected that these values were an underestimation of the actual prevalence, particularly for excitatory responses. This is because activity immediately following stimulation was masked by the electrical artifact, requiring spikes during and shortly after the stimulation to be removed. Therefore, the prevalence of fast, transient excitatory responses may have been under-counted.

SINGLE-UNIT ANALYSIS IDENTIFIES A THIRD NAC RESPONSE TYPE FOLLOWING CB STIMULATION

One way to avoid this artifact masking is by sorting units using individual waveforms. Although a short refractory period is still necessary, assessing neuronal activity by single-unit firing rate bypasses much of the mask and allows for better quantification of NAc responses. Additionally, while multi-unit analyses (MUA) is crucial to understand population dynamics in response to CB stimulation, single-unit analysis (SUA) can also add new insight. SUA allows for separating firing rate information into individual neurons, which is necessary to identify unique populations that may respond to stimulation differently within a trial.

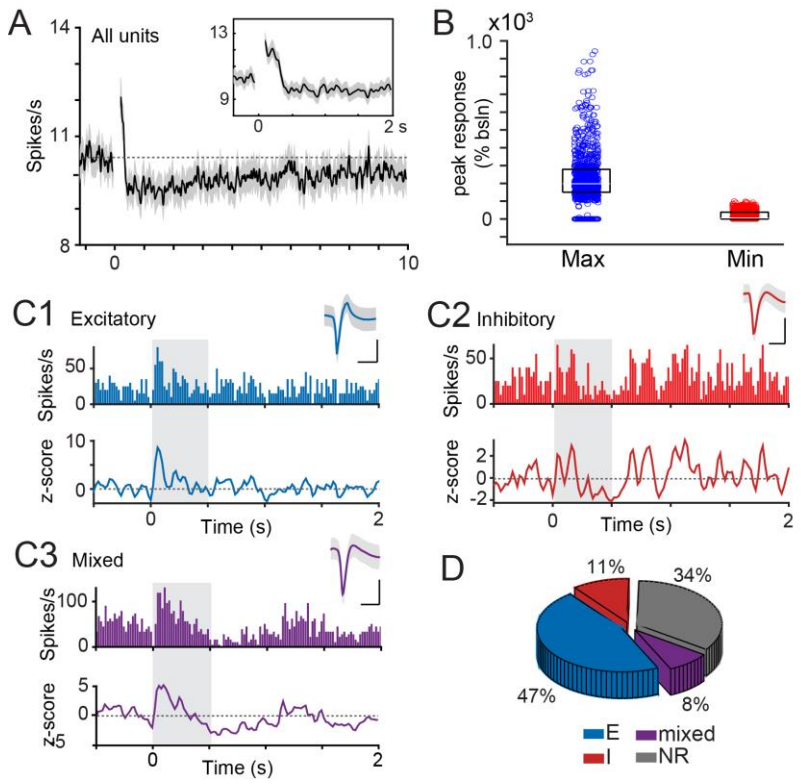

Figure 2.3. Single units in NAc display 3 response-types. A, Average spiking activity (spikes/s) across all recorded units (N = 42 mice). Inset shows zoom-in of first two seconds after stimulation. **B,** Maximum (max) and minimum (min) response for all units normalized to baseline. Max values cut off at 1000%. **C**, Examples of excitatory (**C1**), inhibitory (**C2**), and mixed (**C3**) responses. *Top,* Peri-stimulus time histogram (PSTH) of the average firing rate across trials. *Bottom,* Baseline-normalized firing rate (z-score) across time. *Inset*, Example average waveform of putative single unit. Scale bars: 1 ms, 10 µV. Shaded area marks response window. **D** Distribution of response types elicited in NAc by DCN stimulation. *Blue*: Excitatory (E), *Red*: inhibitory (I), *Purple:* mixed, *Gray*: non-responders (NR).

The averaged spiking activity of all single units is consistent with bidirectional influence of CB stimulation (Fig. 2.3A). The spiking activity averaged across all recorded units, initially increased to 12.2 ± 0.5 spikes/s from a pre-stimulus baseline of 10.7 ± 0.4 spikes/s, followed by a modest, slow-recovering decrease to 9.8 ± 0.4 spikes/s. The average response will underestimate the amplitude of modulation of CB stimulation if individual units do not respond with the exact same timing. In fact, in response to stimulation, average maximum activity for individual units increased significantly to 19.4 ± 0.6 spikes/s (t_{1017} = -33, $p < 0.001$), and decreased to an average minimum of 4.6 ±

0.3 spikes/s ($t_{1017} = 37$, $p < 0.001$) (n = 1018 units x stimulation sites). Plotting the distribution of the maximum and minimum percent of baseline across all units (Fig. 2.3B) clearly demonstrates not only that units are modulated following stimulation, but also that inhibitory modulation must have a physiologically determined floor as neurons cannot spike less frequently than 0 spikes/s. Nevertheless, like multi-unit activity, single units displayed excitatory (Fig. 2.3C1) and inhibitory (Fig. 2.3C2) responses; however, we were surprised to see that individual units could have a mixed response in which their response to stimulation contained both excitatory and inhibitory components (Fig. 2.3C3). Of the 546 recorded NAc neurons, 66% responded to DCN stimulation, with most (47%) displaying an excitatory response (Fig. 2.3D). An inhibitory response was elicited in 11% of neurons, and 8% of neurons displayed mixed responses. As speculated above, the ability to identify spiking within a shorter window following electrical stimulation did in fact lead to an increase in the proportion of excitatory responses. The amplitude of this modulation was significant as excitatory response amplitude was 22 ± 0.9 spikes/s, or 349 ± 15% of baseline ($t_{430} = -26.8$, $p < 0.001$), and the average inhibitory response amplitude was 4.7 ± 0.4 spikes/s, or 30 ± 2% of baseline ($t_{135} = 14.6$, $p < 0.001$).

EFFECTS OF DCN MICROSTIMULATION ON NAC CORE AND MEDIAL SHELL SINGLE-UNIT SPIKING ACTIVITY

We hypothesized that the difference in prevalence between DCN-evoked excitatory and inhibitory responses in NAc could stem from regional differences at NAc recording sites. Our axial multi-electrode array approach enabled recordings from multiple NAc sites in both NAc_{Core} and NAc_{Med} (Fig. 2.4A). Out of 169 neurons we

recorded in NAc_{Core}, more than half (53%) responded with excitatory modulation to 100-µA stimulation of at least one site in DCN, while 8% responded with inhibitory modulation, and another 8% with mixed modulation (Fig. 2.4B *left*). In the NAc_{Med}, 377 neurons were recorded and 44% responded to DCN stimulation with excitation, 12% with inhibition, and 8% with mixed modulation of spiking activity. The frequency distributions of these response-types in NAc_{Core} and NAc_{Med} were not statistically different ($\chi^2_{(3)} = 4.7$, $p = 0.19$).

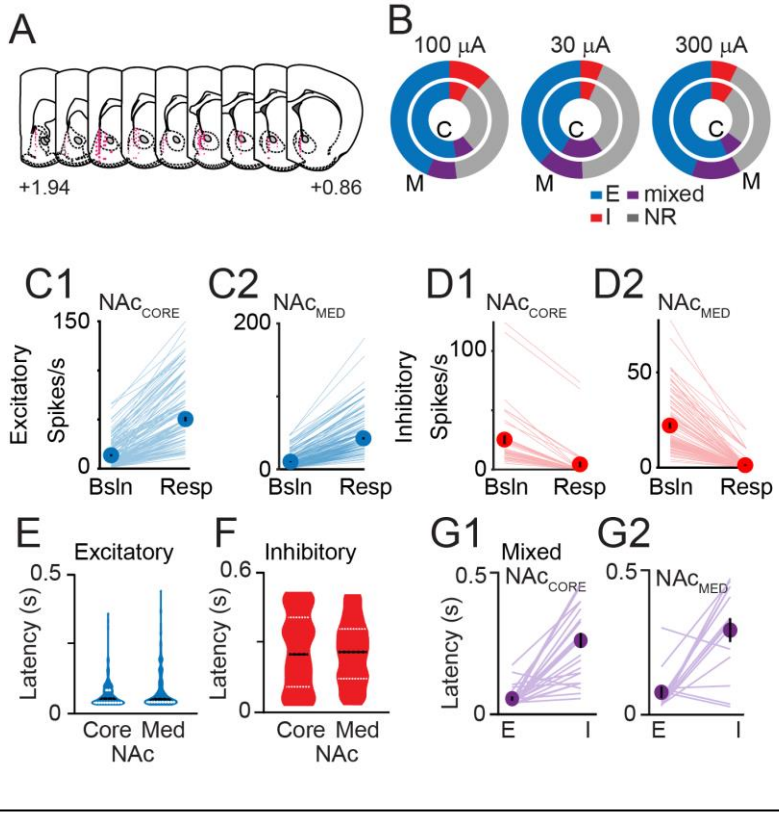

Figure 2.4. Single-unit responses to CB stimulation in NAc Core and Medial Shell. A, Recording sites in NAc_{Core} and NAc_{Med}. Numbers indicate distance (mm) from bregma. **B,** Distribution of response types elicited by 30-, 100-, or 300-µA DCN stimulation. M: NAc_{Med}; C: NAc_{Core}. E: excitatory, I: inhibitory, NR: non-responders. **C,** Average baseline (Bsln) and peak firing rate (Resp) elicited by 100-µA DCN stimulation for excitatory responses in NAc_{Core} (**C1**) and MAc_{Med} (**C2**). Circles and black lines show average and SEM respectively. **D1**,**2**, Same as C but inhibitory responses. **E**,**F**, Violin plots of onset latencies for excitatory (**E**) and inhibitory (**F**) responses in NAc_{Core} and NAc_{Med}. Black lines: median; white lines: interquartile range (Q1-Q3). **G**, Onset latencies for excitatory (E) and inhibitory (I) components of mixed responses in NAc_{Core} (**G1**) and NAc_{Med} (**G2**).

We examined whether the amplitude of excitatory and/or inhibitory responses varied between NAc_{Core} and NAc_{Med} (Figs. 2.4C,D). In both NAc_{Core} and NAc_{Med} DCN stimulation elicited significant excitatory modulation of firing rate (spikes/s in NAc_{Core}: baseline: 12.2 ± 1.1, peak excitatory response: 52.2 ± 2.5, paired $t_{162} = -24.2$, $p <$

0.0001; in NAc_{Med}: baseline: 7.9 ± 0.6, peak excitatory response: 42.2 ± 1.5, paired t_{267} = -32.4, p < 0.0001), which did not differ between subregions (% baseline: NAc_{Core}: 856.2 ± 79.2, NAc_{Med}: 978.8 ± 62.5, t_{429}= -1.2, p = 0.23). Similarly, both NAc_{Core} and NAc_{Med} showed significant inhibitory modulation (mean ± sem, spikes/s in NAc_{Core}: baseline: 24.3 ± 3.9, peak inhibitory response: 4.0 ± 2.3, paired t_{42} = 9.7, p < .0001; in NAc_{Med}: baseline: 22.1 ± 1.6, peak inhibitory response: 1.3 ± 0.4, paired t_{92} = 15.5, p < 0.0001), which did not differ between subregions (% baseline: NAc_{Core}: 4.3 ± 2.1, NAc_{Med}: 2.6 ± 0.8, t_{134} = 0.9, p = 0.36)(p-values corrected for multiple comparisons). It became apparent that irrespective of subregion, the baseline firing rate of excitatory responses was significantly lower than the baseline of inhibitory responses (F(1,563) = 88, p < 0.001). Differences in baseline between excitatory and inhibitory responses could arise from potentially different NAc cellular properties, although the fact that neurons with elevated firing rates are more likely to satisfy our criterion for inhibitory responses should also be considered.

TEMPORAL PROFILES OF NAc RESPONSES

We subsequently evaluated the temporal profiles of NAc responses evoked by DCN microstimulation (Fig. 2.4E-G). In both NAc_{Core} and NAc_{Med}, excitatory responses had earlier onset than inhibitory ones (Fig. 2.4E, F). Excitatory responses of NAc_{Core} neurons had an average onset latency of 75 ± 5 ms (10^{th} percentile: 35 ms), and excitatory responses of NAc_{Med} neurons had an average onset latency of 83 ± 5 ms (10^{th} percentile: 33 ms). Note that the electrical stimulus artifact prevented us from identifying responses with onset latency shorter than 32 ms. Inhibitory responses of NAc_{Core} neurons had an average onset latency of 268 ± 25 ms (10^{th} percentile: 42 ms),

and inhibitory responses of NAc_{Med} neurons had an average onset latency of 259 ± 14 ms (10^{th} percentile: 60 ms). Neither the NAc subregion ($F(1, 563) = 0.01$; $p = 0.93$), nor the interaction of subregion and response-type ($F(1, 563) = 0.82$; $p = 0.37$) showed a statistically significant effect on response onset latencies. There was, however, a significant effect of response-type on latencies ($F(1, 563) = 353.5$; $p<0.001$), with excitatory responses occurring at shorter latencies than inhibitory ones. Finally, excitatory components preceded inhibitory ones also for mixed response-types (t-test for paired samples in NAc_{Core}: $t_{13} = 4.4$; $p < 0.001$; in NAc_{Med}: $t_{25} = 7.4$; $p < 0.001$) (Fig 4G). Collectively, these results indicate that both NAc subregions respond to electrical microstimulation of DCN, with most neurons displaying excitatory modulation with relatively short latency.

DIFFERENTIAL AND NON-LINEAR DEPENDENCE OF SINGLE-UNIT NAc RESPONSES ON DCN STIMULATION INTENSITY

To further probe the functional connectivity between DCN and NAc, we assessed the effectiveness of DCN microstimulation at two more intensities, 30 μA and 300 μA, in addition to 100 μA (Fig. 2.4B; *middle* and *right*). In $NAc_{Core,}$ the proportion of excitatory responses changed from 42% (with 30 μA stimulation) to 53% (with 100 μA), to 57% (with 300 μA); the proportion of inhibitory responses changed from 7% (30 μA) to 8% (100 μA) to 10% (300 μA); and finally, the proportion of mixed responses changed from 18% (30 μA) to 8% (100 μA) to 8% (300 μA). Contingency table analysis did not find a significant effect of stimulation intensity on the frequency distribution of response-types in NAc_{Core} ($\chi^2_{(6)} = 9.4$; $p = 0.15$). In NAc_{Med}, the proportion of excitatory responses changed from 38% (30 μA) to 44% (100 μA) to 45% (300 μA); the proportion of

inhibitory responses changed from 6% (30 μA) to 12% (100 μA) to 7% (300 μA); and the proportion of mixed responses changed from 13% to 8% to 14%. The effect of stimulation intensity on the frequency distribution of response-types in NAc_{Med} was statistically significant ($\chi^2_{(6)} = 13.6$; $p < 0.05$), suggesting that the NAc subregions displayed differential sensitivity to the intensity of DCN microstimulation. For both NAc subregions, the prevalence of the different response-types did not change proportionally to the ~3-fold change in stimulation intensity, which suggests non-linear dependence to stimulation intensity.

In addition to prevalence, we also calculated the maximum response amplitude across stimulation intensities. Changing stimulation intensity had no effect on response amplitude for excitatory (NAc_{Core}: 1109%, 1070%, 1378% change from baseline for 30, 100, and 300 μA respectively. NAc_{Med}: 1161%, 1064%, 1250% change from baseline for 30, 100, and 300 μA respectively) ($F_{2,1067} = 1.53$, $p = .21$) nor inhibitory (NAc_{Core}: 3.2%, 3.6%, 4.7% change from baseline for 30, 100, and 300 μA respectively. NAc_{Med}: 1.6%, 2.6%, 2.3% change from baseline for 30, 100, and 300 μA respectively) ($F_{2,312} = 0.28$, $p = .76$) responses in either subregion. This has implications for the circuitry involved in eliciting NAc responses, suggesting a potential all-or-nothing modulation for each NAc neuron.

THE BIDIRECTIONAL NAc MODULATION IS NOT A REFLECTION OF TOPOGRAPHICAL DCN ORGANIZATION

In our experiments we used bipolar stimulation electrodes to contain the spread of electrical current at DCN stimulation sites. To confirm that the stimulation was indeed localized, we examined the likelihood of NAc neurons that responded to stimulation of

individual DCN sites to also respond to adjacent stimulation sites in the same experiment. We found that the probability of a NAc_{Core} neuron that responded to stimulation of a DCN site to also respond to stimulation of a site ~100 μm away dropped by 66%. In NAc_{Med}, this probability dropped by 33%. The subregion-dependent difference in the likelihood of adjacent DCN sites to evoke a response in the same neuron most likely reflects differences in the architecture of the neural circuits. This loss of response is consistent with localized stimulation.

Given that DCN stimulation appeared spatially restricted, could the observed differences in NAc response-types arise from regional differences within DCN? To address this question, we examined whether there was topographical clustering of DCN sites with respect to their effectiveness to evoke significant excitatory or inhibitory responses in NAc_{Core} and/or NAc_{Med}.

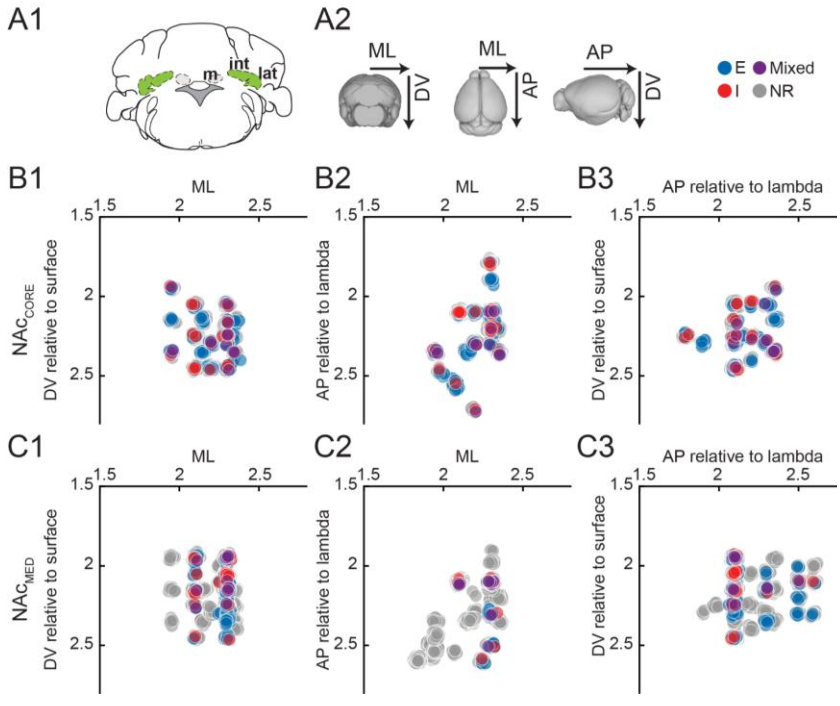

Figure 2.5. The distribution of response-types in nucleus accumbens subregions is not due to topographical specialization within deep cerebellar nuclei. A, The lateral (lat) or interposed (int) DCN (**A1**) was electrically stimulated. M: medial n. **A2,** Demarcation of anatomical planes: ML: medio-lateral; DV: dorsoventral; AP: antero-posterior. **B,C,** Stereotactic coordinates of DCN stimulation sites in ML-DV (B1,C1), ML-AP (B2,C2), and AP-DV (B3,C3) planes. Colored dots denote sites that evoked excitatory (E), inhibitory (I), both, or no response (NR) in NAc_{Core} (B1-3) and NAc_{Med} (C1-3).

We did not find any obvious indications of such clustering (Fig. 2.5B,C), which argues

against topographical organization of lateral/interposed DCN with respect to NAc response types. Using a similar approach, we examined whether there was topographical clustering of sites with excitatory and/or inhibitory responses within NAc subregions, but we did not find evidence for any such organization either.

Discussion

In this study we examined the previously uncharted functional connectivity between the cerebellum and nucleus accumbens using in vivo electrophysiology and neuroanatomy. Results from electrical microstimulation studies reveal that the cerebellum sends strong signals to the NAc that can significantly and bidirectionally modulate spiking activity. Excitatory and inhibitory responses were recorded in both NAc_{Core} and NAc_{Med}. Additionally, we observed single cells in both regions of NAc that responded in a mixed manner, with both excitatory and inhibitory modulation to a single stimulus paradigm. Neuroanatomical studies identified three disynaptic pathways through which cerebellar signals can reach the NAc. These pathways go through the VTA or the intralaminar thalamus (centromedial or parafascicular nucleus).

TECHNICAL CONSIDERATIONS

Our recordings were performed in ketamine-anesthetized mice. Although ketamine at anesthetic doses does not alter the number of spontaneously active striatal neurons (Kelland et al., 1991), it affects the pattern of spontaneous activity, promoting step-like membrane potential fluctuations between “up-” and “down-states” (Mahon et al., 2001). Such bursting behavior would contribute to “noisy” baseline activity; however, we would not expect it to distort our analyses because we have defined neural responses as changes in spiking rate from the preceding baseline. Moreover, by using

electrical, rather than sensory, stimuli to probe connectivity, we have overcome any concerns stemming from the known inhibitory effect of ketamine on sensory-evoked activity in the cerebellum.

In addition to anesthesia, the stimulation modality warrants consideration. Electrical stimulation causes an artifact that distorts the recording for tens of milliseconds. This was to some extent overcome by using spike sorting analyses to view individual waveforms and eliminate part of the artifact. Moreover, although electrical current propagates widely in the brain, the use of bipolar electrodes allowed us to restrict the spread of DCN stimulation to ~100 µm, as shown by the substantial drop in the probability to bilitte the same NAc neuron with DCN stimuli delivered 100 µm apart. Ultimately the next steps in characterizing this circuitry will require the use of a more specific, non-artifact-inducing method for stimulation.

INSIGHTS GAINED BY ANALYZING MULTI-UNIT AND SINGLE-UNIT RESPONSE PROFILES

Our ability to identify different response types in the NAc changed depending on whether we looked at multi-unit, or population, activity or single-unit activity. Our multi-unit analysis (MUA) identified a far fewer number of excitatory responses (35%) than the number identified with single-unit analysis (SUA) (47%), especially when including the excitatory component of mixed responses (55%). This difference is likely due to our ability to identify spikes occurring within a shorter latency of the stimulus artifact. This is supported by the fact that the change was specific to excitatory responses, whose temporal profile is much faster and more transient than inhibitory ones (discussed more below). It may appear at first glance that the prevalence of inhibition is decreased when

switching from MUA to SUA. This could be because inhibition is a feature limited to population coding, as the baseline firing rate of multiple neurons is required to see attenuation in spiking activity. This would be especially pertinent in regions, or conditions in which basal spike rate is low (e.g., under anesthesia). However, almost all the calculated attrition can be accounted for by bilityy to identify individual units in which a mixed response occurred (9%, combined with inhibitory prevalence: 20%; MUA prevalence: 23%). It is also possible that some differences between MUA and SUA are caused by the fact that MUA favors larger spikes, possibly skewing the data towards activity of larger neurons. By switching to SUA, we may be including more non-primary medium spiny neural data, such as inhibitory or cholinergic interneurons. Ultimately the two forms of analysis converge on similar conclusions: that CB stimulation is effective in eliciting significant changes in NAc activity, and that excitatory signals from CB are more predominant than inhibitory ones. It has been effectively shown that SUA often reaches similar conclusions as does MUA (ref); however, the results discussed above suggest that each is valuable in drawing conclusions from electrophysiological data.

SOURCES OF VARIABILITY IN SINGLE-UNIT RESPONSE FEATURES

The prevalence of each response type, excitatory, inhibitory, and mixed, does not show any NAc subregion-dependence. Nor does the strength, in terms of the amplitude of modulation, or the latency of responses. However, latencies between excitatory and inhibitory responses are significantly different. Consistently, excitatory responses have faster onsets than do inhibitory ones. This includes the excitatory component of mixed responses, which nearly always precedes the inhibitory component (Fig.2.4). This difference in latency could indicate that excitatory modulation serves the purpose of

rapidly communicating information critical to the control of motivated behavior. Because the CB is a known instructor for updating responses based on external stimuli, these excitatory responses could represent the neural underpinnings of reward prediction error. On the other hand, the slower, longer-lasting inhibitory responses could serve a regulatory function, such as gain control. Additionally, the difference in latency could be a result of differing circuitry. For example, inhibitory responses could be receiving cerebellar signal through a greater number of synapses than excitatory ones. Or rather than a longer route, the inhibitory circuitry could involve slower neurotransmission (e.g., dopaminergic neuromodulation).

One feature that does appear to be subregion-specific is how the response prevalence varies with changes in stimulation intensity. In neither NAc_{Core} nor NAc_{Med} did stimulation intensity alter the amplitude of responses relative to baseline firing rates. It is possible that this is a feature of the circuit, in which responses CB stimulation activates all-or-nothing changes in NAc neurons' firing rates, or it could be an artificially induced feature due to the anesthesia. Another possibility is that even at the lowest stimulation intensity, response amplitudes are already reaching their maximum potential. While this would be surprising given the large range of intensities used in our experiments, this in itself could be a feature of the synapses. Such "saturating" neuron types have been previously described (Davis et al., 2007; Barriga-Rivera et al., 2017; Komssi et al., 2004), and are characterized by their sharp response curve that quickly reaches and maintains maximum firing rate with increasing stimulation intensity. Both NAc_{Med} and NAc_{Core} increase response prevalence to increasing stimulation. However, only in the NAc_{Med} did the ratio of response types change significantly with increased

intensity. Despite this effect, the intensity of stimulation had little effect on the amplitude of modulation in either subregion. Thus, the degree to which NAc neurons increase or decrease their spiking activity is not dependent on the intensity of stimulation, but the number of neurons that alter their spiking activity could be. One potential explanation for this is that the downstream circuitry responsible for these responses has largely one-to-one connectivity with NAc neurons. If, for example, the circuit had converging connectivity onto individual NAc neurons, increased recruitment of nodal cells would likely lead to increased amplitude of response. One possible explanation for the change in distribution of response types in the NAc_{Med} is that increasing stimulation recruits a greater number of DCN neurons, which thereby activates different downstream circuitry responsible for each response type. Therefore, the next logical question is if the circuit is organized in the DCN by the type of response elicited in the NAc.

Ultimately, we found that the DCN is unlikely to give rise to these differences in response features. Mapping of the topographical organization of effective DCN stimulation sites indicate widespread and overlapping distributions of sites that evoke excitatory and inhibitory responses in both NAc_{Med} and/or NAc_{Core}. If these different response profiles in NAc arise from distinct sources within DCN, these sources are likely organized at a scale below the resolution of our study (e.g., at the cellular level). If distinct pools of DCN neurons transmit signals to the two NAc subregions, the onset-latency differential between response types suggests at least some divergence in the downstream routes that DCN signals take to arrive at their NAc destinations.

There is already an abundance of evidence to support differences in connectivity based on NAc subregion. The fact that there is divergence in response distributions

between NAc_{Med} and NAc_{Core} could suggest that the two subregions do not receive the same copy of the CB signal. Alternatively, the signal from the CB could vary based on the type of modulation rather than the subregion. Excitatory and inhibitory responses occurred at very different timescales, further suggesting unique underlying circuitry.

Further experiments are necessary to tap into the mechanisms of how CB signals influence NAc activity. Here, we have broken new ground by providing the first evidence of functional connectivity between CB and NAc, and offering an anatomical blueprint that could serve as its foundation.

References

Aquili, Luca, Andrew W. Liu, Mayumi Shindou, Tomomi Shindou, and Jeffery R. Wickens. “Behavioral Flexibility Is Increased by Optogenetic Inhibition of Neurons in the Nucleus Accumbens Shell during Specific Time Segments.” *Learning & Memory (Cold Spring Harbor, N.Y.)* 21, no. 4 (April 1, 2014): 223–31. https://doi.org/10.1101/lm.034199.113.

Badrinarayan, Aneesha, Seth A. Wescott, Caitlin M. Vander Weele, Benjamin T. Saunders, Brenann E. Couturier, Stephen Maren, and Brandon J. Aragona. “Aversive Stimuli Differentially Modulate Real-Time Dopamine Transmission Dynamics within the Nucleus Accumbens Core and Shell.” *The Journal of Neuroscience: The Official Journal of the Society for Neuroscience* 32, no. 45 (November 7, 2012): 15779–90. https://doi.org/10.1523/JNEUROSCI.3557-12.2012.

Benjamini, Yoav, and Yosef Hochberg. “Controlling the False Discovery Rate: A Practical and Powerful Approach to Multiple Testing.” *Journal of the Royal Statistical Society: Series B (Methodological)* 57, no. 1 (January 1995): 289–300. https://doi.org/10.1111/j.2517-6161.1995.tb02031.x.

Corbit, Laura H., and Bernard W. Balleine. “The General and Outcome-Specific Forms of Pavlovian-Instrumental Transfer Are Differentially Mediated by the Nucleus Accumbens Core and Shell.” *The Journal of Neuroscience: The Official Journal of the Society for Neuroscience* 31, no. 33 (August 17, 2011): 11786–94. https://doi.org/10.1523/JNEUROSCI.2711-11.2011.

Corbit, Laura H., Janice L. Muir, and Bernard W. Balleine. “The Role of the Nucleus Accumbens in Instrumental Conditioning: Evidence of a Functional Dissociation between Accumbens Core and Shell.” *The Journal of Neuroscience* 21, no. 9 (May 1, 2001): 3251–60. https://doi.org/10.1523/JNEUROSCI.21-09-03251.2001.

D’Ambra, Alexa F., Se Jung Jung, Swetha Ganesan, Evan G. Antzoulatos, and Diasynou Fioravante. “Cerebellar Activation Bidirectionally Regulates Nucleus Accumbens Medial Shell and Core.” *BioRxiv*, January 1, 2021, 2020.09.28.283952. https://doi.org/10.1101/2020.09.28.283952.

Floresco, Stan B. “The Nucleus Accumbens: An Interface Between Cognition, Emotion, and Action.” *Annual Review of Psychology* 66, no. 1 (2015): 25–52. https://doi.org/10.1146/annurev-psych-010213-115159.

Groenewegen, H. J., C. I. Wright, A. V. Beijer, and P. Voorn. “Convergence and Segregation of Ventral Striatal Inputs and Outputs.” *Annals of the New York Academy of Sciences* 877 (June 29, 1999): 49–63. https://doi.org/10.1111/j.1749-6632.1999.tb09260.x.

Ito, Rutsuko, and Anja Hayen. “Opposing Roles of Nucleus Accumbens Core and Shell Dopamine in the Modulation of Limbic Information Processing - PubMed.” Accessed May 5, 2023. https://pubmed.ncbi.nlm.nih.gov/21508225/.

Kelland, Mark D., Louis A. Chiodo, and Arthur S. Freeman. “Dissociative Anesthesia and Striatal Neuronal Electrophysiology.” *Synapse* 9, no. 1 (1991): 75–78. https://doi.org/10.1002/syn.890090111.

Klawonn, Anna M., and Robert C. Malenka. “Nucleus Accumbens Modulation in Reward and Aversion.” *Cold Spring Harbor Symposia on Quantitative Biology* 83 (January 1, 2018): 119–29. https://doi.org/10.1101/sqb.2018.83.037457.

Komssi, Soile, Seppo Kähkönen, and Risto J. Ilmoniemi. “The Effect of Stimulus Intensity on Brain Responses Evoked by Transcranial Magnetic Stimulation.” *Human Brain Mapping* 21, no. 3 (January 15, 2004): 154–64. https://doi.org/10.1002/hbm.10159.

Loriaux, Amy L., Jamie D. Roitman, and Mitchell F. Roitman. “Nucleus Accumbens Shell, but Not Core, Tracks Motivational Value of Salt.” *Journal of Neurophysiology* 106, no. 3 (September 2011): 1537–44. https://doi.org/10.1152/jn.00153.2011.

Shan, Qiang, You Hu, Shijie Chen, and Yao Tian. “Nucleus Accumbens Dichotomically Controls Social Dominance in Male Mice.” *Neuropsychopharmacology* 47, no. 3 (February 2022): 776–87. https://doi.org/10.1038/s41386-021-01220-1.

West, Elizabeth A., and Regina M. Carelli. “Nucleus Accumbens Core and Shell Differentially Encode Reward-Associated Cues after Reinforcer Devaluation.” *The Journal of Neuroscience: The Official Journal of the Society for Neuroscience* 36, no. 4 (January 27, 2016): 1128–39. https://doi.org/10.1523/JNEUROSCI.2976-15.2016.

Zahm, D. S. “Functional-Anatomical Implications of the Nucleus Accumbens Core and Shell Subterritories.” *Annals of the New York Academy of Sciences* 877 (June 29, 1999): 113–28. https://doi.org/10.1111/j.1749-6632.1999.tb09264.x.

Chapter 3: Disynaptic cerebellar pathways through ventral tegmental area and intralaminar thalamus modulate nucleus accumbens spiking activity

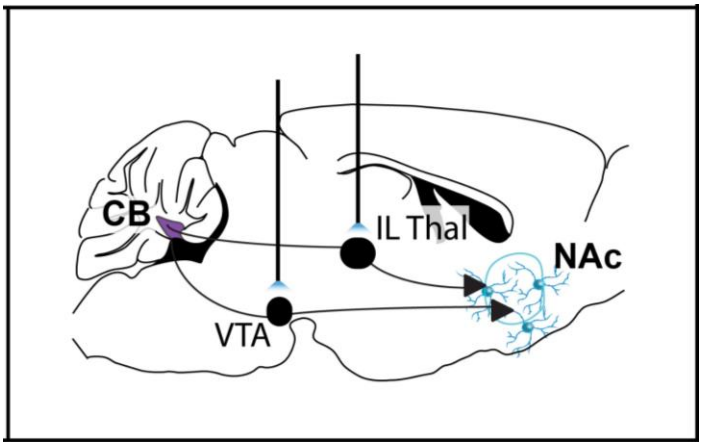

Figure 3.0 Graphical Abstract Depicting Findings Described in Chapter 3

Preface

The following chapter includes data and analyses reported in the following manuscript published in *eLife*: D'Ambra AF, Vlasov K, Jung SJ, Ganesan S, Anztoulatos EG, Fioravante D (2023). Cerebellar Activation Bidirectonally Regulates Nucleus Accumbens Core and Medial Shell.DOI: 10.7554/eLife.87252. Figure 3 presents data included in the following published manuscript: Jung SJ*, Vlasov K*, D'Ambra AF, Parigi A, Baya M, Frez EP, Villalobos J, Fernandez-Frentzel M, Anguiano M, Ideguchi Y, Antzoulatos EG and Fioravante D (2022) Novel Cerebello-Amygdala Connections Provide Missing Link Between Cerebellum and Limbic System. Front. Syst. Neurosci. 16:879634. doi: 10.3389/fnsys.2022.879634. Author contributions to the work presented in this chapter is as follows: **AFD**: conceptualization, methodology, animal care, investigation, data analysis and visualization, project administration, supervision; **KV**: methodology, investigation, data analysis and visualization; **SJJ**: methodology, investigation, data visualization; **AP**: investigation (Fig. 3); **SG**: histological analysis; **EGA**: conceptualization, methodology, data analysis and visualization, resources, project administration, supervision; **DF**: conceptualization, animal care, data analysis and visualization, project administration, supervision, project funding acquisition. Funding: **AFD** was supported by NIH T32 GM007377 and a UC Davis Dean's Distinguished Graduate Fellowship; **KV** was supported by NIMH T32 MH112507 and F31MH131405 by NIMH. **EA** was supported by a NARSAD 2018 Young Investigator Grant. This work was supported by a Whitehall fellowship, BRFSG-2017-02, R21MH114178, NSF1754831 and R01MH128744 to **DF**.

Introduction

In the previous chapter, I showed electrophysiological evidence that cerebellar (CB) activation, specifically in the deep cerebellar nucleus (DCN), drives changes in spiking activity in the nucleus accumbens (NAc). This modulation of NAc activity could be excitatory, inhibitory, or both, with response types differing in properties such as prevalence and latency, but not topographical origin within the CB. Despite extensive exploration of DCN output (Fujita et al., 2020; Lu et al., 2013; Sultan et al., 2012), no direct connection between the CB and NAc has been identified. Thus, the anatomical basis for this functional connection remains unknown. This suggests that CB signal is relayed to the NAc through at least one nodal region. As differences between response types do not emerge from DCN topography, this variability could be due to differences in downstream circuitry, indicating that multiple routes could be responsible for NAc responses to CB electrical stimulation. Lastly, gaining understanding of the circuit mediating CB-NAc connectivity can offer more insight on the role of CB modulation. Investigation of CB circuitry in a non-motor context is still limited but is crucial for understanding the CB's many non-motor roles. For example, whether this signal is passed through motor, or reward, or other similarly dedicated pathways can help interpret the behavioral implications for this connection. In this chapter, we seek to identify the multi-synaptic connectivity responsible for CB influence on NAc activity.

Materials and Methods

MICE

C57Bl/6J mice of both sexes were used in accordance with the National Institutes of Health guidelines and the policies of the University of California Davis Committee for Animal Care.

SURGERY FOR ANATOMICAL STUDIES

For anatomical tracing, juvenile mice of both sexes were injected with AAVs and tracers using the procedure described above for in vivo optophysiology. For co-localization experiments: AAV9-CAG-GFP (2 x 10^{12} viral particles/ml, UNC viral core) was injected in DCN (from bregma, in mm: medial n.: -2.55 AP, ± 0.75 ML, -2.1 DV, 50 nl; interposed n. : -2.5 AP, ± 1.55 ML, -2.1 DV, 50 nl; lateral n.: -2.2 AP, ± 2.3 ML, -2.12 DV, 50 nl; and -1.8, ± 2.35 ML, -2.12 DV, 50 nl). Cholera toxin subunit B (ctb)- 640 or -568 (5 mg/ml, Biotium) was injected in NAc medial shell and core (from bregma, in mm: 1.8 AP, ± 0.8 ML, -4.2 DV, 200 nl). For anterograde transsynaptic tracing: AAV1-hSyn-Cre-WPRE-hGH (10^{13} gc/ml, Addgene; 1:10 dilution) was injected in DCN (coordinates as above). AAV5-CAG-FLEX-tdTomato (7.8 x 10^{12} viral particles/ml, UNC viral core; 1:2 dilution) or AAV5-pCAG-FLEX-EGFP-WPRE (1.1 x 10^{13} gc/ml, Addgene; 1:2 dilution) was injected in VTA (from bregma, in mm: 2.8 AP, ± 0.35 ML, -4.2 DV, 100 nl; and -2.85 AP, ± 0.6 ML, -4.2 DV, 100 nl) or thalamus (from bregma, in mm: -0.85 AP, ± 0.3 ML, -3.3 DV, 300 nl; and -1.2 AP, ± 0.5 ML, -3.5 DV, 300 nl; 1:5 dilution). Following surgery, mice remained in the colony for 2-3 weeks to allow for recovery and retrograde labeling/virus expression prior to euthanasia and tissue collection/processing.

HISTOLOGY AND FLUORESCENCE MICROSCOPY FOR ANATOMICAL STUDIES

Two to three weeks following tracer/virus injections, mice were anesthetized with the anesthetic cocktail and perfused transcardially with 4% (w/v) PFA in PB. Brains were post-fixed in 4% PFA for 6 h and transferred to 30% sucrose in PBS for overnight incubation at 4°C. Brains were coronally sectioned (60 µm) on a sliding microtome, stained with DAPI, mounted to slides, coverslipped with Mowiol-based antifade solution and imaged. VTA sections were immunostained for tyrosine hydroxylase (TH) prior to mounting, as follows: slices were first incubated with blocking solution [10% normal goat serum (NGS) in PBS supplemented with 0.3% Triton-X100; PBST] for 1 h at room temperature, then with mouse anti-TH (clone LNC11, Millipore Sigma, Burlington, MA; 1:1000) in blocking solution with 2% NGS overnight at 4^{o}C. Sections were washed with PBST (3 x 20 min) and incubated for 1 h at room temperature with goat anti-mouse Alexa fluor 488 secondary antibody (1:1000), washed with PBS (3 x 20 min), mounted, coverslipped and imaged. Epifluorescence image mosaics were acquired on an Olympus VS120 slide scanner with a 10x air objective. High magnification confocal images were taken sequentially with different laser lines and a 63x oil-immersion objective on a Zeiss LSM800 microscope with Airyscan. Image brightness/contrast was adjusted using ImageJ (NIH) for display purposes. Data from a total of N = 13 mice with successful injections, without spill to neighboring regions, are presented.

SURGERY FOR SLICE ELECTROPHYSIOLOGY

Mice were induced to a surgical plane of anesthesia with 5% isoflurane and maintained at 1-2% isoflurane. Mice were placed in a stereotaxic frame (David Kopf Instruments, Tujunga, California) on a feedback-controlled heating pad. Following skin incision, small

craniotomies were made above the target regions with a dental drill. The following coordinates (in mm) were used (from bregma): for medial DCN -6.4 AP, ± 0.75 ML, -2.2 DV; for interposed DCN: -6.3 AP, ± 1.6 ML, -2.2 DV; for lateral DCN: -5.7 AP, ± 2.35 ML, -2.18 DV. For limbic thalamus: -0.85 AP, ± 0.3 ML, -3.3 DV, and -1.2 AP, ± 0.5 ML, -3.5 DV. A small amount of tracer (50 - 100 nl for DCN, 300 - 500 nl for thalamus) was pressure-injected in the targeted site with a UMP3-1 ultramicropump (WPI, Sarasota, FL) and glass pipettes (Wiretrol II, Drummond) (tip diameter: 25-50 µm) at a rate of 30 nl/min. The pipette was retracted 10 min after injection, the skin was sutured (Ethilon P-6 sutures, Ethicon, Raritan, NJ) and/or glued (Gluture, Abbott labs, Abbott Park, IL) and animal was allowed to recover completely prior to returning to the home cage. Preoperative analgesia consisted of a single administration of local lidocaine (VetOne, MWI, Boise, ID; 1 mg/kg) and Meloxicam (Covetrus, Portland, ME; 5 mg/kg), both SC. Postoperative analgesia consisted of a single administration of Buprenex (AmerisourceBergen Drug Corp, Sacramento, CA; 0.1 mg/kg) and Meloxicam 5 mg/kg, both SC, followed by Meloxicam at 24 and 48 hr. The following adeno-associated viruses (AAV) and tracers were used: AAV1-hSyn-Cre-WPRE-hGH (Addgene, 10^13 gc/ml, diluted 1:5) AAV5-CAG-FLEX-tdtomato (UNC Viral Core, 7.8*10^12 gc/ml, diluted 1:5), AAV9-EF1a-DIO-hChR2(H134R)-EYFP (Addgene, 1.8*10^13 gc/ml, diluted 1:10). Three to five weeks were allowed for viral expression/labelling.

PREPARATION OF BRAIN SLICES FOR ELECTROPHYSIOLOGY

Mice of either sex (P39-60) (Fig. 3, N=9; Fig. 5, N=5) were anesthetized through intraperitoneal injection of ketamine/xylazine/acepromazine anesthetic cocktail and transcardially perfused with ice-cold artificial cerebrospinal fluid (aCSF; in mM: 127

NaCl, 2.5 KCl, 1.25 NaH_2PO_4, 25 $NaHCO_3$, 1 $MgCl_2$, 2 $CaCl_2$, 25 glucose; supplemented with 0.4 sodium ascorbate and 2 sodium pyruvate; ~310 mOsm). Brains were rapidly removed, blocked, and placed in choline slurry (110 choline chloride, 25 $NaHCO_3$, 25 glucose, 2.5 KCl, 1.25 NaH_2PO_4, 7 $MgCl_2$, 0.5 $CaCl_2$, 11.6 sodium ascorbate, 3.1 sodium pyruvate; ~310 mOsm). Coronal sections (250 μm) containing the thalamus were cut on a vibratome (Leica VT1200S) and allowed to recover in aCSF at 32°C for 25 min before moving to room temperature until further use. All solutions were bubbled with 95% O_2-5% CO_2 continuously. Chemicals were from Sigma.

SLICE ELECTROPHYSIOLOGY

Slices were mounted onto poly-l-lysine-coated glass coverslips and placed in a submersion recording chamber perfused with aCSF (2-3 ml/min) at near physiological temperature (30-32ºC). Whole-cell voltage-clamp recordings were made from tdTomato+ (Figs. 3,5) cells in the thalamus using borosilicate glass pipettes (3-5 MΩ) filled with internal solution containing (in mM): $CsMSO_3$ 120, CsCl 15, NaCl 8, TEA-Cl 10, HEPES 10, EGTA 0.5, QX314 2, MgATP 4 and NaGTP 0.3, biocytin 0.3. Recordings were acquired in pClamp11 using a Multiclamp 700B amplifier (Molecular Devices, San Jose, CA), digitized at 20 kHz and low-pass filtered at 8 kHz. Membrane potential was maintained at -70 mV. Series resistance and leak current were monitored, and recordings were terminated if either of these parameters changed by more than 50%. Optical stimulation of ChR2+ fibers surrounding tdTomato+ thalamic neurons was performed under a 60x water immersion lens (1.0 N.A.) of an Olympus BX51W microscope, using an LED system (Excelitas X-cite; or Prizmatix UHP-T) mounted on the microscope and driven by a Master9 stimulator (AMPI). Optical stimulation

consisted of 488 nm light pulses (1-5 ms duration). Power density was set to 1.5-2x threshold (max: 0.25 mW/mm^2). A minimum of 5 response-evoking trials (inter-trial interval: 60 s) were delivered and traces were averaged. Postsynaptic current (PSC) amplitude was computed from the maximum negative deflection from baseline within a time window (2.5 - 40 ms) from stimulus onset. Onset latency was measured at 10% of peak amplitude. To confirm monosynaptic inputs, action potentials were blocked with TTX (1 µM), followed by TTX+ 4AP (100 µM) to prolong ChR2-evoked depolarization. A connection is monosynaptic if prolonged ChR2-induced presynaptic depolarization in TTX+4AP is sufficient to evoke release (Petreanu et al., 2009).

SURGERY FOR IN VIVO OPTOPHYSIOLOGY

Mice of both sexes (P35 - P49; N = 11) were used for optogenetic experiments. Animals were anesthetized with isoflurane (4% - 5% induction; 1.5% maintenance) and secured to a stereotactic frame (Kopf). After exposing the top of the skull, the head was leveled and small craniotomies were drilled over the DCN. Channelrhodopsin-expressing adeno-associated virus (AAV2-hSyn-hChR2(H134R)-EYFP, UNC Vector Core; 100 nl, 5.6x10^{12} gc/ml, 1:2 dilution) was injected into the three DCN using a Micro4 controller and UltraMicroPump 3 (VWR). Glass needles were made from 1-mm outer diameter glass pipettes (Wiretrol II, Drummond) pulled to a fine tip (20 - 50 µm tip diameter, 3 - 4 mm tip length) using a pipette puller (P-97, Sutter). Injection needles were left in place for 5-10 min following injections to minimize diffusion. The following coordinates were used for targeting pipettes to each nucleus (relative to lambda): medial n.: -2.55 AP, +/-0.8 ML, -2.15 DV; interposed n.: -2.45 AP, +/-1.7 ML, -2.15 DV; lateral n.: -1.82 AP, +/- 2.37 ML, -2.17 DV. Following surgery and analgesia

administration (0.1 mg/kg buprenorphine, 5 mg/kg meloxicam), mice were allowed to recover on a warm heating pad before being transferred back to the vivarium. Animals were given 4-5 weeks expression time before being used in in vivo recording experiments.

Optic fibers were implanted over the CM (relative to bregma: -1.3 AP; -.85 ML; -3.55 DV, 10^{o} angle), PF (relative to bregma: -1.87 AP; -.95 ML; -2.95 DV, 12^{o} angle), or VTA (relative to bregma: -3.1 AP; -0.5 ML; -4.05 DV) ipsilaterally to recording site and secured with temporary resin acrylic (Keystone Industries).

OPTICAL STIMULATION FOR IN VIVO OPTOPHYSIOLOGY

20-50 trials of ten 5-ms light pulses (473-nm DPSS laser, Opto Engine) were delivered at 20 Hz (inter-trial interval: 30 s or 1 min). Optical stimulation was primarily delivered at 10 mW intensity at fiber tip, but lower intensities were also tested (1 and 5 mW).

ACQUISITION OF IN VIVO ELECTROPHYSIOLOGICAL DATA

Recordings were performed with a 12-channel (platinum; 0.2 - 2 MΩ impedance) axial multi-electrode array (FHC Inc., Bowdoin, ME; 150 μm distance between channels), dipped in fluorescein or Texas red dextran (3000 MW) and lowered into the NAc at a depth of 3.75 - 5.25 mm below the brain surface (DV axis). Electrode signals were fed to a digital headstage (RHD 2132, Intan Technologies, Los Angeles, CA) for amplification (x20), filtering (0.7 - 7500 Hz) and digitization (30 kS/s with 16-bit resolution), before transfer to an open-source acquisition system (OpenEphys) for display and storage.

HISTOLOGY FOR VERIFICATION OF ELECTRODE/OPTIC FIBER PLACEMENT

Verification was performed the same way as in Chapter 2. Positioning of electrodes was initially guided by atlas-based stereotactic coordinates (Paxinos & Franklin) and, upon completion of experiments, histologically verified through electrolytic lesions (single 10-s cathodal pulse of 300 μA) and fluorescence imaging (fluorescein dye track). Coordinates for subsequent animals of the same litter were further adjusted accordingly. At the end of experiments, electrodes were retracted, and animals were perfused with 4% (w/v) paraformaldehyde (PFA) in 0.1 M phosphate buffer (PB). Brains were dissected and post-fixed in 4% PFA, sliced in phosphate buffered saline (PBS) and inspected under a fluorescence stereoscope (Olympus SZX2). Slices containing the dye track from the recording array were identified under 488 nm light; CB slices with electrolytically lesioned tissue were identified under brightfield illumination. Slices of interest were subsequently stained with DAPI (1:20,000, Thermo Fisher Scientific), mounted on slides, and imaged using a VS120 Olympus slide scanner. Images were manually registered to the Paxinos and Franklin Mouse Brain Atlas and the location of the recording electrode tip and optic fiber were mapped. Only channels along the recording array that were determined to be within NAc_{Core} and/or NAc_{Med} were included in analysis. Experiments with misplaced optic fibers, viral expression outside the DCN region, or cerebellar electrolytic lesions localized outside the lateral and/or interposed DCN, were excluded from analysis.

STATISTICS

Statistical analyses were performed in Graphpad Prism 9.3.0 and Matlab. Comparisons of the relative frequency distribution of response types were performed

with Contingency Table analyses (Chi-square tests). Comparisons of response latencies and firing rates were performed with t-tests and ANOVA. To correct for multiple comparisons, we followed the Benjamini-Hochberg method (Benjamini and Hochberg, 1995) with False Discovery Rate (FDR) set at 10%.

RESULTS

ANATOMICAL BLUEPRINT OF DCN-NAc CONNECTIVITY

There is no evidence for direct, monosynaptic connections between DCN and NAc (Allen Brain Atlas, and our own observations); we therefore hypothesized the existence of at least disynaptic anatomical pathways between the two areas. To test this hypothesis, we adopted a 2-pronged approach. First, we combined injection of a retrograde tracer (cholera toxin subunit B (ctb) -640 or -568) in NAc with injection of an anterograde viral tracer (AAV9-CAG-GFP) in DCN to identify areas of overlap (nodes) in a putative disynaptic CB-NAc circuit (Fig. 3.1A,B). Histological processing and high-resolution confocal imaging of brain sections revealed two regions of overlap between ctb-filled neurons that project to NAc and GFP-labelled DCN axonal projections: the VTA and limbic thalamus (Fig. 3.1C,D). In VTA, most areas of overlap localized medially and caudally and involved both TH+ (dopaminergic) neurons (Fig. 3.1C) and TH- neurons. In the thalamus, we found areas of overlap in centromedial (CM) and parafascicular (PF) intralaminar nuclei (Fig. 3.1D). We found overlap in these same regions also when DCN injections were restricted to the lateral cerebellar nucleus only (Fig. 3.1E,F). These results are consistent with the existence of a disynaptic DCN-NAc anatomical circuit and point to VTA, and CM and PF thalamic nuclei, as putative circuit nodes.

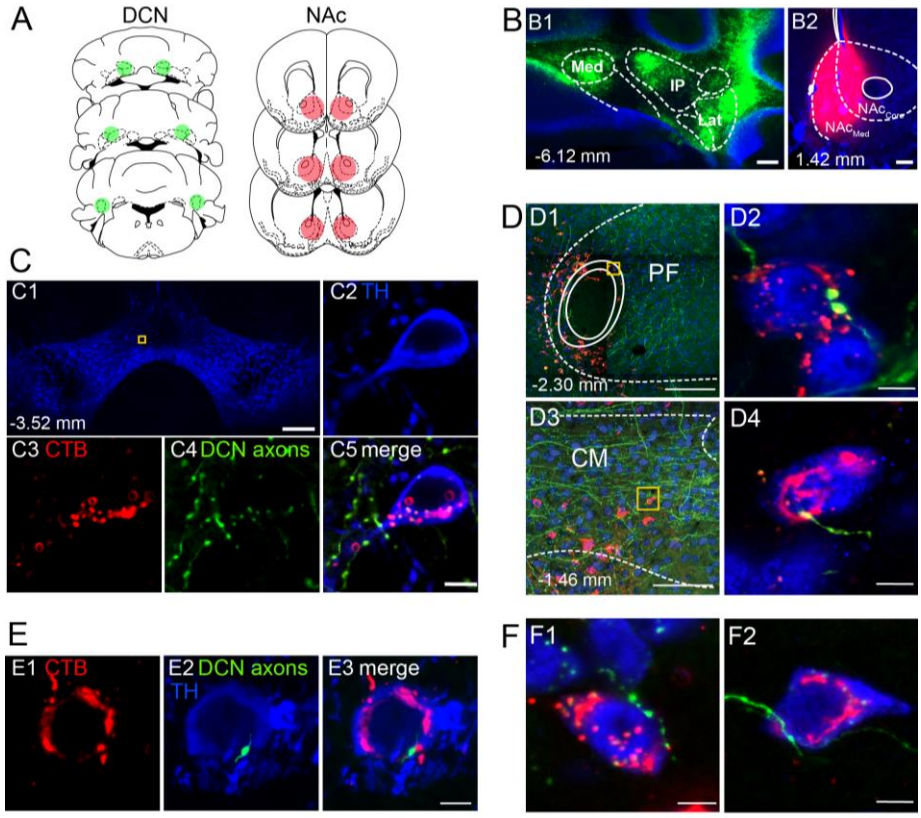

Figure 3.1. **Co-localization of nucleus accumbens-projecting neurons with cerebellar projections in VTA and intralaminar thalamus**. **A**, Schematic diagrams of stereotactic injections in DCN and NAc. **B1**, Expression of GFP at DCN injection sites. **B2**, Ctb-Alexa 568 injection site in NAc. **C**, Overlap of ctb-labeled NAc projectors and DCN axons in VTA. **C1**, VTA identification through TH immunostaining. **C2**, TH+ neuron. **C3**, Retrograde ctb-Alexa 568 labelling in NAc-projecting cell. **C4**, GFP-expressing DCN axons. **C5**, C2-C4 merged. **D**, Overlap of ctb retrograde label (red) in NAc projectors (blue; NeuN) and GFP-expressing DCN axons (green) in intralaminar thalamic nuclei. **D1**-**D2**, Overlap in parafascicular (PF) n. **D3**-**D4**, Overlap in centromedial (CM) n. Yellow boxes in C1,D1,D3 denote zoom-in areas depicted in C2-C5, D2 and D4, respectively. **E**-**F**, Airyscan confocal images from experiments similar to **A** but with only lateral DCN injected with AAV-GFP. **E1**, Ctb-labeled (red) NAc-projecting cell in the VTA. **E2,** TH+ cell (blue) with overlapping GFP-labeled axonal projection (green) from lateral DCN. **E3,** E1-2 merged. **F1**, GFP-labeled axon from lateral DCN (green) overlaps with ctb-labeled (red) NAc-projecting cell (blue: NeuN) in the PF n. **F2,** Same as in F1 but for neuron in the CM n. Scale bars: B1-2,C1,D1: 200 µm; C2-C5,D2,D4,E1-3,F1,F2: 5 µm; D3: 100 µm. N = 6 mice. Numbers denote distance from bregma.

To confirm these observations through an independent approach, we performed AAV1-mediated anterograde transsynaptic tracing experiments [18] via stereotactic injections of AAV1-Cre in DCN and AAV-FLEX-tdTomato in VTA or limbic thalamus

(Fig. 3.2A,B). This approach relies on the transsynaptic transfer of Cre to postsynaptic neurons, which, once infected with a floxed fluorophore, become fluorescently labeled.

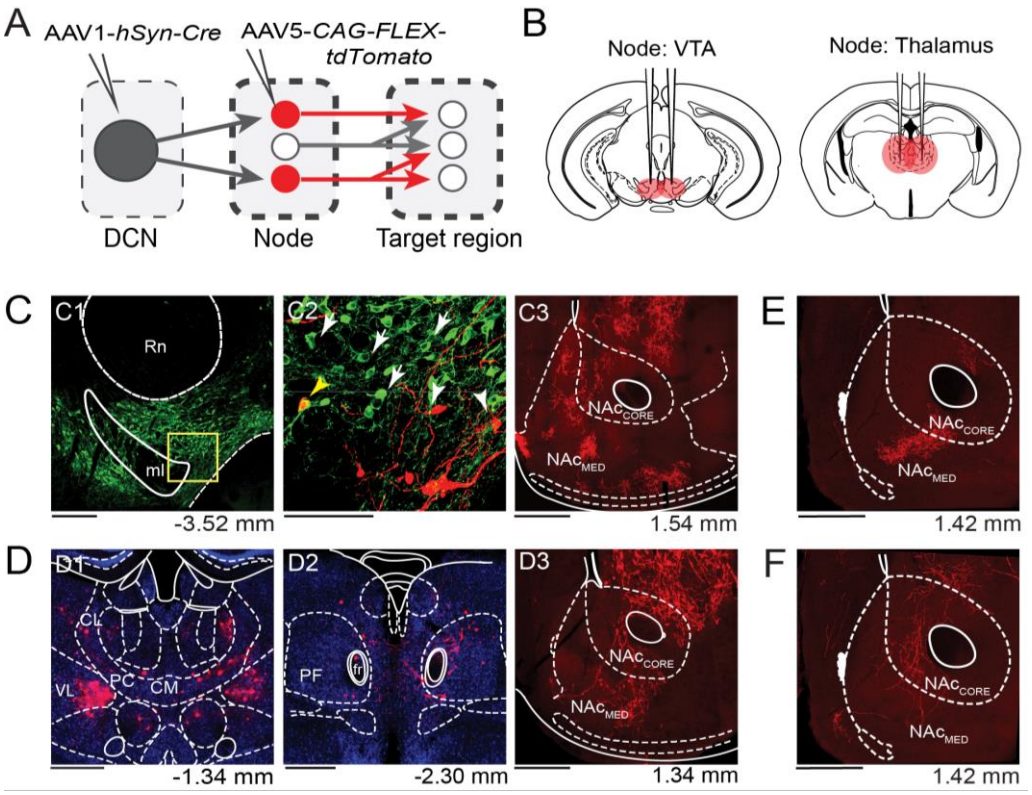

Figure 3.2. **Disynaptic cerebellum - nucleus accumbens connectivity is confirmed via anterograde transsynaptic viral tracing**. **A**, Schematic diagram of AAV1-mediated transsynaptic labeling approach. **B**, Schematic diagrams of stereotactic injections of floxed fluorophore in VTA and thalamic nodes. **C1**, The VTA is visualized via TH immunostaining (green). Yellow box denotes zoom-in area depicted in C2. Rn: red nucleus; ml: medial lemniscus. **C2**, Neurons that receive DCN input are labeled with tdTomato (red; white arrowheads). Green: TH+ neurons (white arrows). Yellow arrowhead: TH+, tdTomato+ neuron. **C3**, Projections of CB-VTA neurons in NAc_{Core} and NAc_{Med}. **D1**, Neurons that receive DCN input in thalamus are labeled with tdTomato (red). Blue: NeuN. CM: centromedial n.; PC: paracentral n.; CL: centrolateral n.; VL: ventrolateral n. **D2**, Same as D1, but for parafascicular n. (PF). fr: fasciculus retroflexus. **D3**, Projections of CB-thalamic neurons in NAc_{Core} and NAc_{Med}. **E**-**F**, Fluorescence images from experiments similar to A-B but with only lateral DCN injected with AAV1-Cre. **E**, NAc projections of VTA neurons receiving input from lateral DCN. **F**, Same as in E but for thalamic neurons. Scale bars below images: C1: 200 µm; C2: 100 µm; C3,D1-3,E,F: 500 µm. N = 7 mice. Numbers denote distance from bregma.

With this method, we confirmed the existence of neurons receiving CB input in VTA (Fig. 3.2C1,C2) and CM, PF intralaminar thalamus (Fig. 3.2D1,D2). Importantly, we were able to localize their labeled axonal projections in NAc, in both NAc_{Core} and NAc_{Med}

(Fig. 3.2C3,D3). We observed similar patterns of cell labeling and projections to the NAc_{Core} and NAc_{Med} when AAV1-Cre was injected in lateral DCN only (Fig. 3.2E,F). These findings chart the blueprint of disynaptic DCN-NAc connectivity and could provide an anatomical foundation for our newly discovered DCN-NAc functional connection.

ELECTROPHYSIOLOGICAL CONFIRMATION OF TRANS-NEURONAL TRACING

To confirm that targets identified with the transneuronal Cre method receive cerebellar synaptic input, we performed optophysiological experiments in acute thalamic slices from mice injected with AAV1-Cre in the DCN and AAV-FLEX-tdTomato in the thalamus (Fig. 3.3A). To activate cerebellar inputs, channelrhodopsin (ChR2-H134R) was conditionally expressed in DCN through AAV-DIO-ChR2-EYFP injection. DCN axonal projections were stimulated in the thalamus with 488-nm light pulses applied through the objective. Light-evoked synaptic responses were monitored in whole-cell voltage-clamp recordings (V_m = -70 mV) from thalamic neurons, which were selected based on tdTomato expression, their anatomical location and position in the slice, i.e., surrounded by ChR2-EYFP-expressing axons. In the intralaminar nuclei of the thalamus, light stimulation elicited synaptic responses (mean response in pA: 311.7 ± 100) (Fig. 3.3B1) with short latencies (mean latency in ms: 2.5 ± 0.28) (Fig. 3.3B2). These data support the specificity of the anatomical connectivity and establish the existence of active DCN terminals (as opposed to just passing axons) in the intralaminar nuclei of the thalamus.

Next, we tested whether these connections, specifically in the CM and PF, were monosynaptic. Under basal conditions, CM/PF neurons received synaptic inputs from the DCN (at Vm = -70 mV; average amplitude ± SEM: -197.5 pA ± - 80.14, n = 6) (Fig.

3.3C1,D1) with short onset latency (average latency ± SEM: 2.4 ms ± 0.18) (Fig. 3.3E), which is consistent with direct monosynaptic connections. Application of the sodium channel blocker tetrodotoxin (TTX) abolished the inputs (average amplitude ± SEM: -5.1 pA ± -2.03) (Fig. 3C2, C4 D1), which recovered upon addition of the potassium channel blocker 4-AP (average amplitude ± SEM: -151.8 pA ± -39.52) (Fig., 3.3C3,4,D1) (Friedman's non-parametric repeated measures ANOVA: $x^2_r = 9$, n = 6, p = 0.008; Dunn's multiple comparison test: Baseline vs TTX: p = 0.02, Baseline vs TTX+4AP: p = 0.99, TTX vs TTX+4AP: p = 0.01), confirming that these connections identified by transsynaptic neuronal tracing are in fact monosynaptic.

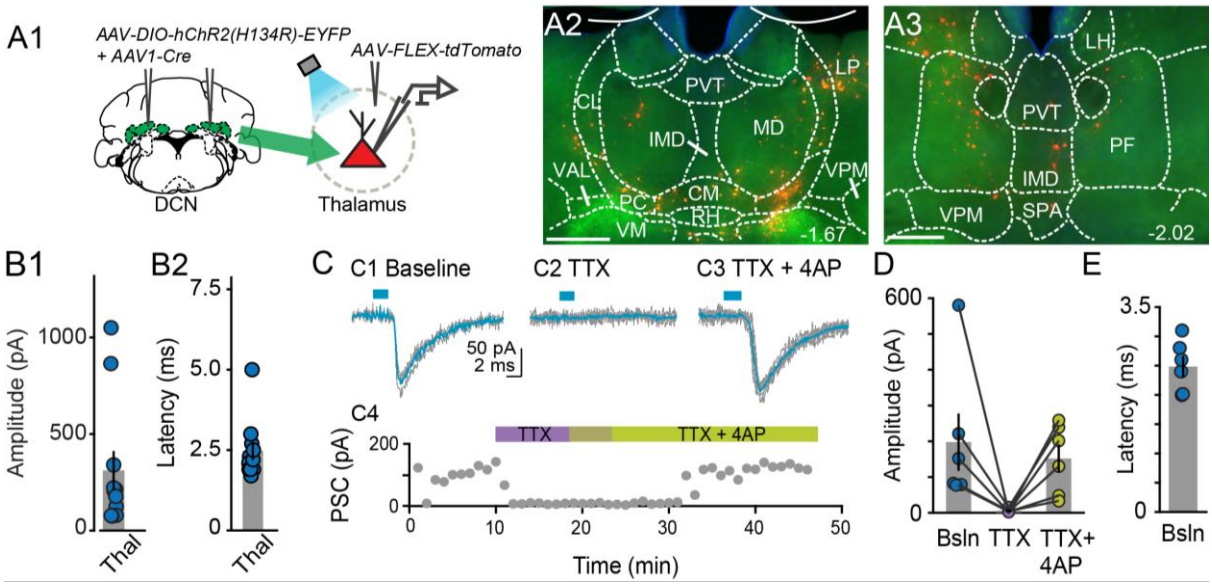

Figure 3.3. Electrophysiological validation of virally-identified cerebello-thalamic connectivity. **A1,** Schematic of experimental approach. **A2,A3,** Epifluorescence images of anterior (A2) and posterior (A3) thalamic slices acutely prepared for recordings. DCN input-receiving neurons are tdTomato+. ChR expressing (green) fibers are from the DCN Scale bars: 500 µm. **B,** Average (± SEM) amplitude (**B1**) and onset latency (**B2**) of ChR2-evoked synaptic currents in the intralaminar thalamus (Thal). **C** Example ChR2-evoked synaptic response in neuron in centromedial (CM) thalamus. Average trace (teal) overlaid onto single trials (gray). **D,** Average (± SEM) amplitude **E,** onset latency of ChR2-evoked synaptic currents at DCN-CM/PF synapses.

PHOTOSTIMULATION OF DCN AXONAL PROJECTIONS IN NODES SUPPORTS THE EXISTENCE OF DISYNAPTIC CIRCUITS BETWEEN CEREBELLUM AND NAc

The novel neuroanatomical data point to the existence of neural circuits connecting the CB to the NAc_{Core} and NAc_{Med}, with putative nodal regions in VTA and/or intralaminar thalamus. We sought to determine whether these anatomically defined nodes are also functional nodes serving CB-NAc connectivity. To this end, we performed additional electrophysiological experiments combined with optogenetic stimulation of DCN projections in the putative nodes (Figs. 3.4,5). We expressed channelrhodopsin (ChR2) in DCN projection neurons through viral injection (Figs. 3.4A,3.5B) and recorded responses in NAc_{Core} and NAc_{Med} following photostimulation of DCN axons (10 pulses at 20 Hz, 10 mW at fiber tip) in VTA (Fig. 3.4C1,C2), CM (Fig. 3.4D1,D2), or PF (Fig. 3.4E1,E2). All DCN nuclei were injected in order to maximize ChR2 expression and the chances of successful stimulation of projections.

Targeted photostimulation of ChR2-expressing DCN axons in each of the three putative nodes modulated spiking activity in both NAc_{Core} and NAc_{Med} (example units in Fig. 3.4C2,D2,E2; group averages in Fig. 3.5A1,B1,C1), establishing the VTA, CM and PF as functional nodes of the CB-NAc circuitry. Figure 3.5 shows the normalized group average excitatory responses of NAc_{Core} and NAc_{Med} neurons elicited by photostimulation in VTA (Fig. 3.5A1), CM (Fig. 3.5B1), and PF (Fig. 3.5C1). Because of jitter, the group average response underestimates the true magnitude of modulation, as discussed previously for electrical responses. Therefore, to further evaluate the connectivity strength in the three CB-NAc circuits, we computed the average peak amplitude of light-evoked excitatory responses in NAc subregions and asked whether it

varied across nodes or between NAc subregions. In NAc_{Core}, neurons displayed an average peak excitatory response to photostimulation in VTA of 43 ± 8 spikes/s; in CM: 44 ± 5 spikes/s; in PF: 36 ± 4 spikes/s. In NAc_{Med}, the average peak excitatory response to photostimulation in VTA was 39 ± 6 spikes/s; in CM: 34 ± 3 spikes/s; and in PF: 41 ± 6 spikes/s. There was no statistically significant effect of NAc subregion, or of node, on peak responses (NAc subregion: $F(1,120) = 0.4$; $p = 0.5$; node: $F(2,120) = 0.1$; $p = 0.9$), and no significant interaction ($F(2,120) = 0.9$; $p = 0.4$). These NAc responses were specific to ChR2 expression, as no-opsin (EGFP-alone) controls did not show an effect of photostimulation on peak firing rate, even at 15 mW (response window vs. baseline: NAc_{Core}: $t_4 = 0.53$, $p = 0.62$; NAc_{Med}: $t_{35} = -1.41$, $p = 0.17$) (Fig. 3.5D).

Light-evoked responses were excitatory in their majority, with frequency distribution that varied between NAc_{Core} and NAc_{Med} in a node-dependent manner: photostimulation of DCN projections in VTA evoked more excitatory responses in NAc_{Core} than in (excitatory responses in NAc_{Core}: 86%, in NAc_{Med}: 38%; $\chi^2_{(1)} = 13.6$; $p < 0.001$) (Fig. 5A2), whereas no such differences were observed upon photostimulation in CM (NAc_{Core}: 77%, NAc_{Med}, 72%; $\chi^2_{(1)} = 0.20$; $p = 0.44$) (Fig. 3.5B2) or PF (excitatory responses in NAc_{Core}: 65%, in NAc_{Med} : 85%; $\chi^2_{(1)} = 2.63$; $p = 0.11$) (Fig. 3.5C2) (p-values corrected for multiple comparisons). Excitatory responses were also readily elicited in NAc_{Core} and NAc_{Med} with as little as 1 or 5 mW photostimulation (Table 3.1). Even at the lowest intensity (1 mW), a single pulse was sufficient to elicit a response (percent responses elicited by first pulse in VTA: NAc_{Core}: 54%, NAc_{Med}, 58%; in CM: NAc_{Core}: 72%, NAc_{Med}, 57%; in PF: NAc_{Core}: 67%, NAc_{Med}: 58%) (Table 2), pointing to high-fidelity connectivity that does not strictly require activity-dependent synaptic

enhancement to propagate information to NAc. The proportion of responses elicited by the first light pulse increased with photostimulation intensity in (permutation test: $p < 0.001$, $n = 41$, $N = 4$) and CM ($p < 0.01$, $n = 52$, $N = 4$), but not in PF ($p = 0.08$, $n = 45$, $N = 3$) (p-values corrected for multiple comparisons). This finding could potentially suggest convergent connectivity within the CB-VTA-NAc and CB-CM-NAc circuits.

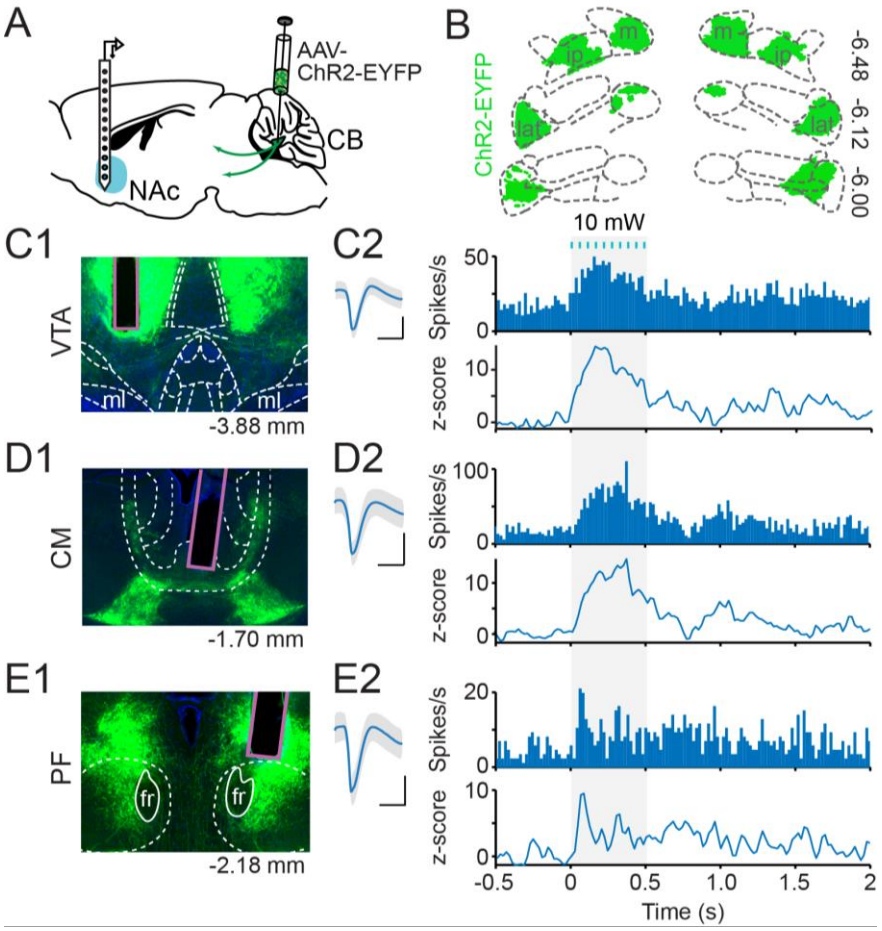

Figure 3.4. Photostimulation of cerebellar projections in VTA and thalamus elicits responses in nucleus accumbens. A, Schematic diagram of optophysiological approach. *NAc:* nucleus accumbens, *CB:* cerebellum. **B,** Example ChR2-EYFP expression in DCN. lat: lateral n.; ip: interposed n; m: medial n. **C**,**D**,**E**, Histology and NAc responses to optogenetic stimulation of VTA (**C1,2**), CM (**D1**,**2**), and PF (**E1**,**2**). **C1**,**D1**,**E1**: Representative images of optic fiber placement. ml: medial lemniscus; fr: fasciculus retroflexus. **C2**,**D2**,**E2**: Example single units. *Left*: Average spike waveform. Scale bars: 1 ms, 10 µV. *Top*: PSTH (10-ms bins) of firing rate (spikes/s). B*ottom*: Baseline-normalized firing rate (z-score) across time. Blue lines denote photostimulation; Shaded area marks response window. Numbers below or next to images indicate distance from bregma (in mm).

In contrast to excitatory responses, inhibitory responses were scarce in photostimulation experiments (Fig. 3.5A2, B2, C2). This finding appeared to be stimulation regime-dependent, because lowering the photostimulation intensity increased the prevalence of inhibitory responses in NAc more than expected by chance alone (permutation test, 1 vs. 5 vs. 10 mW: VTA: $p < 0.01$, $n = 64$, $N = 4$; CM: $p < 0.05$, $n = 82$, $N = 4$; PF: $p < 0.05$, $n = 60$, $N = 3$; p-values corrected for multiple comparisons) (Table 3.1). Finally, we asked whether each NAc subregion was differentially responsive to photostimulation in each of the nodes. We found no differential effect of 10 mW-photostimulation among the three nodes on the distribution of response-types in either NAc_{Core} ($\chi^2_{(2)} = 5.4$; $p = 0.07$) or NAc_{Med} ($\chi^2_{(2)} = 4.9$; $p = 0.09$).

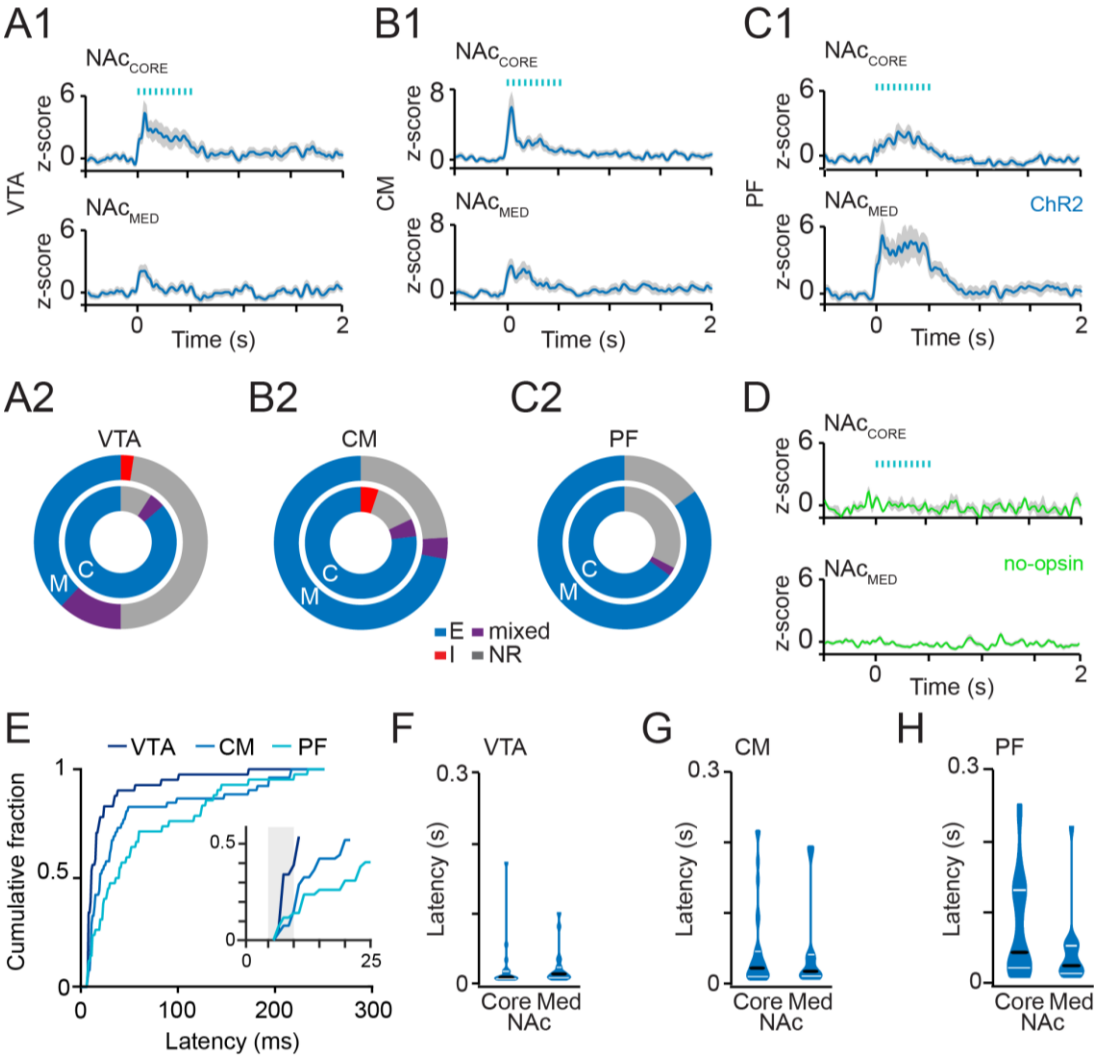

Figure 3.5. Node-dependent differences in nucleus accumbens responses to photostimulation of cerebellar projections. A1,**B1**,**C1**, Average normalized activity (z-score) in NAc_{Core} (*top*) and NAc_{Med} (*bottom*) as a function of time, for cerebellar fiber photostimulation (blue lines) in VTA (**A1**), CM (**B1**) and PF (**C1**). **A2**,**B2**,**C2**, Distribution of response-types in NAc_{Core} (C: inner ring) and NAc_{Med} (M: outer ring) upon photostimulation of cerebellar projections in VTA (**A2**), CM (**B2**), and PF (**C2**). *Blue:* excitatory (E), *Red*: inhibitory (I), *Purple:* mixed, *Gray:* non-responders (NR). **D**, Average normalized activity (z-score) in NAc_{Core} (*top*) and NAc_{Med} (*bottom*) as a function of time, for no-opsin controls. **E**, Cumulative histogram of NAc response onset latencies upon cerebellar fiber photostimulation in VTA, CM and PF. Inset: 0-25 ms zoom-in. **F**,**G**,**H**, Violin plots of onset latencies of excitatory responses in NAc_{Core} (Core) and NAc_{Med} (Med), upon cerebellar fiber photostimulation in VTA (**F**), CM (**G**) and PF (**H**). Black lines: Median; White lines: interquartile range (Q1-Q3). VTA: N = 4 mice, $n_{NAcCORE}$ = 22 units, n_{NAcMED} = 42 units; CM: N = 4 mice, $n_{NAcCORE}$ = 39 units, n_{NAcMED} = 25 units; PF: N = 3 mice, $n_{NAcCORE}$ = 40 units, n_{NAcMED} = 20 units. D, no-opsin controls: N = 4 mice, $n_{NAcCORE}$ = 5 units, n_{NAcMED} = 36 units.

		Percent (%) responses					
		VTA		**CM**		**PF**	
Photostimulation Intensity		*NAc Core*	*NAc Med*	*NAc Core*	*NAc Med*	*NAc Core*	*NAc Med*
1 mW	Exc.	59	37	54	41	43	60
	Inh.	5	17	3	6	3	5
	Mixed	0	10	3	0	3	0
	No Res.	36	37	41	53	53	35
	n =	22	41	39	17	40	20
5 mW	Exc.	82	45	54	58	58	75
	Inh.	0	7	13	4	3	0
	Mixed	5	5	5	8	0	15
	No Res.	14	43	29	31	40	10
	n =	22	42	56	26	40	20
10 mW	Exc.	86	38	77	72	65	85
	Inh.	0	2	5	0	0	0
	Mixed	5	12	5	4	3	0
	No Res.	9	48	13	24	33	15
	n =	22	42	39	25	40	20

Table 1. Percent responses in NAc_{Core} and NAc_{Med} elicited by photostimulation of cerebellar axons in VTA, CM and PF at different intensities.

		Proportion of responses elicited by 1st light pulse	
	Photostimulation Intensity	*NAc Core*	*NAc Med*
VTA	1 mW	7/13 (54%)	11/19 (58%)
	5 mW	16/19 (84%)	14/21 (67%)
	10 mW	18/20 (90%)	19/21 (90%)
CM	1 mW	16/22 (72%)	4/7 (57%)
	5 mW	27/33 (82%)	14/17 (82%)
	10 mW	26/32 (81%)	16/19 (84%)
PF	1 mW	12/18 (67%)	7/12 (58%)
	5 mW	15/23 (65%)	16/18 (89%)
	10 mW	14/27 (52%)	14/17 (82%)

Table 2. Proportion of excitatory responses in NAc_{Core} and NAc_{Med} elicited by the first light pulse, at different photostimulation intensities.

TEMPORAL ASPECTS OF LIGHT-EVOKED RESPONSES

We wondered whether temporal aspects of CB-NAc communication differed between excitatory and inhibitory responses. Analysis of onset latency of responses elicited by 10 mW CB axonal photostimulation indicated that, overall, excitatory responses had significantly shorter onset latencies than inhibitory ones (mean ± sem: excit.: 45.4 ± 5.0 ms, inh.: 256.7 ± 46.2 ms, t_{147}= -10.0, $p < 0.001$; N = 10, $n_{exc.}$= 136, $n_{inh.}$= 13). To dissect node-specific effects, we computed the cumulative distributions of onset latencies for excitatory responses elicited by photostimulation in VTA, CM and PF (Fig. 3.5E). A relatively broad distribution of onset latencies was evident in all nodes, with half-rise latencies of 11 ms for VTA, 20 ms for CM and 40 ms for PF. Further analysis indicated that the probability of eliciting short-latency responses (≤ 10 ms), which are consistent with disynaptic connectivity (Chen et al., 2014; Gao et al., 2018; Assous et al., 2019; Yang et al., 2021), was greater for photostimulation in VTA compared to CM and/or PF (proportion of latencies ≤ 10 ms: VTA: 0.34, CM: 0.08, PF: 0.11; VTA vs CM: $\chi^2_{(1)} = 10.3$, $p < 0.01$; VTA vs PF: $\chi^2_{(1)} = 6.4$, $p < 0.01$; CM vs PF: $\chi^2_{(1)} = 0.4$, $p = 0.54$; p-values corrected for multiple comparisons) (Fig. 3.5E *inset*). In the VTA, lower intensity stimulation led to a decreased proportion of short latencies within the VTA alone (13%, 15%, and 34% of latencies less than or equal to 10ms following 1, 5 and 10-mW stimulation paradigms respectively) ($X^2_{(2)}$=6.5, $p = 0.04$), and thus this node no longer had a significantly different proportion of short latencies compared to CM and PF (1mW: $X^2_{(2)} = 0.85$, $p = 0.65$; 5mW: $X^2_{(2)} = 3.7$, $p = 0.25$). This further supports the idea that the CB-VTA-NAc circuit exhibits unique convergent properties. Similar analysis could not be applied to inhibitory responses because of their limited

prevalence (Fig. 3.5A2-C2 and Table 1). Finally, we examined NAc subregion-specific effects on excitatory response latencies (Fig. 3.5F-H). A two-way ANOVA corroborated the significant main effect of nodes ($F(2,130) = 4.7$; $p < 0.05$) but did not find significant main effect of NAc subregion ($F(1,130) = 1.7$; $p = 0.19$), or significant interaction effect between node and NAc subregion ($F(2,130) = 1.7$; $p = 0.18$).

Collectively, these results support and expand the conclusions of our neuroanatomical studies that signals originating in DCN can reach NAc through pathways that involve the VTA and the intralaminar thalamus.

Discussion

In this study we examined the anatomical basis of functional connectivity between the cerebellum and nucleus accumbens using neuroanatomy, and optogenetics, and in vivo electrophysiology. Our investigations into this connection identify three disynaptic pathways through which cerebellar signals can reach the NAc. These pathways go through the VTA or the intralaminar thalamus (centromedial or parafascicular nucleus). Optogenetic activation of DCN axons in each of these intermediary nodes revealed that all three pathways can communicate cerebellar signals to NAc, albeit with distinct node-dependent properties.

TECHNICAL CONSIDERATIONS

Our recordings were performed in ketamine-anesthetized mice. As discussed in Chapter 2, although ketamine at anesthetic doses does not alter the number of spontaneously active striatal neurons (Kelland et al., 1991), it affects the pattern of spontaneous activity, promoting step-like membrane potential fluctuations between “up-”

and “down-states” (Mahon et al., 2001). Such bursting behavior would contribute to “noisy” baseline activity; however, we would not expect it to distort our analyses because we have defined neural responses as changes in spiking rate from the preceding baseline. Moreover, by using optogenetic, rather than sensory, stimuli to probe connectivity, we have overcome any concerns stemming from the known inhibitory effect of ketamine on sensory-evoked activity in the cerebellum (Bengtsson and Jörntell, 2007).

With this, the stimulation modality warrants consideration. Optogenetic stimulation of DCN axons in a node could induce back-propagating action potentials that could, in turn, elicit NAc responses through axonal collaterals. However, to the best of our knowledge, there is no evidence for DCN collaterals that form synapses onto NAc-projecting neurons in both VTA and intralaminar thalamic nuclei. Even if such collaterals existed, their activation would result in unreliable responses with relatively long latencies, due to synaptic delays and the failure-prone asymmetric nature of action potential conduction velocity (Grill et al., 2008; Mateus et al., 2021).

NOVELTY OF ANATOMICAL CONNECTIONS

Anatomical and functional connections between DCN and VTA, and DCN and intralaminar nucleus nodes, have been described previously (Snider and Maiti, 1976; Hendry et al., 1979; Phillipson, 1979; Watabe-Uchida et al., 2012; Gornati et al., 2018; Carta et al., 2019; Jung et al., 2022). VTA and thalamic projections to NAc are also well established (Beckstead et al., 1979; Su and Bentivoglio, 1990; Bentivoglio et al., 1991; Bassareo and Di Chiara, 1999; Garris et al., 1999; Groenewegen et al., 1999; Van der Werf et al., 2002; Ikemoto, 2007; Taylor et al., 2014). It might therefore be unsurprising

that the DCN recruit these nodes to communicate with NAc. However, the VTA and thalamus are exquisitely complex areas with multiple output streams. For example, the VTA projects not only to NAc but also to hippocampus, hypothalamus, lateral habenula, entorhinal cortex, etc. (Oades and Halliday, 1987; Stamatakis et al., 2013; Beier et al., 2015). None of these downstream target regions appears to be disynaptically connected to DCN through the VTA, which points to specificity in circuit wiring. Our study is the first one, to our knowledge, to map DCN-NAc circuits through VTA and thalamus. We also effectively extended observations of DCN-thalamic outputs to the CM and PF nuclei, including confirming monosynaptic inputs from DCN to CM and PF.

FAST EXCITATORY MODULATION THAT DIFFERS BETWEEN MIDBRAIN AND THALAMIC ROUTES

Results from optogenetic stimulation of projections in these newly identified nodes support the previously identified strong excitatory signals from CB to NAc. The strength of these excitatory signals does not show any NAc subregion-, or node-, dependence. However, the relative frequency of NAc neurons that receive excitatory vs. inhibitory (or mixed) signals vary depending on the route that the DCN signals follow: the CB-VTA pathway is more likely to communicate excitatory signals to neurons in NAc_{Core} than in NAc_{Med}, whereas the CB-thalamic pathways do not show a clear preference for either NAc subregion, barring a slight preference for NAc_{Med} from the CB-PF pathway.

Disynaptic pathways that utilize fast classical neurotransmitters (e.g., glutamate) would be expected to support the rapid signal propagation and result in short-latency responses, whereas neuromodulatory (e.g., dopaminergic) pathways would be expected to operate at longer time scales (Chen et al., 2014; Gao et al., 2018; Assous

et al., 2019; Liu et al., 2021; Yang et al., 2021; Sippy and Tritsch, 2023). The shortest-latency responses we recorded upon photostimulation of cerebellar axons in each of the intermediary nodes occur within 10 ms, a finding that is consistent with the monosynaptic connections known to exist, between DCN and VTA, and DCN and thalamus (Carta et al., 2019; Baek et al., 2022; Jung et al., 2022), and which is corroborated by our newly identified monosynaptic structural connectivity. Particularly for responses elicited by photostimulation in VTA, DCN axons are known to synapse onto both dopaminergic and non-dopaminergic VTA neurons (Beier et al., 2019; Carta et al., 2019; Baek et al., 2022), including vesicular glutamate transporter 2-positive (vGlut2+) VTA neurons, which project to NAc (Beier et al., 2015) and which could, at least partly, mediate cerebellar signaling.

The CB-VTA-NAc circuit is unique in how stimulation intensity influences the latency of evoked responses. Higher stimulation intensities cause increasingly shorter response latencies only when stimulation was in the VTA, not in either thalamic nucleus. This effect could be due to convergent circuitry from CB input-receiving VTA neurons onto NAc neurons. This is not unexpected considering the known strong connection between VTA and NAc. This is also corroborated by our own anatomy, in which the transsynaptic labeling approach showed somewhat sparse expression in the VTA, but offered much more abundant expression in the NAc compared to expression of transsynaptically labeled CB-thalamus projections (Fig. 2). Longer-latency excitatory responses dominate CB-NAc communication through the intralaminar thalamus and could arise from polysynaptic circuitry, in agreement with the diffuse patterning of intralaminar projections (Jones and Leavitt, 1974; Van der Werf et al., 2002).

Subthreshold synaptic signaling that requires activity-dependent short-term facilitation in order to propagate to NAc neurons could also account for longer latencies. While short-term plasticity is unlikely to be strictly required for successful CB-NAc communication, given that a single pulse of optogenetic stimulation can elicit NAc responses; it may account for the longer-latency portion of the excitatory responses. For example, some of the responses evoked in the PF display more gradual buildup than excitatory responses through the other nodes and therefore may require the short-term plasticity induced through repeated stimulation.

Inhibitory responses (and/or inhibitory components of mixed responses), though more rare, are seen following stimulation in the nodes. They also appear to depend on photostimulation intensity, with higher prevalence at lower photostimulation intensities for all three nodes. Multiple cellular mechanisms could underlie inhibitory responses and could involve dopamine release as well as non-dopaminergic signaling through the VTA (Brown et al., 2012; Beier et al., 2019; Carta et al., 2019; Baek et al., 2022) and/or CB-thalamic (CM, PF) projections to NAc, which are known to contact not only medium spiny neurons but also cholinergic inhibitory interneurons (Yamanaka et al., 2018). Polysynaptic pathways could also be involved, although their recruitment seems at odds with the inverse relationship between inhibitory response prevalence and photostimulation intensity.

The results of these experiments offer novel insight on the long-range, functional connectivity of the non-motor CB. These data open many doors for future investigation of these CB-NAc circuits. The cellular makeup, as well as the nature of synaptic plasticity, in CB-NAc circuits is an exciting route for further investigation. As techniques

for di/polysynaptic circuit manipulation continue to improve, the behavioral influence of this connection will undoubtedly be pursued in future study.

Acknowledgments

Particular thanks are extended to Amber Arif and Alicia Dye for help with tissue sectioning; Drs. Brian Wiltgen, Karen Zito, Marty Usrey and Brian Mulloney of UC Davis for access to equipment; Dr. Ditterich for comments on a previous version of the manuscript; and Dr. Chaudhuri for helpful discussions.

References

Assous, Maxime, Daniel Dautan, James M. Tepper, and Juan Mena-Segovia. "Pedunculopontine Glutamatergic Neurons Provide a Novel Source of Feedforward Inhibition in the Striatum by Selectively Targeting Interneurons." *Journal of Neuroscience* 39, no. 24 (June 12, 2019): 4727–37. https://doi.org/10.1523/JNEUROSCI.2913-18.2019.

Bassareo, V., and G. Di Chiara. "Differential Responsiveness of Dopamine Transmission to Food-Stimuli in Nucleus Accumbens Shell/Core Compartments." *Neuroscience* 89, no. 3 (March 1999): 637–41. https://doi.org/10.1016/s0306-4522(98)00583-1.

Beckstead, R. M., V. B. Domesick, and W. J. Nauta. "Efferent Connections of the Substantia Nigra and Ventral Tegmental Area in the Rat." *Brain Research* 175, no. 2 (October 19, 1979): 191–217. https://doi.org/10.1016/0006-8993(79)91001-1.

Beier, Kevin T., Xiaojing J. Gao, Stanley Xie, Katherine E. DeLoach, Robert C. Malenka, and Liqun Luo. "Topological Organization of Ventral Tegmental Area Connectivity Revealed by Viral-Genetic Dissection of Input-Output Relations." *Cell Reports* 26, no. 1 (January 2, 2019): 159-167.e6. https://doi.org/10.1016/j.celrep.2018.12.040.

Beier, Kevin T., Elizabeth E. Steinberg, Katherine E. DeLoach, Stanley Xie, Kazunari Miyamichi, Lindsay Schwarz, Xiaojing J. Gao, Eric J. Kremer, Robert C. Malenka, and Liqun Luo. "Circuit Architecture of VTA Dopamine Neurons Revealed by Systematic Input-Output Mapping." *Cell* 162, no. 3 (July 2015): 622–34. https://doi.org/10.1016/j.cell.2015.07.015.

Bengtsson, Fredrik, and Henrik Jorntell. "Ketamine and Xylazine Depress Sensory-Evoked Parallel Fiber and Climbing Fiber Responses." Accessed May 5, 2023. https://doi.org/10.1152/jn.00057.2007.

Benjamini, Yoav, and Yosef Hochberg. "Controlling the False Discovery Rate: A Practical and Powerful Approach to Multiple Testing." *Journal of the Royal Statistical Society: Series B (Methodological)* 57, no. 1 (January 1995): 289–300. https://doi.org/10.1111/j.2517-6161.1995.tb02031.x.

Bentivoglio, M., G. Balercia, and L. Kruger. "The Specificity of the Nonspecific Thalamus: The Midline Nuclei." *Progress in Brain Research* 87 (1991): 53–80. https://doi.org/10.1016/s0079-6123(08)63047-2.

Brown, Holden D., Phillip M. Baker, and Michael E. Ragozzino. "The Parafascicular Thalamic Nucleus Concomitantly Influences Behavioral Flexibility and Dorsomedial Striatal Acetylcholine Output in Rats." *The Journal of Neuroscience: The Official Journal of the Society for Neuroscience* 30, no. 43 (October 27, 2010): 14390–98. https://doi.org/10.1523/JNEUROSCI.2167-10.2010.

Carta, Ilaria, Christopher H. Chen, Amanda L. Schott, Schnaude Dorizan, and Kamran Khodakhah. “Cerebellar Modulation of the Reward Circuitry and Social Behavior.” *Science* 363, no. 6424 (January 18, 2019): eaav0581.

Chen CH, Fremont R, Arteaga-Bracho EE, Khodakhah K (2014) Short latency cerebellar modulation of the basal ganglia. Nature Neuroscience 17:1767–1775.https://doi.org/10.1126/science.aav0581.

Fujita, Hirofumi, Takashi Kodama, and Sascha du Lac. “Modular Output Circuits of the Fastigial Nucleus for Diverse Motor and Nonmotor Functions of the Cerebellar Vermis.” *ELife* 9 (July 8, 2020): e58613. https://doi.org/10.7554/eLife.58613.

Gao, Zhenyu, Courtney Davis, Alyse M. Thomas, Michael N. Economo, Amada M. Abrego, Karel Svoboda, Chris I. De Zeeuw, and Nuo Li. “A Cortico-Cerebellar Loop for Motor Planning.” *Nature* 563, no. 7729 (November 2018): 113–16. https://doi.org/10.1038/s41586-018-0633-x.

Garris, P. A., M. Kilpatrick, M. A. Bunin, D. Michael, Q. D. Walker, and R. M. Wightman. “Dissociation of Dopamine Release in the Nucleus Accumbens from Intracranial Self-Stimulation.” *Nature* 398, no. 6722 (March 4, 1999): 67–69. https://doi.org/10.1038/18019.

Gornati, Simona V., Carmen B. Schäfer, Oscar H. J. Eelkman Rooda, Alex L. Nigg, Chris I. De Zeeuw, and Freek E. Hoebeek. “Differentiating Cerebellar Impact on Thalamic Nuclei.” *Cell Reports* 23, no. 9 (May 29, 2018): 2690–2704. https://doi.org/10.1016/j.celrep.2018.04.098.

Grill, Warren M., Meredith B. Cantrell, and Matthew S. Robertson. “Antidromic Propagation of Action Potentials in Branched Axons: Implications for the Mechanisms of Action of Deep Brain Stimulation.” *Journal of Computational Neuroscience* 24, no. 1 (February 2008): 81–93. https://doi.org/10.1007/s10827-007-0043-9.

Groenewegen, H. J., C. I. Wright, A. V. Beijer, and P. Voorn. “Convergence and Segregation of Ventral Striatal Inputs and Outputs.” *Annals of the New York Academy of Sciences* 877 (June 29, 1999): 49–63. https://doi.org/10.1111/j.1749-6632.1999.tb09260.x.

Hendry, S. H., E. G. Jones, and J. Graham. “Thalamic Relay Nuclei for Cerebellar and Certain Related Fiber Systems in the Cat.” *The Journal of Comparative Neurology* 185, no. 4 (June 15, 1979): 679–713. https://doi.org/10.1002/cne.901850406.

Ikemoto, Satoshi. “Dopamine Reward Circuitry: Two Projection Systems from the Ventral Midbrain to the Nucleus Accumbens-Olfactory Tubercle Complex.” *Brain Research Reviews* 56, no. 1 (November 2007): 27–78. https://doi.org/10.1016/j.brainresrev.2007.05.004.

Jones, E. G., and R. Y. Leavitt. “Retrograde Axonal Transport and the Demonstration of Non-Specific Projections to the Cerebral Cortex and Striatum from Thalamic Intralaminar Nuclei in the Rat, Cat and Monkey.” *The Journal of Comparative*

Neurology 154, no. 4 (April 15, 1974): 349–77. https://doi.org/10.1002/cne.901540402.

Jung, Se Jung, Ksenia Vlasov, Alexa F. D'Ambra, Abhijna Parigi, Mihir Baya, Edbertt Paul Frez, Jacqueline Villalobos, et al. "Novel Cerebello-Amygdala Connections Provide Missing Link Between Cerebellum and Limbic System." *Frontiers in Systems Neuroscience* 16 (2022): 879634. https://doi.org/10.3389/fnsys.2022.879634.

Kelland, Mark D., Louis A. Chiodo, and Arthur S. Freeman. "Dissociative Anesthesia and Striatal Neuronal Electrophysiology." *Synapse* 9, no. 1 (1991): 75–78. https://doi.org/10.1002/syn.890090111.

Liu, Changliang, Pragya Goel, and Pascal S. Kaeser. "Spatial and Temporal Scales of Dopamine Transmission." *Nature Reviews Neuroscience* 22, no. 6 (June 2021): 345–58. https://doi.org/10.1038/s41583-021-00455-7.

Mahon, S., J. M. Deniau, and S. Charpier. "Relationship between EEG Potentials and Intracellular Activity of Striatal and Cortico-Striatal Neurons: An in Vivo Study under Different Anesthetics." *Cerebral Cortex (New York, N.Y.: 1991)* 11, no. 4 (April 2001): 360–73. https://doi.org/10.1093/cercor/11.4.360.

Mateus, JC, Cdf Lopes, M Aroso, AR Costa, A Geros, J Meneses, P Faria, et al. "Bidirectional Flow of Action Potentials in Axons Drives Activity Dynamics in Neuronal Cultures - IOPscience." Accessed May 5, 2023. https://iopscience.iop.org/article/10.1088/1741-2552/ac41db.

Oades, R. D., and G. M. Halliday. "Ventral Tegmental (A10) System: Neurobiology. 1. Anatomy and Connectivity." *Brain Research Reviews* 12, no. 2 (May 1, 1987): 117–65. https://doi.org/10.1016/0165-0173(87)90011-7.

Oden, Anders, and Hans Wedel. "Arguments for Fisher's Permutation Test." *The Annals of Statistics* 3, no. 2 (March 1975): 518–20. https://doi.org/10.1214/aos/1176343082.

Petreanu, Leopoldo, Tianyi Mao, Scott M. Sternson, and Karel Svoboda. "The Subcellular Organization of Neocortical Excitatory Connections." *Nature* 457, no. 7233 (February 2009): 1142–45. https://doi.org/10.1038/nature07709.

Phillipson, O. T. "Afferent Projections to the Ventral Tegmental Area of Tsai and Interfascicular Nucleus: A Horseradish Peroxidase Study in the Rat." *Journal of Comparative Neurology* 187, no. 1 (1979): 117–43. https://doi.org/10.1002/cne.901870108.

Sippy, Tanya, and Nicolas X. Tritsch. "Unraveling the Dynamics of Dopamine Release and Its Actions on Target Cells." *Trends in Neurosciences* 46, no. 3 (March 2023): 228–39. https://doi.org/10.1016/j.tins.2022.12.005.

Snider, R. S., and A. Maiti. "Cerebellar Contributions to the Papez Circuit." *Journal of Neuroscience Research* 2, no. 2 (1976): 133–46. https://doi.org/10.1002/jnr.490020204.

Stamatakis, Alice M., Joshua H. Jennings, Randall L. Ung, Grace A. Blair, Richard J. Weinberg, Rachael L. Neve, Frederick Boyce, et al. “A Unique Population of Ventral Tegmental Area Neurons Inhibits the Lateral Habenula to Promote Reward.” *Neuron* 80, no. 4 (November 20, 2013): 1039–53. https://doi.org/10.1016/j.neuron.2013.08.023.

Su, H. S., and M. Bentivoglio. “Thalamic Midline Cell Populations Projecting to the Nucleus Accumbens, Amygdala, and Hippocampus in the Rat.” *The Journal of Comparative Neurology* 297, no. 4 (July 22, 1990): 582–93. https://doi.org/10.1002/cne.902970410.

Sultan, Fahad, Mark Augath, Salah Hamodeh, Yusuke Murayama, Axel Oeltermann, Alexander Rauch, and Peter Thier. “Unravelling Cerebellar Pathways with High Temporal Precision Targeting Motor and Extensive Sensory and Parietal Networks.” *Nature Communications* 3, no. 1 (June 26, 2012): 924. https://doi.org/10.1038/ncomms1912.

Taylor, Seth R., Sylvia Badurek, Ralph J. Dileone, Raad Nashmi, Liliana Minichiello, and Marina R. Picciotto. “GABAergic and Glutamatergic Efferents of the Mouse Ventral Tegmental Area.” *The Journal of Comparative Neurology* 522, no. 14 (October 1, 2014): 3308–34. https://doi.org/10.1002/cne.23603.

Van der Werf, Ysbrand D, Menno P Witter, and Henk J Groenewegen. “The Intralaminar and Midline Nuclei of the Thalamus. Anatomical and Functional Evidence for Participation in Processes of Arousal and Awareness.” *Brain Research Reviews* 39, no. 2 (September 1, 2002): 107–40. https://doi.org/10.1016/S0165-0173(02)00181-9.

Watabe-Uchida, Mitsuko, Lisa Zhu, Sachie K. Ogawa, Archana Vamanrao, and Naoshige Uchida. “Whole-Brain Mapping of Direct Inputs to Midbrain Dopamine Neurons.” *Neuron* 74, no. 5 (June 7, 2012): 858–73. https://doi.org/10.1016/j.neuron.2012.03.017.

Yamanaka, Ko, Yukiko Hori, Takafumi Minamimoto, Hiroshi Yamada, Naoyuki Matsumoto, Kazuki Enomoto, Toshihiko Aosaki, Ann M. Graybiel, and Minoru Kimura. “Roles of Centromedian Parafascicular Nuclei of Thalamus and Cholinergic Interneurons in the Dorsal Striatum in Associative Learning of Environmental Events.” *Journal of Neural Transmission (Vienna, Austria: 1996)* 125, no. 3 (March 2018): 501–13. https://doi.org/10.1007/s00702-017-1713-z.

Yang, Hongbin, Johannes W. de Jong, Ignas Cerniauskas, James R. Peck, Byung Kook Lim, Hui Gong, Howard L. Fields, and Stephan Lammel. “Pain Modulates Dopamine Neurons via a Spinal–Parabrachial–Mesencephalic Circuit.” *Nature Neuroscience* 24, no. 10 (October 2021): 1402–13. https://doi.org/10.1038/s41593-021-00903-8.

Chapter 4: Concluding Remarks

The thesis work described in this dissertation offers new insights on the long-range connectivity of the non-motor cerebellum. Through in vivo and ex vivo electrophysiology, optogenetics, and anatomical tracing, we have determined that the cerebellum is disynaptically connected to the nucleus accumbens through at least three circuits: CB-VTA-NAc, CB-CM-NAc, and CB-PF-NAc. It is tempting to speculate on the network-wide implications as well as the cellular mechanisms of the different CB-NAc pathways, and thus I will begin to do so below.

Cerebellar signals that arrive to NAc_{Core} through VTA could be behaviorally relevant for reward learning through signaling of value, which has been correlated with dopamine release in NAc_{Core}, but not in NAc_{Med} (Mohebi et al., 2019). Alternatively (or additionally), the CB-VTA-NAc_{Core} pathway could be rewarding in itself, as stimulation of dopaminergic projections from VTA to NAc_{Core} are sufficient to establish self-stimulation (Han et al., 2017) and previous studies have shown that the CB can signal reward (Wagner et al., 2017; Carta et al., 2019; Medina, 2019). The CB-VTA-NAc_{Core} pathway could also be involved in social cognition, given that NAc_{Core} activation promotes social dominance in mice and that cerebellar Purkinje neurons are known to modulate social aggression in mice (Jackman et al., 2020). Finally, the CB-VTA-NAc_{Core} pathway could also be important for signaling salience, regardless of valence, to promote learned responses to behaviorally relevant stimuli (Kutlu et al., 2010). The short response latencies of the CB-VTA-NAc_{Core} pathway could be key for temporally precise control of behavioral states including attentional control (Flores-Dourojeanni et al., 2021), and could gate incoming signals to NAc, including signals from PF (Akaike et al., 1981; Hara et al., 1989).

CB-VTA projections preferentially project to NAc_{Core}, but a substantial portion still arrive at NAc_{Med}. It has been shown that VTA cells that co-transmit dopamine (DA) and glutamate preferentially project to the NAc_{Med}, and that these neurons elicit strong excitatory responses in cholinergic interneurons, though they also have weaker connections directly onto medium spiny neurons and inhibitory interneurons (Mingote et al., 2019). This activation of intrinsic circuitry could help explain several features of the CB-VTA-NAc_{Med} circuit. The direct release of glutamate and dopamine onto NAc_{Med} neurons may be responsible for the fast and slower excitatory responses observed, respectively. Additionally, activation of cholinergic interneurons can cause increased release of GABA from inhibitory interneurons onto medium spiny neurons. Thus, slower inhibitory responses, seen predominantly in NAc_{Med} could be in response to polysynaptic activation of these interneurons. Lastly, the dual effect on medium spiny neurons, both direct activation and polysynaptic inhibition could be responsible for the mixed responses recorded in the NAc_{Med} following activation of CB-VTA projections.

CB-PF-NAc neurons were observed to preferentially influence NAc_{Med} over NAc_{Core}. This preference could also support a role in behavioral flexibility. Indeed, both NAc_{Med} and NAc_{Core} neurons encode rewarding and aversive stimuli via changes in neural firing rate, however, only neurons in NAc_{Med} adaptively shift population response type to track the motivational value of a stimulus (Loriaux et al., 2011), suggesting that NAc_{Med} can flexibly modulate encoding based on relative stimulus valence and/or acquired salience (Aquili et al., 2014; West and Carelli, 2016). Given that the PF is known to play a role in behavioral flexibility (Brown et al., 2010; Kato et al., 2021), the

CB-PF-NAc_{Med} circuit may communicate teaching signals for updating past learning and altering behavior adaptively.

Future investigations into the cellular basis of DCN-NAc communication as well as potential circuit-specificity of behavioral contributions are clearly in order. Here, we have broken new ground by providing the first evidence of rapid functional connectivity between CB and NAc, through the midbrain and intralaminar thalamus.

References

Akaike, A., M. Sasa, and S. Takaori. “Inhibition from Ventral Tegmental Area of Nucleus Accumbens Neurons in the Rat.” *Brain Research* 225, no. 1 (November 23, 1981): 189–94. https://doi.org/10.1016/0006-8993(81)90329-2.

Aquili, Luca, Andrew W. Liu, Mayumi Shindou, Tomomi Shindou, and Jeffery R. Wickens. “Behavioral Flexibility Is Increased by Optogenetic Inhibition of Neurons in the Nucleus Accumbens Shell during Specific Time Segments.” *Learning & Memory (Cold Spring Harbor, N.Y.)* 21, no. 4 (April 1, 2014): 223–31. https://doi.org/10.1101/lm.034199.113.

Brown, Holden D., Phillip M. Baker, and Michael E. Ragozzino. “The Parafascicular Thalamic Nucleus Concomitantly Influences Behavioral Flexibility and Dorsomedial Striatal Acetylcholine Output in Rats.” *The Journal of Neuroscience: The Official Journal of the Society for Neuroscience* 30, no. 43 (October 27, 2010): 14390–98. https://doi.org/10.1523/JNEUROSCI.2167-10.2010.

Carta, Ilaria, Christopher H. Chen, Amanda L. Schott, Schnaude Dorizan, and Kamran Khodakhah. “Cerebellar Modulation of the Reward Circuitry and Social Behavior.” *Science* 363, no. 6424 (January 18, 2019): eaav0581. https://doi.org/10.1126/science.aav0581.

Flores-Dourojeanni, Jacques P., Coby van Rijt, Marleen H. van den Munkhof, Linde Boekhoudt, Mieneke C. M. Luijendijk, Louk J. M. J. Vanderschuren, and Roger A. H. Adan. “Temporally Specific Roles of Ventral Tegmental Area Projections to the Nucleus Accumbens and Prefrontal Cortex in Attention and Impulse Control.” *The Journal of Neuroscience: The Official Journal of the Society for Neuroscience* 41, no. 19 (May 12, 2021): 4293–4304. https://doi.org/10.1523/JNEUROSCI.0477-20.2020.

Han, Jeong-Kyu, Sun-Ho Kwon, Yong Gyu Kim, Jaeyong Choi, Jong-Il Kim, Yong-Seok Lee, Sang-Kyu Ye, and Sang Jeong Kim. “Ablation of STAT3 in Purkinje Cells Reorganizes Cerebellar Synaptic Plasticity in Long-Term Fear Memory Network.” Edited by Gary L Westbrook, Jennifer L Raymond, Dagmar Timmann, and Keiko Tanaka-Yamamoto. *ELife* 10 (January 18, 2021): e63291. https://doi.org/10.7554/eLife.63291.

Hara, M., M. Sasa, and S. Takaori. “Ventral Tegmental Area-Mediated Inhibition of Neurons of the Nucleus Accumbens Receiving Input from the Parafascicular Nucleus of the Thalamus Is Mediated by Dopamine D1 Receptors.” *Neuropharmacology* 28, no. 11 (November 1989): 1203–9. https://doi.org/10.1016/0028-3908(89)90212-8.

Jackman, Skyler L, Christopher H Chen, Heather L Offermann, Iain R Drew, Bailey M Harrison, Anna M Bowman, Katelyn M Flick, Isabella Flaquer, and Wade G Regehr. “Cerebellar Purkinje Cell Activity Modulates Aggressive Behavior.” *ELife* 9 (n.d.): e53229. https://doi.org/10.7554/eLife.53229.

Kutlu, Munir Gunes, Jennifer E. Zachry, Patrick R. Melugin, Stephanie A. Cajigas, Maxime F. Chevee, Shannon J. Kelly, Banu Kutlu, Lin Tian, Cody A. Siciliano, and Erin S. Calipari. “Dopamine Release in the Nucleus Accumbens Core Signals Perceived Saliency.” *Current Biology: CB* 31, no. 21 (November 8, 2021): 4748-4761.e8. https://doi.org/10.1016/j.cub.2021.08.052.

Loriaux, Amy L., Jamie D. Roitman, and Mitchell F. Roitman. “Nucleus Accumbens Shell, but Not Core, Tracks Motivational Value of Salt.” *Journal of Neurophysiology* 106, no. 3 (September 2011): 1537–44. https://doi.org/10.1152/jn.00153.2011.

Medina, Javier F. “Teaching the Cerebellum about Reward.” *Nature Neuroscience* 22, no. 6 (June 2019): 846. https://doi.org/10.1038/s41593-019-0409-0.

Mingote, Susana, Aliza Amsellem, Abigail Kempf, Stephen Rayport, and Nao Chuhma. “Dopamine-Glutamate Neuron Projections to the Nucleus Accumbens Medial Shell and Behavioral Switching.” *Neurochemistry International* 129 (October 1, 2019): 104482. https://doi.org/10.1016/j.neuint.2019.104482.

Mohebi, Ali, Jeffrey R. Pettibone, Arif A. Hamid, Jenny-Marie T. Wong, Leah T. Vinson, Tommaso Patriarchi, Lin Tian, Robert T. Kennedy, and Joshua D. Berke. “Dissociable Dopamine Dynamics for Learning and Motivation.” *Nature* 570, no. 7759 (June 2019): 65. https://doi.org/10.1038/s41586-019-1235-y.

Wang, Samuel S. -H., Alexander D. Kloth, and Aleksandra Badura. “The Cerebellum, Sensitive Periods, and Autism.” *Neuron* 83, no. 3 (August 6, 2014): 518–32. https://doi.org/10.1016/j.neuron.2014.07.016.

West, Elizabeth A., and Regina M. Carelli. “Nucleus Accumbens Core and Shell Differentially Encode Reward-Associated Cues after Reinforcer Devaluation.” *The Journal of Neuroscience: The Official Journal of the Society for Neuroscience* 36, no. 4 (January 27, 2016): 1128–39. https://doi.org/10.1523/JNEUROSCI.2976-15.2016.

Appendix i: *Chd8* and the developing cerebellum: implications for the adult non-motor cerebellum

Preface

The studies from our lab described in this dissertation expand upon the role of the cerebellum in non-motor functions by elucidating cerebellar connectivity to regions involved in reward, motivation, emotion, attention, and social behaviors. This growing knowledge highlights the importance of studying the cerebellum (CB) in the context of neurological disorders and identifying potential targets for therapeutic intervention. In this chapter, I will discuss completed and ongoing work probing the role of the clinically relevant gene, *CHD8*, on CB development. The work presented in this appendix is the result of a collaboration between the Nord and Fioravante labs and has partly appeared in abstract form: D'Ambra, Canales, C, Seban, N, Jung, SJ, Chu, N, Cichewicz, K, Lozano, S, Smith, E, Ortiz, R, Zhu, J, Fioravante, D, Nord A. Identifying the behavioral, genomic, and circuit-specific effects of Chd8 mutations in the developing and adult mouse cerebellum. Program No. 299.11. 2022 Neuroscience Meeting Planner. San Diego, CA. Society for Neuroscience, 2022. Online. The following individuals have contributed to the work included in this appendix: Alexa D'Ambra, Cesar Canales, Se Jung Jung, Jade Lin Dungca, Alex Nord and Diasynou Fioravante. Author contribution is as follows: **AFD**: conceptualization, methodology, investigation, data analysis and visualization, project administration, supervision; **CC**: animal care, project administration; **SJJ**: investigation and data visualization (Fig. i.2); **JLD**: data analysis and visualization (Fig. i.2; **AN**: conceptualization, resources, project funding acquisition; **DF**: conceptualization, methodology, supervision, project funding acquisition. Funding: This work was supported by R21MH126413 to **DF** and **AN**; and R01MH120513 to **AN**.

Introduction

CHD8 is a gene that encodes a protein involved in the regulation of gene expression and the development of various organs, including the brain. Substantial evidence suggests that mutations in the *CHD8* gene may contribute to the development of autism spectrum disorder (ASD), a complex neurodevelopmental disorder characterized by deficits in social communication and interaction, and repetitive or restrictive behaviors (Sugathan et al., 2014). In addition to ASD, human individuals harboring *CHD8* mutations exhibit macrocephaly, distinct craniofacial morphology, mild-to-severe intellectual disability (ID) and gastrointestinal problems (Bernier et al., 2014).

Several studies have created transgenic mouse lines with varying *Chd8* mutations to model those seen in humans. The most translationally relevant of these models are those that recreate the heterozygous mutation of the gene. To create a heterozygous deletion of *Chd8* in mice, researchers have used several different techniques, including CRISPR/Cas9 genome editing and gene trapping. The resulting *Chd8*+/- mice displayed ASD-like behaviors, including deficits in social interaction and increased repetitive behaviors, with some variability in phenotypes depending on the technique used. Specifically, germline haploinsufficiency induced by using CRISPR/Cas9 to generate a 5-base-pair deletion in *Chd8* exon 5 leads to several clinically relevant phenotypic changes (Fig. i.1A). These include alterations in cortical and subcortical volume, deficits in cognitive assays, altered neurogenesis, and changes in the transcriptomic landscape that exist in early and later neurodevelopment (Gompers et al., 2017)(Fig. i.1B-D).

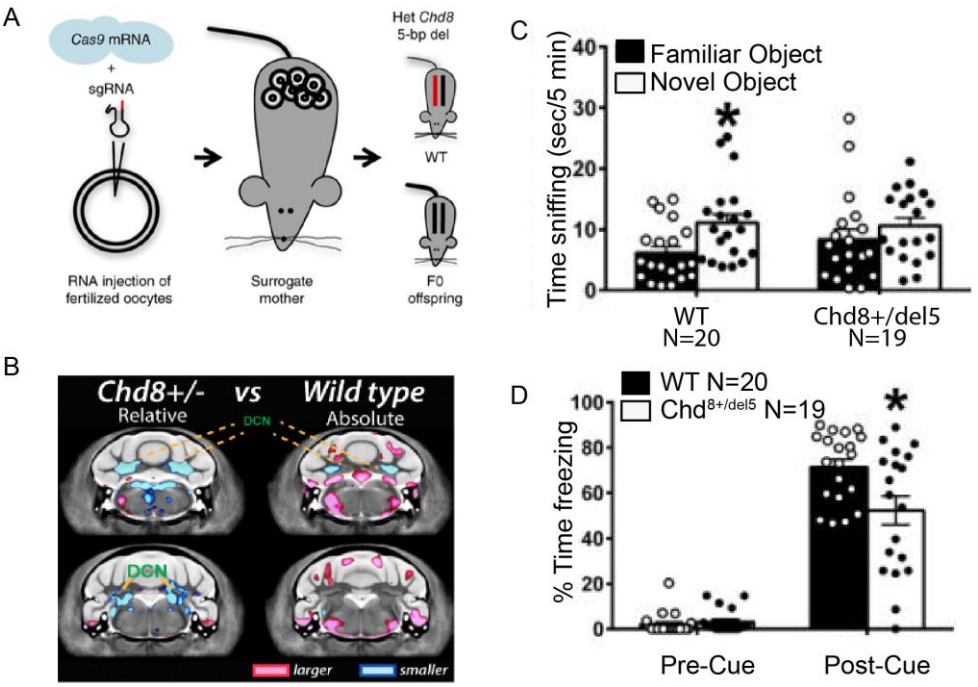

Figure i.1. Germline *Chd8* Haploinsufficiency alters brain volume and cognitive performance. **A**, Schematic depicting CRISPR/Cas9 technique for generating transgenic animals. *Het:* heterozygous, *Del*: deletion **B,** Changes in CB volume. *DCN*: deep cerebellar nucleus **C**, $Chd8^{+/del5}$ animals perform poorly on the novel object recognition task WT: *p = 0.0031; $Chd^{8+/del5}$: p = 0.0867 **D,** $Chd8^{+/del5}$ mice exhibit reduced freezing to cue after tone-shock conditioning (WT vs $Chd8^{+/del5}$ *p = 0.0104). ***Adapted from Gompers et al., 2017.***

Studies on the role of *CHD8* in the cerebellum (CB) have provided insights into the molecular mechanisms underlying the pathogenesis of ASD. For instance, *CHD8* has been shown to regulate the expression of several genes that are involved in the development and function of the cerebellum, such as *Pcdh10*, *Cntn4*, and *Dlgap2* (Cotney et al., 2015). Moreover, recent studies have suggested that *Chd8* mutations may disrupt the balance of excitatory and inhibitory synaptic transmission in the cerebellum, leading to altered neural circuitry and impaired motor and social behavior. For instance, *Chd8* mutations have been associated with abnormal CB architecture, decreased Purkinje cell density, and altered properties of synapses onto Purkinje cells, which are believed to contribute to the motor and social deficits observed in ASD

(Kawamora et al., 2021; Chen et al., 2022). To date, there has yet to be investigation of the effect of *Chd8* haploinsufficiency on cerebellar development.

In this study we use the previously described transgenic mouse line modeling *Chd8* haploinsufficiency ($Chd8^{+/del5}$) to investigate the role of *Chd8* in cerebellar development. Specifically, we use ex vivo electrophysiology, pharmacology, and histology to examine changes in inhibitory synaptic connectivity and morphology of the sole CB cortical output cells, Purkinje neurons (PNs).

Material and Methods

ELECTROPHYSIOLOGICAL RECORDINGS

Slice preparation

Mice (postnatal day 11-12; both sexes) were placed in a chamber with isoflurane for anesthesia. Brains were rapidly removed, blocked, and placed in ice cold sucrose solution (in mM: 81.2 NaCl, 23.4 NaHCO3, 69.9 sucrose, 23.3 glucose, 2.4 KCl, 1.4 NaH2PO4, 6.7 MgCl2, 0.5 CaCl2; ~315 mOsm). Sagittal sections (250 μm) of the cerebellum were cut on a vibratome (Leica VT1200S) and transferred to an incubation chamber containing sucrose solution at 32^{o} for 20 minutes after which they were transferred to a second incubation chamber containing artificial cerebrospinal fluid (aCSF; in mM: 127 NaCl, 2.5 KCl, 1.25 NaH_2PO_4, 25 $NaHCO_3$, 1 $MgCl_2$, 2 $CaCl_2$, 25 glucose; supplemented with 0.4 sodium ascorbate and 2 sodium pyruvate; ~315 mOsm) at 32°C. After 25 minutes of incubation, slices were moved to room temperature until used for recordings. All solutions were bubbled with 95% O2-5% CO2 continuously. Chemicals were from Sigma.

Whole-cell patch clamp recordings

For recordings, slices were mounted onto glass coveslips coated with poly-l-lysine and placed in a submersion chamber perfused with aCSF (2-3 ml/min) containing TTX (1µM) and NBQX (1µM) at 30-32 °C. Whole-cell patch-clamp recordings were made from visually identified PNs using borosilicate glass pipettes (1.5–3.5 MΩ) filled with internal solution containing (in mM): 140 CsCl, 4 NaCl, 0.5 $CaCl_2$, 10 HEPES, 5 EGTA , 5 QX314, 2 MgATP, and 0.05% biocytin; pH: 7.3. Recordings were acquired in pClamp11 using a Multiclamp 700B amplifier (Molecular Devices, San Jose, CA), digitized at 20 kHz and low-pass filtered at 8 kHz. Membrane potential was maintained at -70 mV. Series resistance and leak current were monitored and recordings were terminated if either of these parameters changed by more than 50%. Cells were excluded if leak exceeded 400pA or resistance was greater than 20MΩ.

ANALYSIS OF PURKINJE NEURON MORPHOLOGY

Following recording, slices were fixed in 4% (w/v) paraformaldehyde (PFA) for 24-48 hours. For immunohistochemistry, slices were blocked with 10% normal goat serum (NGS, Millipore, Burlington, MA) and streptavidin Alexa Fluor 488 (1:500) in PBST (0.3% Triton X-100 in PBS) for 1 h. After four 15-minute rinses in PBS, slices were mounted to slides, coverslipped with Mowiol-based antifade solution containing DAPI, and imaged using a LSM800 confocal microscope. Using ImageJ software, we created maximum projection images from z-stacks and saved them as .tif files. The SNT plugin on ImageJ was then used to manually trace individual dendritic branches and label individual pathways and to perform Sholl analysis as follows: Concentric rings around the soma were drawn with a step size of 4 microns from the base of the primary dendrite and covered the entire cell. The number of times any tracing crossed each

circle is counted as an “intersection”. Total branch length and number of branches were also calculated.

Results

CHD8 AND PURKINJE NEURON DENDRITIC ARBORIZATION

In order to determine if *Chd8* haploinsufficiency influences PN morphology during development, we first evaluated its expression in the CB cortex in P11-P12 mice. We found that *Chd8* is broadly expressed in the CB and is highly concentrated in the granule cell layer and in the Purkinje cell layer (Fig. i.2A). PN dendritic arborization was compared between wildtype animals (WT) and $Chd8^{+/del5}$ (Fig. i.2B). The data suggest that $Chd8^{+/del5}$ animals have a more complex arborization than WTs, with a greater number of radial intersections (Fig. i.2C). Additionally, $chd8^{+/del5}$ animals had a trend toward greater average total branch length, number of branches, and number of terminal dendrites (Fig. i.2D-F). On the other hand, WTs appeared to have longer PN dendritic arbors overall, with more cells intersecting at radii above 120μm (Fig. i.2C). These experiments are ongoing, and as such the sample size is insufficient to perform statistics. Further data collection will ensure appropriately powered statistical analyses to confirm the noticeable trend that constitutive heterozygous loss of *Chd8* leads to PN dendritic overgrowth. If this trend is indeed indicative of a significant effect of *Chd8* haploinsufficiency, it could be suggestive of an important role in the formation or functionality of synaptic transmission onto PNs.

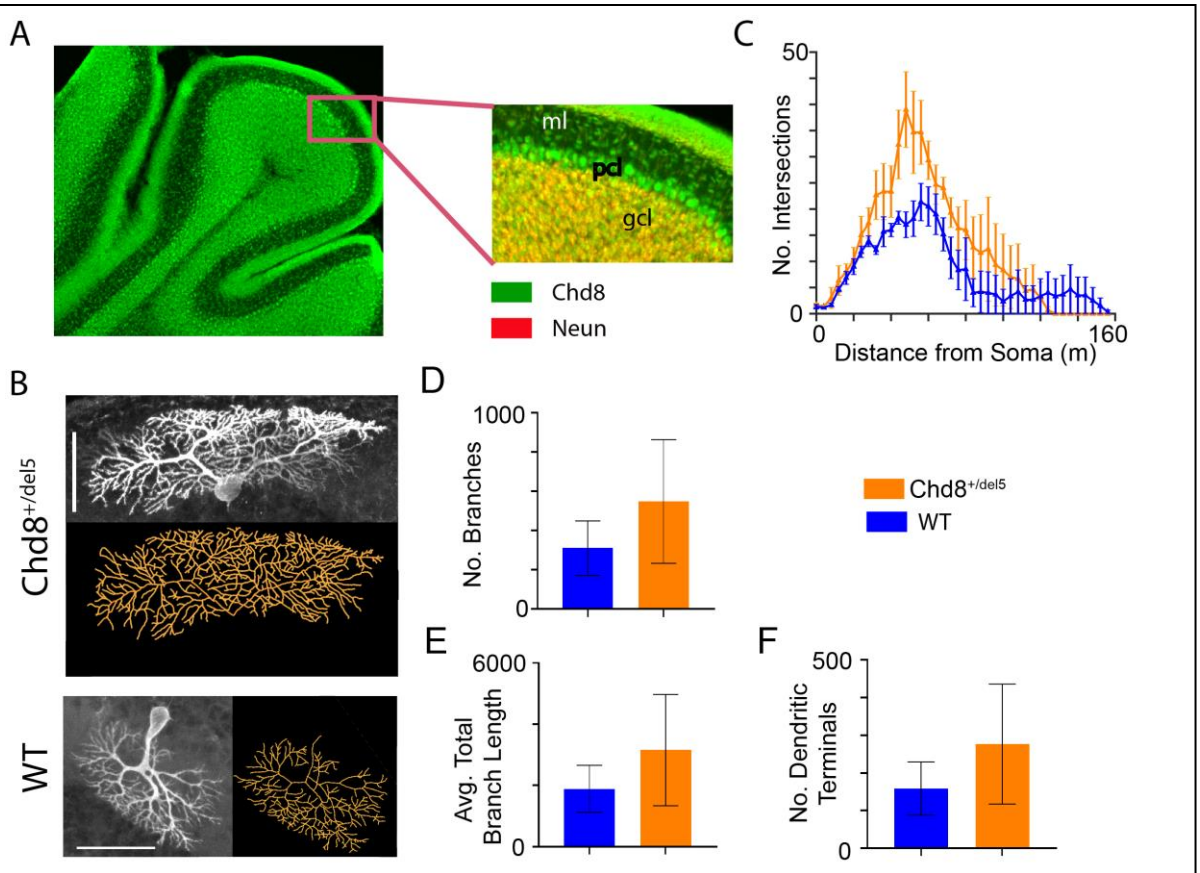

Figure 2. Chd8$^{+/del5}$ animals exhibit trend towards greater PN dendritic arborization. A, Chd8 expression in sagittal CB section. *Green:* Chd8, *Red:* NEUN. **B,** Example images of PN from Chd8$^{+/del5}$ (top) and WT (bottom) animals with manual dendritic tracing. **C**, Results of Sholl analysis show higher peak in Chd8$^{+/del5}$ PNs. **D,** Total number of branches across genotypes. **E**, Average total branch length (in microns) across genotypes. **F,** Total number of dendritic terminals across genotypes.

INHIBITORY TRANSMISSION IN CEREBELLAR CORTEX IS UNALTERED BY *CHD8* HAPLOINSUFFICIENCY

Studies suggest that *Chd8* may play a role in synaptic transmission in the CB cortex. To determine if heterozygous deletion of *Chd8* altered inhibitory transmission onto PNs, we recorded spontaneous inhibitory postsynaptic currents (mIPSCs) in both WT and Chd8$^{+/del5}$ animals of both sexes (Fig. i.3A-C). In both females (Fig. i.3D1, left) and males (Fig. 3D1, right) amplitude of mIPSCs was not significantly different between genotypes. There was also no significant difference in the frequency of mIPSCs (Fig. i.3D2). This may have been due to the large variability for these two properties;

however, plotting the distribution of amplitudes (Fig. i.3E1) and frequencies (Fig. i.3E2) corroborate this finding. Ultimately these data suggest that inhibitory synaptic transmission is not altered in in Chd8$^{+/del5}$ animals.

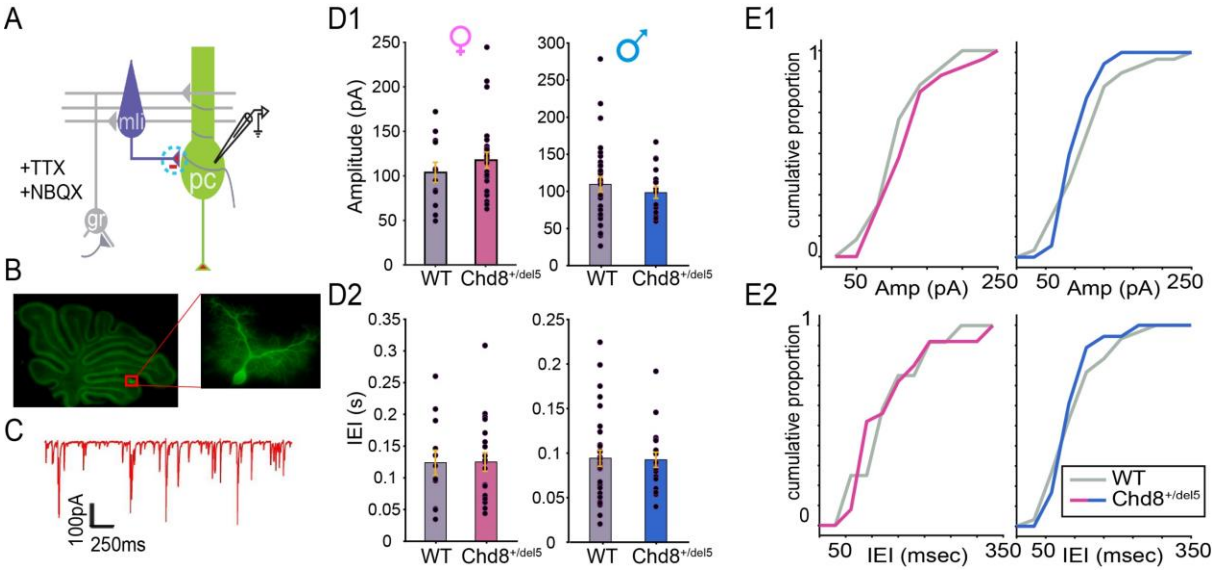

Figure 3. *Chd8* haploinsufficiency has no effect on inhibitory synaptic transmission onto PNs. **A,** Schematic illustrating the protocol for slice electrophysiology experiments. *TTX:* tetrodotoxin, *NBQX*: **B,** Example biocytin-labeled PN that was recorded from. **C,** Example trace of mIPSCs in PN. **D,** Amplitude (**D1**) and Frequency (**D2**) of mIPSCs in females and males across genotypes. *IEI:* inter-event interval. **E,** Cumulative histograms of amplitude (**E1**) and frequency (**E2**) of mIPSCs in both sexes across genotypes. *Amp*: amplitude, *IEI:* inter-event interval.

Discussion

In this appendix chapter, I have described preliminary work investigating the impact of *Chd8* haploinsufficiency on cerebellar development. Histological evaluations of PN morphology begin to uncover a potential effect of heterozygous *Chd8* deletion. Results from these preliminary data seem to suggest that *Chd8* plays a role in slowing or controlling dendritic growth. We also found no evidence that this mutation has any effect on inhibitory inputs onto PNs.

The finding that $Chd8^{+/del5}$ animals have no change in inhibitory inputs onto PNs suggests that *Chd8* may not play a role in the development of synapses from molecular layer interneurons (MLIs) onto PNs. MLIs are the primary inhibitory inputs onto PNs, and are important for modulating the strength and timing of excitatory inputs arriving from climbing and parallel fibers (Mittmann et al., 2004; Jörntell et al., 2010). This inhibitory feedback is crucial for directing plasticity at excitatory synapses and plays an important role in CB-relevant learning (Sergaki et al., 2017). One possibility for the lack of effect on spontaneous inputs suggests either that MLI inputs are unaffected, or that by postnatal day 11/12, homeostatic changes have already compensated for the loss. An important follow up study will be to probe PN evoked IPSCs following stimulation of MLIs.

An additional possibility is that the effect of *Chd8* knockdown is not seen until later into adulthood. Our lab has found that *Chd8* continues to express into adulthood in the CB (not shown), which is not seen in most other areas of the brain. Additionally, there is some evidence from collaborators that adult $Chd8^{+/del5}$ mice have noticeably reduced PN

density (not shown). Thus a more prominent effect on synaptic transmission may exist at later time points.

Finally, while it is not necessary that morphological changes in dendritic arborization result in changes in synaptic properties, it is unlikely that PN connectivity is unchanged. In addition to MLI's, the two key synaptic connections onto PNs are climbing fibers, arising from the inferior olive, and granule cell projections in the form of parallel fibers. Because climbing fibers form multiple synapses along the PN dendritic branch, this connection would be likely to be affected by changes in PN dendritic morphology. Prior manipulations of *chd8* in granule cell progenitors have already identified that this population is sensitive to *chd8* manipulations, and such mutations can lead to altered parallel fiber-PN synaptic integrity (Kawamura et al., 2021). Thus, in addition to exploring potential changes in evoked currents, spontaneous excitatory transmission is another avenue for future study.

This work expands on previous studies that have investigated the role of *Chd8* in cerebellar development, including PN morphology and synaptic transmission. The data described in this appendix chapter are the first, to our knowledge, to look both at the clinically relevant constitutive germline haploinsufficiency (as opposed to homozygous knock out and/or cell-type specific deletion), and at its effect in juvenile animals in which the CB is still developing.

References

Bernier, Raphael, Christelle Golzio, Bo Xiong, Holly A. Stessman, Bradley P. Coe, Osnat Penn, Kali Witherspoon, et al. “Disruptive CHD8 Mutations Define a Subtype of Autism Early in Development.” *Cell* 158, no. 2 (July 17, 2014): 263–76. https://doi.org/10.1016/j.cell.2014.06.017.

Chen, Xiang, Tong Chen, Chen Dong, Huiyao Chen, Xinran Dong, Lin Yang, Liyuan Hu, et al. “Deletion of CHD8 in Cerebellar Granule Neuron Progenitors Leads to Severe Cerebellar Hypoplasia, Ataxia, and Psychiatric Behavior in Mice.” *Journal of Genetics and Genomics* 49, no. 9 (September 1, 2022): 859–69. https://doi.org/10.1016/j.jgg.2022.02.011.

Cotney, Justin, Rebecca A. Muhle, Stephan J. Sanders, Li Liu, A. Jeremy Willsey, Wei Niu, Wenzhong Liu, et al. “The Autism-Associated Chromatin Modifier CHD8 Regulates Other Autism Risk Genes during Human Neurodevelopment.” *Nature Communications* 6, no. 1 (March 10, 2015): 6404. https://doi.org/10.1038/ncomms7404.

Gompers, Andrea L., Linda Su-Feher, Jacob Ellegood, Nycole A. Copping, M. Asrafuzzaman Riyadh, Tyler W. Stradleigh, Michael C. Pride, et al. “Germline Chd8 Haploinsufficiency Alters Brain Development in Mouse.” *Nature Neuroscience* 20, no. 8 (August 2017): 1062–73. https://doi.org/10.1038/nn.4592.

Ito-Ishida, Aya, Wataru Kakegawa, Kazuhisa Kohda, Eriko Miura, Shigeo Okabe, and Michisuke Yuzaki. “Cbln1 Downregulates the Formation and Function of Inhibitory Synapses in Mouse Cerebellar Purkinje Cells.” *European Journal of Neuroscience* 39, no. 8 (2014): 1268–80. https://doi.org/10.1111/ejn.12487.

Jung, Hwajin, Haram Park, Yeonsoo Choi, Hyojin Kang, Eunee Lee, Hanseul Kweon, Junyeop Daniel Roh, et al. “Sexually Dimorphic Behavior, Neuronal Activity, and Gene Expression in Chd8-Mutant Mice.” *Nature Neuroscience* 21, no. 9 (September 2018): 1218–28. https://doi.org/10.1038/s41593-018-0208-z.

Katayama, Yuta, Masaaki Nishiyama, Hirotaka Shoji, Yasuyuki Ohkawa, Atsuki Kawamura, Tetsuya Sato, Mikita Suyama, Toru Takumi, Tsuyoshi Miyakawa, and Keiichi I. Nakayama. “CHD8 Haploinsufficiency Results in Autistic-like Phenotypes in Mice.” *Nature* 537, no. 7622 (September 29, 2016): 675–79. https://doi.org/10.1038/nature19357.

Kawamura, Atsuki, Yuta Katayama, Wataru Kakegawa, Daisuke Ino, Masaaki Nishiyama, Michisuke Yuzaki, and Keiichi I. Nakayama. “The Autism-Associated Protein CHD8 Is Required for Cerebellar Development and Motor Function.” *Cell Reports* 35, no. 1 (April 6, 2021): 108932. https://doi.org/10.1016/j.celrep.2021.108932.

Lonchamp, Etienne, Frédéric Gambino, Jean Luc Dupont, Frédéric Doussau, Antoine Valera, Bernard Poulain, and Jean-Louis Bossu. “Pre and Post Synaptic NMDA

Effects Targeting Purkinje Cells in the Mouse Cerebellar Cortex." *PLoS ONE* 7, no. 1 (January 19, 2012): e30180. https://doi.org/10.1371/journal.pone.0030180.

Mittmann, Wolfgang, Ursula Koch, and Michael Hausser. "Feed-forward Inhibition Shapes the Spike Output of Cerebellar Purkinje Cells." Accessed May 5, 2023. https://physoc.onlinelibrary.wiley.com/doi/epdf/10.1113/jphysiol.2004.075028?src=getftr.

Peter, Saša, Michiel M. ten Brinke, Jeffrey Stedehouder, Claudia M. Reinelt, Bin Wu, Haibo Zhou, Kuikui Zhou, et al. "Dysfunctional Cerebellar Purkinje Cells Contribute to Autism-like Behaviour in Shank2-Deficient Mice." *Nature Communications* 7, no. 1 (September 1, 2016): 12627. https://doi.org/10.1038/ncomms12627.

Platt, Randall J., Yang Zhou, Ian M. Slaymaker, Ashwin S. Shetty, Niels R. Weisbach, Jin-Ah Kim, Jitendra Sharma, et al. "Chd8 Mutation Leads to Autistic-like Behaviors and Impaired Striatal Circuits." *Cell Reports* 19, no. 2 (April 11, 2017): 335–50. https://doi.org/10.1016/j.celrep.2017.03.052.

Sergaki, Maria Christina, Juan Carlos López-Ramos, Stefanos Stagkourakis, Agnès Gruart, Christian Broberger, José María Delgado-García, and Carlos F. Ibáñez. "Compromised Survival of Cerebellar Molecular Layer Interneurons Lacking GDNF Receptors GFRα1 or RET Impairs Normal Cerebellar Motor Learning." *Cell Reports* 19, no. 10 (June 6, 2017): 1977–86. https://doi.org/10.1016/j.celrep.2017.05.030.

Sugathan, Aarathi, Marta Biagioli, Christelle Golzio, Serkan Erdin, Ian Blumenthal, Poornima Manavalan, Ashok Ragavendran, et al. "*CHD8* Regulates Neurodevelopmental Pathways Associated with Autism Spectrum Disorder in Neural Progenitors." *Proceedings of the National Academy of Sciences* 111, no. 42 (October 21, 2014). https://doi.org/10.1073/pnas.1405266111.

Tsai, Peter T., Court Hull, YunXiang Chu, Emily Greene-Colozzi, Abbey R. Sadowski, Jarrett M. Leech, Jason Steinberg, Jacqueline N. Crawley, Wade G. Regehr, and Mustafa Sahin. "Autistic-like Behavior and Cerebellar Dysfunction in Purkinje Cell Tsc1 Mutant Mice." *Nature* 488, no. 7413 (August 30, 2012): 647–51. https://doi.org/10.1038/nature11310.

Appendix ii: Polysynaptic cerebello-amygdala connectivity further elucidates the cerebellum's link to the limbic system

Preface

The following work outlines the anatomical connections that link the cerebellum to the basolateral amygdala and was published in in the following manuscript: Jung SJ*, Vlasov K*, D'Ambra AF, Parigi A, Baya M, Frez EP, Villalobos J, Fernandez-Frentzel M, Anguiano M, Ideguchi Y, Antzoulatos EG and Fioravante D (2022) Novel Cerebello-Amygdala Connections Provide Missing Link Between Cerebellum and Limbic System. Front. Syst. Neurosci. 16:879634. doi: 10.3389/fnsys.2022.879634. Author contributions to the work, as it is presented in this appendix chapter, is as follows: **SJJ**: animal care, investigation, data analysis and visualization, project administration, supervision; **KV**: investigation, data analysis and visualization, supervision; **AFD** and **AP**: investigation; **YI**: methodology; **MB**, **EPF**, **JV**, **MFF**, **MA, EGA**: data analysis; **DF**: conceptualization, methodology, animal care, data analysis and visualization, project administration, supervision, project funding acquisition. Funding: **KV** was supported by NIMH T32 MH112507 and F31MH131405 by NIMH; **AFD** was supported by NIH T32 GM007377 and a UC Davis Dean's Distinguished Graduate Fellowship; **EA** was supported by a NARSAD 2018 Young Investigator Grant. This work was supported by a Whitehall fellowship, BRFSG-2017-02, R21MH114178, NSF1754831 and R01MH128744 to **DF**.

Abstract

The cerebellum is emerging as a powerful regulator of cognitive and affective processing and memory in both humans and animals and has been implicated in affective disorders. How the cerebellum supports affective function remains poorly understood. The short-latency (just a few milliseconds) functional connections that were identified between the cerebellum and amygdala -a structure crucial for the processing of emotion and valence- more than 4 decades ago raise the exciting, yet untested, possibility that a cerebellum-amygdala pathway communicates information important for emotion. The major hurdle in rigorously testing this possibility is the lack of knowledge about the anatomy and functional connectivity of this pathway. Our initial anatomical tracing studies in mice excluded the existence of a direct monosynaptic connection between cerebellum and amygdala. Using transneuronal tracing techniques, we have identified a novel disynaptic circuit between the cerebellar output nuclei and the basolateral amygdala. This circuit recruits the understudied intralaminar thalamus as a node. Using ex vivo optophysiology and super-resolution microscopy, we provide the first evidence for the functionality of the pathway, thus offering a missing mechanistic link between the cerebellum and amygdala. This discovery provides a connectivity blueprint between the cerebellum and a key structure of the limbic system. As such, it is the requisite first step toward obtaining new knowledge about cerebellar function in emotion, thus fundamentally advancing understanding of the neurobiology of emotion, which is perturbed in mental and autism spectrum disorders.

Introduction

The cerebellum is increasingly recognized as a regulator of limbic functions (Strick et al., 2009; Buckner, 2013; Reeber et al., 2013; Strata, 2015; Adamaszek et al., 2017; Liang and Carlson, 2019; Schmahmann, 2019; Hull, 2020). The human cerebellum is activated in response to aversive or threatening cues, upon remembering emotionally charged events, and during social behavior, reward-based decision making and violation of expectation (Ploghaus et al., 1999; Damasio et al., 2000; Ernst, 2002; Ahs et al., 2009; Moulton et al., 2010, 2014; Guo et al., 2013; Van Overwalle et al., 2014; Guell et al., 2018; Ernst et al., 2019). Consistent with this, deficits in cerebellar function are associated with impaired emotional attention and perception, as seen in depression, anxiety, schizophrenia and post-traumatic stress disorder (Yin et al., 2011; Roy et al., 2013; Parker et al., 2014; Phillips et al., 2015), as well as cognitive and emotional disturbances collectively known as cerebellar cognitive affective syndrome (Schmahmann and Sherman, 1998). Animal models have recapitulated some of these findings, with selective mutations, damage or inactivation of the rodent cerebellum resulting in altered acquisition or extinction of learned defensive responses, and impaired social and goal-directed behavior, without motor deficits (Supple et al., 1987; Supple and Leaton, 1990; Sebastiani et al., 1992; Bauer et al., 2011; Lorivel et al., 2014; Otsuka et al., 2016; Xiao et al., 2018; Carta et al., 2019; Frontera et al., 2020; Han et al., 2021).

The limited understanding of the anatomical and functional circuits that connect the cerebellum to limbic centers has impeded mechanistic insight into the neural underpinnings of cerebellar limbic functions, which have begun to be dissected only

recently (Xiao et al., 2018; Carta et al., 2019; Frontera et al., 2020; Kelly et al., 2020). Moreover, a neuroanatomical substrate for the functional connections between the cerebellum and a key affective center, the amygdala (Janak and Tye, 2015), has yet to be provided, even though these connections were observed more than 40 years ago (Heath and Harper, 1974; Snider and Maiti, 1976; Heath et al., 1978). The purpose of the present work was to generate a mesoscale map of functional neuroanatomical connectivity between the cerebellum and amygdala. We focused on connections between the deep cerebellar nuclei (DCN), which give rise to most cerebellar output pathways (Ito, 2006), and the basolateral amygdala (BLA), which is known to process affect-relevant salience and valence information (Janak and Tye, 2015; O'Neill et al., 2018; Yizhar and Klavir, 2018), and which was targeted in the early electrophysiological studies of Heath et al. (Heath and Harper, 1974; Heath et al., 1978).

Materials and methods

MICE

C57Bl/6J mice of both sexes were used in accordance with National Institute of Health guidelines. All procedures were reviewed and approved by the Institutional Animal Care and Use Committee of the University of California, Davis. Mice were maintained on a 12-hr light/dark cycle with ad libitum access to food and water. For anatomical tracing experiments, postnatal day P45-65 (at the time of injection) mice were used (N = 13 mice). For slice optophysiology, P18-25 (at the time of injection) mice were used. (Fig. 3: N = 14 mice; Fig. 5: N = 5 mice; Fig. 6: N = 7 mice).

VIRUS AND TRACER INJECTIONS

For stereotaxic surgeries, mice were induced to a surgical plane of anesthesia with 5% isoflurane and maintained at 1-2% isoflurane. Mice were placed in a stereotaxic frame (David Kopf Instruments, Tujunga, California) on a feedback-controlled heating pad. Following skin incision, small craniotomies were made above the target regions with a dental drill. The following coordinates (in mm) were used (from bregma): for medial DCN -6.4 AP, ± 0.75 ML, -2.2 DV; for interposed DCN: -6.3 AP, ± 1.6 ML, -2.2 DV; for lateral DCN: -5.7 AP, ± 2.35 ML, -2.18 DV. For basolateral amygdala: -0.85 AP, ± 3.08 ML, -4.5 DV. For limbic thalamus: -0.85 AP, ± 0.3 ML, -3.3 DV, and -1.2 AP, ± 0.5 ML, -3.5 DV. A small amount of tracer (50 – 100 nl for DCN, 300 – 500 nl for thalamus) was pressure-injected in the targeted site with a UMP3-1 ultramicropump (WPI, Sarasota, FL) and glass pipettes (Wiretrol II, Drummond) (tip diameter: 25-50 µm) at a rate of 30 nl/min. The pipette was retracted 10 min after injection, the skin was sutured (Ethilon P-6 sutures, Ethicon, Raritan, NJ) and/or glued (Gluture, Abbott labs, Abbott Park, IL) and animal was allowed to recover completely prior to returning to the home cage.

Preoperative analgesia consisted of a single administration of local lidocaine (VetOne, MWI, Boise, ID; 1 mg/kg) and Meloxicam (Covetrus, Portland, ME; 5 mg/kg), both SC. Postoperative analgesia consisted of a single administration of Buprenex (AmerisourceBergen Drug Corp, Sacramento, CA; 0.1 mg/kg) and Meloxicam 5 mg/kg, both SC, followed by Meloxicam at 24 and 48 hr. The following adeno-associated viruses (AAV) and tracers were used: AAV8-CMV-TurboRFP (Upenn Vector Core, 1.19*10^14 gc/ml), AAV9-CAG-GFP (UNC Vector Core, 2x10^12 gc/ml), AAV2-retro-CAG-GFP (Addgene, 7x10^12 gc/ml), AAV2-retro-AAV-CAG-tdTomato (Addgene, 7x10^12 gc/ml), Cholera toxin subunit B CF-640 (Biotium, 2 mg/ml, 100 nl), AAV1-hSyn-Cre-WPRE-hGH (Addgene, 10^13 gc/ml, diluted 1:5), AAV5-CAG-FLEX-tdtomato (UNC Viral Core, 7.8*10^12 gc/ml, diluted 1:5), AAV9-EF1a-DIO-hChR2(H134R)-EYFP (Addgene, 1.8*10^13 gc/ml, diluted 1:10), AAV2-hSyn-hChR2(H134R)-EYFP (UNC Vector Core, 5.6x10^12 gc/ml, diluted 1:2). Three to five weeks were allowed for viral expression/labelling.

HISTOLOGY AND IMAGING

Following deep anesthesia (anesthetic cocktail: 100 mg/kg ketamine, 10 mg/kg xylazine, 1 mg/kg acepromazine, IP) mice were paraformaldehyde-fixed (4% paraformaldehyde in 0.1 M phosphate buffer, pH 7.4, EMS Diasum, Hatfield, PA) through transcardial perfusion. Brains were post-fixed overnight, cryo-protected with 30% sucrose in PBS and sliced coronally on a sliding microtome at 60-100 µm thickness. Slices were mounted on slides with Mowiol-based mounting media and scanned using an Olympus VS120 Slide Scanner (Olympus, Germany) (resolution with 10x/0.4 N.A. lens at 488 nm: 645 nm in x,y). For immunohistochemistry, slices were blocked with 10% normal goat serum (NGS, Millipore, Burlington, MA) in PBST (0.3%

Triton X-100 in PBS) for 1 h. Slices were incubated with primary antibodies (anti-Cre IgG1, Millipore, 1:1000; anti-NEUN, Cell Signaling, Danvers, MA, 1:1000; anti-vGLUT2, Synaptic Systems, Goettingen, Germany, 1:700; anti-PSD-95, Neuromab, Davis, CA, 1:500) in 2% NGS-PBST overnight at 4°C. After 4 x 20-min rinses with PBST, secondary antibodies (Alexa fluor-568 goat anti-mouse 1:1000 IgG1; Alexa fluor-488 goat anti-rabbit 1:1000; Dylight-405 goat anti-guinea pig 1:200; Alexa fluor-647 goat anti-mouse 1:1000 IgG2a; Life Technologies, Carlsbad, CA) were applied in 2% NGS-PBST for 1-2 h at room temperature. Following another round of rinses, slices were mounted on slides with Mowiol and scanned on an LSM800 confocal microscope with Airyscan (resolution with 63x/1.4 N.A. oil lens at 488 nm: 120 nm in x,y, 350 nm in z) (Zeiss, Germany). Maximal projections of optical z-stacks were obtained with Zen software (Zeiss) or ImageJ and used for analysis.

PREPARATION OF BRAIN SLICES FOR ELECTROPHYSIOLOGY

Mice of either sex (P39-60) were anesthetized through intraperitoneal injection of ketamine/xylazine/acepromazine anesthetic cocktail and transcardially perfused with ice-cold artificial cerebrospinal fluid (aCSF; in mM: 127 NaCl, 2.5 KCl, 1.25 NaH_2PO_4, 25 $NaHCO_3$, 1 $MgCl_2$, 2 $CaCl_2$, 25 glucose; supplemented with 0.4 sodium ascorbate and 2 sodium pyruvate; ~310 mOsm). Brains were rapidly removed, blocked, and placed in choline slurry (110 choline chloride, 25 $NaHCO_3$, 25 glucose, 2.5 KCl, 1.25 NaH_2PO_4, 7 $MgCl_2$, 0.5 $CaCl_2$, 11.6 sodium ascorbate, 3.1 sodium pyruvate; ~310 mOsm). Coronal sections (250 µm) containing the thalamus were cut on a vibratome (Leica VT1200S) and allowed to recover in aCSF at 32°C for 25 min before moving to room temperature until further use. All solutions were bubbled with 95% O_2-5% CO_2 continuously. Chemicals were from Sigma.

ELECTROPHYSIOLOGY

Slices were mounted onto poly-l-lysine-coated glass coverslips and placed in a submersion recording chamber perfused with aCSF (2-3 ml/min) at near physiological temperature (30-32^{o}C). Whole-cell voltage-clamp recordings were made from tdTomato+ (Figs. 3,5) or CtB+ (Fig. 6) cells in the thalamus using borosilicate glass pipettes (3-5 MΩ) filled with internal solution containing (in mM): $CsMSO_3$ 120, CsCl 15, NaCl 8, TEA-Cl 10, HEPES 10, EGTA 0.5, QX314 2, MgATP 4 and NaGTP 0.3, biocytin 0.3. Recordings were acquired in pClamp11 using a Multiclamp 700B amplifier (Molecular Devices, San Jose, CA), digitized at 20 kHz and low-pass filtered at 8 kHz. Membrane potential was maintained at -70 mV. Series resistance and leak current were monitored and recordings were terminated if either of these parameters changed significantly. Optical stimulation of ChR2+ fibers surrounding tdTomato+ or CtB+ thalamic neurons was performed under a 60x water immersion lens (1.0 N.A.) of an Olympus BX51W microscope, using an LED system (Excelitas X-cite; or Prizmatix UHP-T) mounted on the microscope and driven by a Master9 stimulator (AMPI). Optical stimulation consisted of 488 nm light pulses (1-5 ms duration). Power density was set to 1.5-2x threshold (max: 0.25 mW/mm^2). A minimum of 5 response-evoking trials (inter-trial interval: 60 s) were delivered and traces were averaged. To confirm monosynaptic inputs, action potentials were blocked with TTX (1 µM), followed by TTX+ 4AP (100 µM) to prolong ChR2-evoked depolarization [17].

DATA ANALYSIS

Analysis of ex vivo recordings was performed using custom MATLAB R2019b scripts (MathWorks, Natick, MA). Postsynaptic current (PSC) amplitude was computed from the maximum negative deflection from baseline within a time window (2.5 – 40 ms) from

stimulus onset. Onset latency was measured at 10% of peak amplitude. Cell location was confirmed through biocytin-streptavidin Alexa fluor staining. For slice registration the Paxinos Brain Atlas (Paxinos and Franklin, 2001) and the Allen Brain Atlas (ABA_v3) were used. Location of injection sites was identified and experiments were excluded if there was spill into neighboring nuclei. Cell counting and immunofluorescence intensity analyses were done by raters naïve to the experimental hypotheses using ImageJ (Fiji, National Institutes of Health, Bethesda, Maryland) and Abode Illustrator. Statistical analysis was performed in Matlab (Mathworks) and Prism (GraphPad), with significance set at $p < 0.05$.

Results

PUTATIVE DISYNAPTIC PATHWAYS BETWEEN CEREBELLAR NUCLEI AND BLA THROUGH THE LIMBIC THALAMUS

Given that microstimulation of DCN elicits short-latency responses in the BLA (Heath and Harper, 1974; Snider and Maiti, 1976; Heath et al., 1978), we hypothesized that an anatomical pathway exists between the two regions that involves at most two synapses. Initial anatomical tracing experiments did not support a direct DCN-BLA connection (not shown). We therefore performed simultaneous injections of an anterograde tracer virus (AAV8-CMV-TurboRFP) in the DCN and a retrograde tracer virus (AAV2-retro-CAG-GFP) in the BLA (Fig. 1A,B) to identify potential regions of overlap. In epifluorescence images of brain slices across different animals (N = 8), the limbic thalamus consistently emerged as a prominent site of overlap (**Fig. 1C**). We use the term “limbic thalamus” to refer to a collection of non-sensorimotor thalamic nuclei, including the mediodorsal (MD), midline and intralaminar (IL) nuclei, with diverse projections to cortical (mainly medial prefrontal) and/or subcortical limbic structures (Groenewegen and Witter, 2004; Morgane et al., 2005; Jones, 2007; Vertes et al., 2015). Registration of images to the Allen Brain Atlas localized BLA-projecting thalamic neurons in multiple nuclei of the limbic thalamus (Fig. 1D), in agreement with known connectivity patterns (Van der Werf et al., 2002; Vertes et al., 2015; Amir et al., 2018; Hintiryan et al., 2021). Visual inspection of diffraction-limited epifluorescence images identified overlapping DCN axonal projections and BLA-projecting neurons in several (but not all) of these thalamic nuclei, including the parafascicular (PF) n. and subparafascicular area (SPA), the centromedial (CM) and MD nuclei, and other midline

nuclei (Fig. 1E). Injection of the tracer cholera toxin subunit B (CtB)-CF640 in the limbic thalamus retrogradely labeled neurons in DCN (**Fig. 1F**), confirming the DCN-limbic thalamus connectivity.

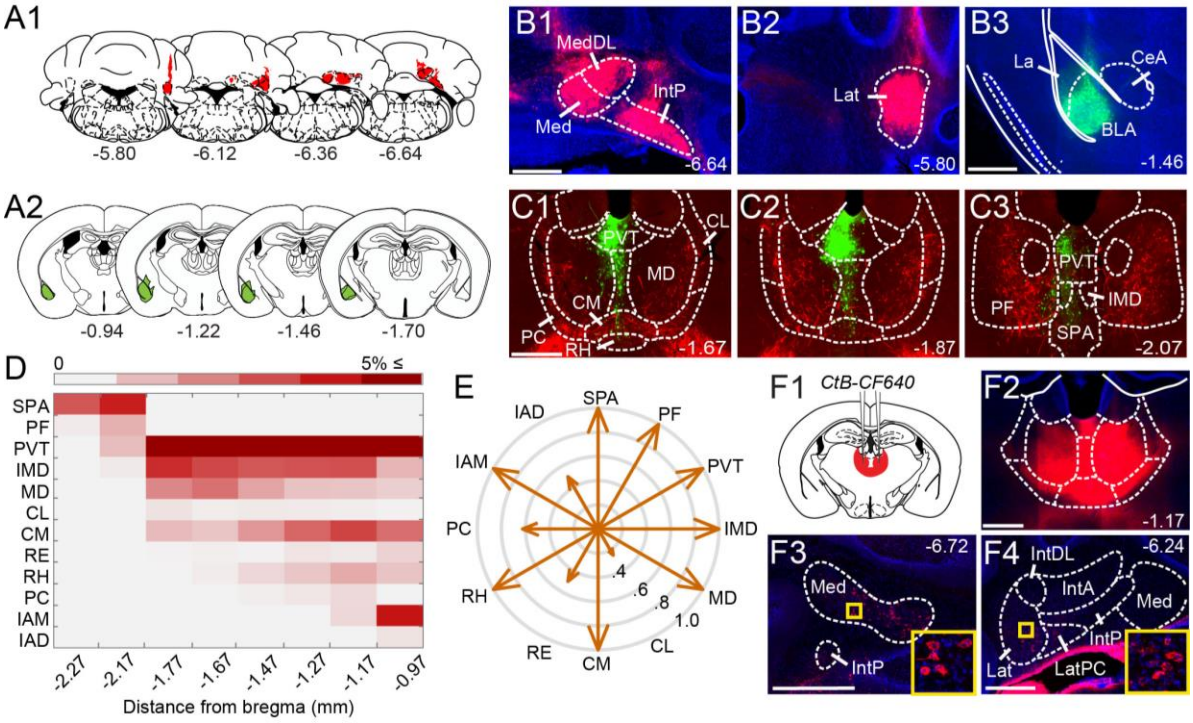

Figure 1. Anatomical tracing uncovers putative disynaptic pathways from cerebellum to basolateral amygdala. A, Unilateral injection sites for anterograde viral tracer in DCN (**A1**, *red*) and retrograde viral tracer in BLA (**A2**, *green*). **B,** Mosaic epifluorescence images of injection sites in DCN (**B1-2**) and BLA (**B3**). **C,** Mosaic epifluorescence images of overlapping DCN axons (red) and BLA-projecting neurons (green) in limbic thalamus. **D,** Relative distribution of BLA-projecting neurons across nuclei of the limbic thalamus, normalized to the total number of labeled neurons and averaged across experiments, as a function of distance from bregma. Antero-posterior coordinates for each nucleus are given in **Table 1**. **E,** Quantification of overlap between DCN axons and BLA-projecting thalamic neurons. Arrow length in radar plot indicates proportion (0-1) of experiments with overlap in each thalamic nucleus. **F1,F2,** Schematic and confocal image of injection site for retrograde tracer CtB CF-640 in limbic thalamus. **F3,F4,** CtB-labeled projection neurons (red) in DCN at different distances from bregma. Insets show high-magnification images of areas in yellow squares. For all panels, numbers denote distance (in mm) from bregma. Scale bars: 500 μm.

TRANSNEURONAL ANATOMICAL TRACING AND OPTOPHYSIOLOGY ESTABLISH SYNAPTIC CONNECTIVITY BETWEEN CEREBELLAR NUCLEI AND LIMBIC THALAMUS

To spatially resolve synaptic connectivity between DCN and BLA-projecting thalamic nuclei, we adopted an AAV-based transneuronal approach (Zingg et al., 2017).

AAV1-Cre in presynaptic neurons is known to propagate across the synapse and induce expression of a floxed tag in postsynaptic neurons, thus identifying synaptic partners (**Fig. 2A**). We injected AAV1-Cre bilaterally in DCN and AAV-FLEX-tdTomato in thalamus and quantified the relative distribution of tdTomato+ neurons in intralaminar and midline thalamic nuclei. Injection coverage for DCN was indicated by Cre immunofluorescence (**Fig. 2B1,2**) and included all cerebellar nuclei. Great care was taken to avoid spill to extracerebellar areas, which resulted in denser coverage of caudal DCN (**Fig. 2B3**). TdTomato+ neurons were observed throughout the limbic thalamus, confirming adequate coverage, and extended into ventromedial nuclei (**Fig. 2C**), which served as positive control (Gornati et al., 2018; Habas et al., 2019). Averaging the relative distribution of tdTomato+ neurons across five successful experiments revealed that the intralaminar cluster, comprised of centrolateral (CL), paracentral (PC), CM, and PF nuclei (Van der Werf et al., 2002), and MD nucleus encompassed most (~95%) tagged neurons (Fig. 2C3), suggesting that these nuclei reliably receive most cerebellar inputs to limbic thalamus.

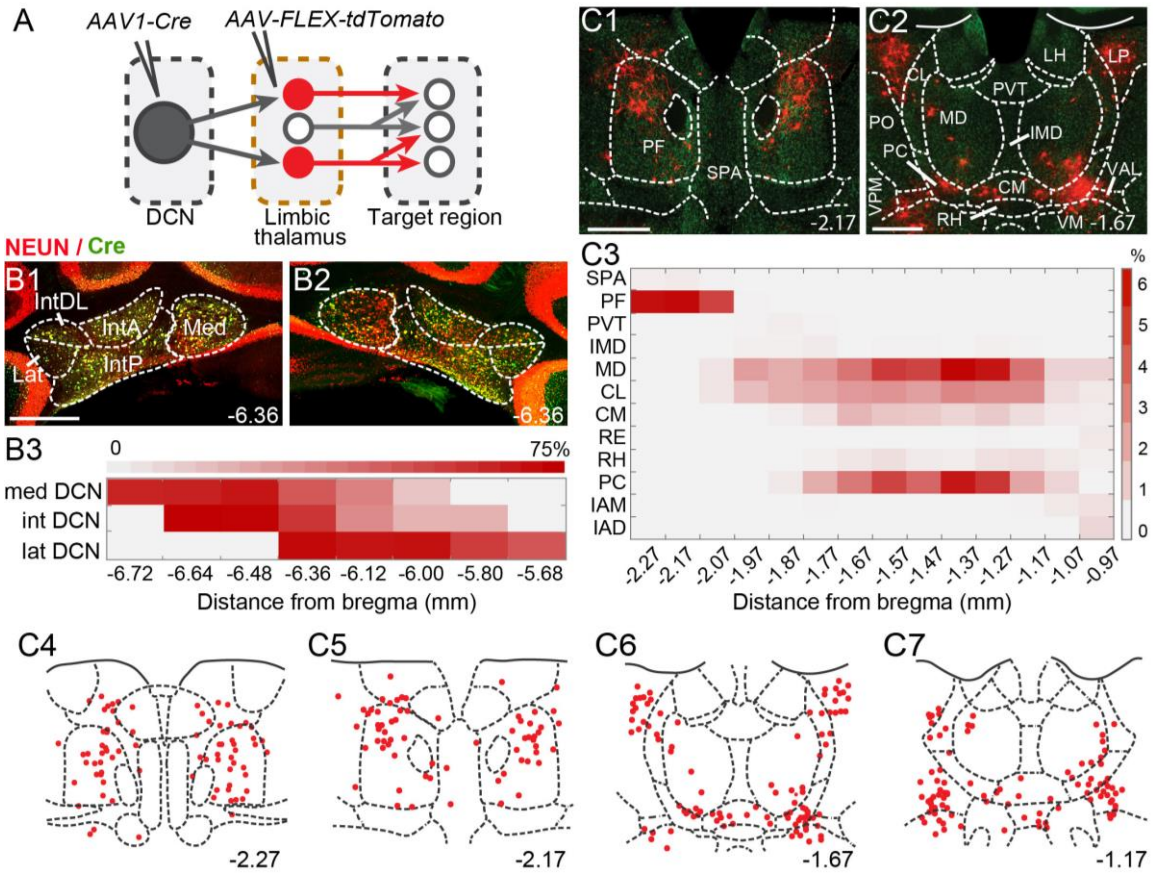

Figure 2. The intralaminar and mediodorsal nuclei are major cerebellar postsynaptic targets in limbic thalamus. A, Schematic of experimental approach for disynaptic pathway tracing. **B1-B2,** Example images of bilateral Cre expression in DCN. Red: immunofluorescence for NeuN neural marker; Green: anti-Cre immunoreactivity; Yellow: merge. **B3,** Heatmap of Cre immunofluorescence in DCN, normalized to NeuN signal and averaged across experiments, as a function of distance (in mm) from bregma. **C1,C2,** Example images of thalamic neurons conditionally expressing tdTomato (red) upon transneuronal transfer of Cre from cerebellar presynaptic axons. Green: NeuN immunofluorescence. **C3,** Heatmap of relative distribution of tdTomato+ neurons across thalamic nuclei, normalized to total number of labeled neurons and averaged across experiments, as a function of distance from bregma. **C4-C7,** Example registration of tdTomato+ neurons to the Allen mouse brain atlas. Numbers at bottom denote distance (in mm) from bregma. Antero-posterior coordinates for each nucleus can be found in **Table 1**. Scale bars: 500 μm.

To confirm that the thalamic targets identified with the transneuronal Cre method receive cerebellar synaptic input, we performed optophysiological experiments in acute thalamic slices from mice injected with AAV1-Cre in the DCN and AAV-FLEX-tdTomato in the thalamus (Fig. 3A). To activate cerebellar inputs, channelrhodopsin (ChR2-H134R) was conditionally expressed in DCN through AAV-DIO-ChR2-EYFP injection.

DCN axonal projections were stimulated in the thalamus with 488-nm light pulses applied through the objective. Light-evoked synaptic responses were monitored in whole-cell voltage-clamp recordings (V_m = -70 mV) from thalamic neurons, which were selected based on tdTomato expression, their anatomical location and position in the slice, i.e., surrounded by ChR2-EYFP-expressing axons. In all thalamic nuclei examined (n = 29 cells), light stimulation elicited synaptic responses (mean response in pA: IL: 311.7 ± 100; MD: 105.7 ± 32.3; midline: 565.8 ± 209.8; VM/VPM: 347.5 ± 112.3; LP: 91.8 ± 2.7) (**Fig. 3B1**) with short latencies (mean latency in ms: IL: 2.5 ± 0.28; MD: 3.3 ± 0.6; midline: 4.2 ± 0.7; VM/VPM: 3.2 ± 0.2; LP: 2.9 ± 0.8) (**Fig. 3B2**). These data support the specificity of the anatomical connectivity and establish the existence of active DCN terminals (as opposed to just passing axons) across limbic thalamus.

Abbreviation	**Structure**	**AP coordinates**
BLA	Basolateral amygdaloid nucleus	-0.67 mm to -3.07 mm
CeA	Central amygdala	-0.57 mm to -2.07 mm
CL	Central lateral nucleus of the thalamus	-0.97 mm to -1.97 mm
CM	Central medial nucleus of the thalamus	-0.67 mm to -1.97 mm
DCN	Deep cerebellar nuclei	
IAM	Interanteromedial thalamic nucleus	-0.77 mm to -1.07 mm
IMD	Intermediodorsal nucleus of the thalamus	-0.87 mm to -2.07 mm
Int	Interposed cerebellar nucleus	-6.64 mm to -5.8 mm
IntA	- anterior part	
IntDL	- dorsolateral part	
IntP	- posterior part	
La	Lateral amygdaloid nucleus	-0.87 mm to -2.47 mm
Lat	Lateral cerebellar nucleus	-6.36 mm to -5.68 mm
LP	Lateral posterior thalamic nucleus	-1.27 mm to -3.17 mm
Med	Medial cerebellar nucleus	-6.84 mm to -5.88 mm
MD	Mediodorsal nucleus of the thalamus	-0.57 mm to -1.97 mm

NAc	Nucleus accumbens	
PC	Paracentral nucleus of the thalamus	-1.07 mm to -1.87 mm
PF	Parafascicular nucleus	-1.97 mm to -2.37 mm
PVT	Paraventicular thalamus	-0.17 mm to -2.07 mm
PO	Posterior thalamic nucleus	-1.27 mm to 2.37 mm
PrL	Prelimbic cortex	
RE	Reuniens thalamic nucleus	-0.37 mm to -1.77 mm
RH	Rhomboid thalamic nucleus	-0.77 mm to -1.67 mm
SPA	Subparafascicular area	-2.07 mm to -2.27 mm
VL	Ventrolateral thalamic nucleus	-0.67 mm to -2.27 mm
VM	Ventromedial thalamic nucleus	-0.67 mm to -2.07 mm

Table 1. Anatomical abbreviations (in alphabetical order) and antero-posterior coordinates (in mm, from bregma)

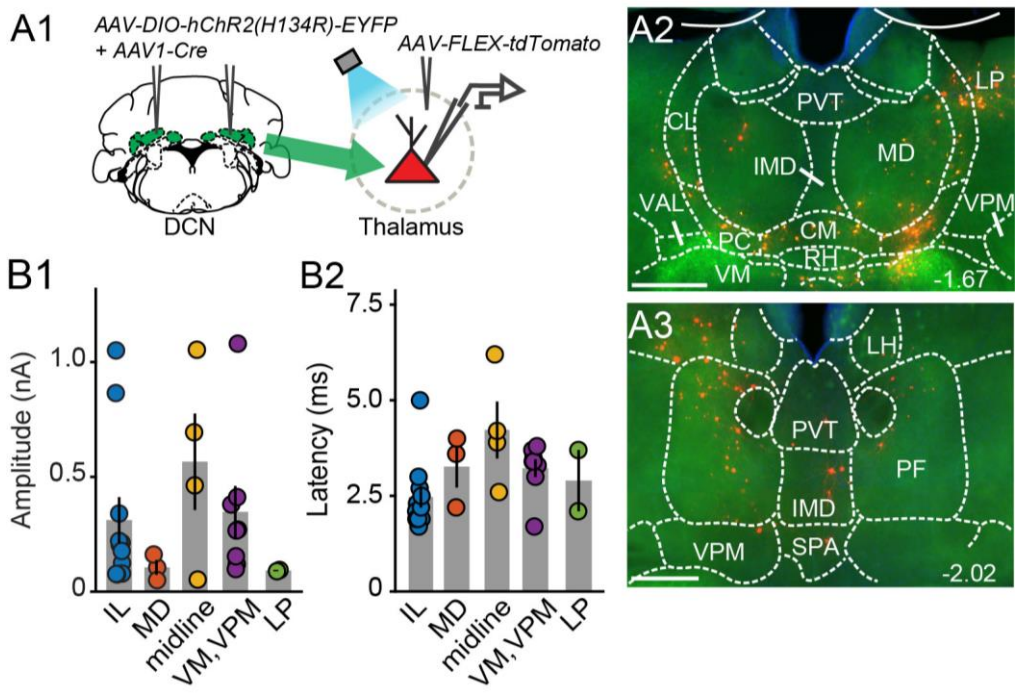

Figure 3. Electrophysiological validation of virally-identified cerebello-thalamic connectivity. **A1,** Schematic of experimental approach for ex vivo optophysiology. **A2,A3,** Epifluorescence images of anterior (A2) and posterior (A3) thalamic slices acutely prepared for recordings. DCN input-receiving neurons are tdTomato+. Scale bars: 500 µm. **B,** Average (± SEM) amplitude (**B1**) and onset latency (**B2**) of ChR2-evoked synaptic currents as a function of recording location in the thalamus. Intralaminar (IL) group: CL, PC, CM and PF; midline group: IMD and RH.

THALAMIC NEURONS RECEIVING CEREBELLAR INPUT PROJECT TO BLA

If the thalamus is a functional node of the disynaptic DCN-BLA circuit, then we would expect to find axons of DCN input-receiving thalamic neurons in BLA. To this end, we imaged BLA-containing slices from transsynaptic Cre experiments (Fig. 4A). We detected tdTomato+ axons at several antero-posterior distances from bregma (Fig. 4B1-B6). Using immunohistochemistry with antibodies against pre- and postsynaptic markers of excitatory synapses (vesicular glutamate transporter, vGLUT2; PSD-95), and super-resolution airyscan confocal imaging, we found tight colocalization between tdTomato+ axonal varicosities, vGLUT2 and PSD-95, an example of which is shown in Fig. 4C. This finding suggests that axons of thalamic neurons receiving cerebellar input form morphological synapses in the BLA. Axonal projections of DCN input-receiving thalamic neurons were also observed in other limbic regions including the nucleus accumbens core and shell (Fig. 4D1,D2) and anterior cingulate/prelimbic cortex (**F**ig. 4D3,D4).

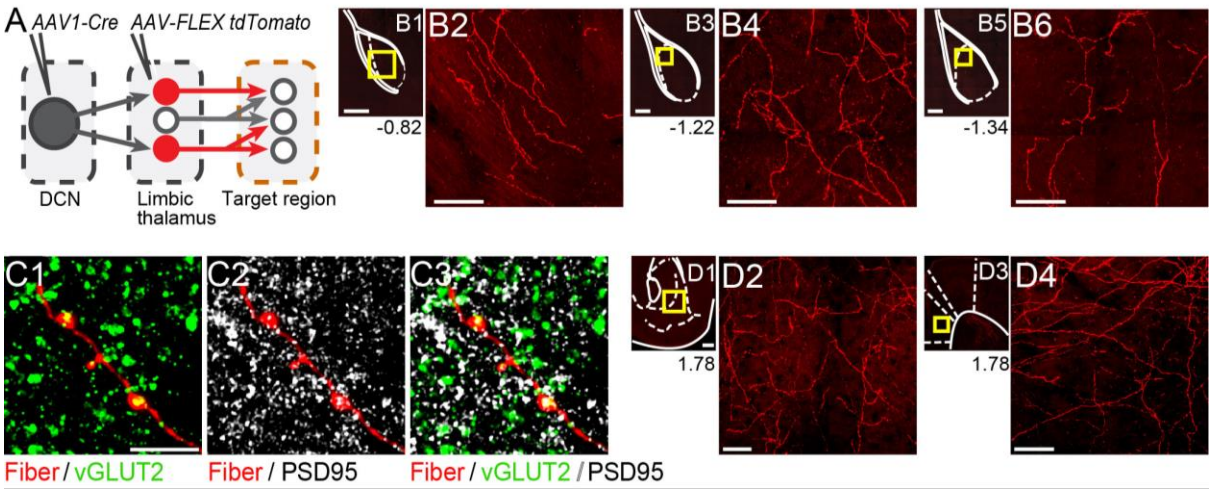

Figure 4. Thalamic neurons receiving cerebellar input form synapses in basolateral amygdala and also target the nucleus accumbens and prelimbic cortex. A, Schematic diagram of experimental approach. Targets of tdTomato+ axons of thalamic neurons receiving cerebellar input were identified through imaging. **B,** Mosaic confocal images of tdTomato+ axons along the anterior-posterior axis of the BLA. **C,** High resolution airyscan confocal images of tdTomato+ axons in the BLA colocalizing with presynaptic (vGLUT2) (**C1**) and postsynaptic (PSD95) (**C2**) markers of excitatory synapses. Green: vGLUT2, gray: PSD95, yellow/white in **C3**: overlay. **D,** tdTomato+ axons in nucleus accumbens (**D1,D2**) and prelimbic cortex (**D3,D4**). Yellow squares in B1,B3,B5 and D1,D3 show zoom-in areas for B2,B4,B6 and D2,D4 images, respectively. Numbers at bottom of images indicate distance (in mm) from bregma. Scale bars: B1,B3,B5,D1,D3: 200 μm; B2,B4,B6,D2,D4: 50 μm; C1-C3: 5 μm.

THE CENTROMEDIAL AND PARAFASCICULAR NUCLEI EMERGE AS FUNCTIONAL NODES IN CEREBELLO-AMYGDALA CIRCUIT

Our tracer overlap studies pointed to multiple thalamic nuclei as potential relays of cerebellar signals to BLA (Fig. 1E). Among them, the MD, CM and PF nuclei showed higher relative distribution of both BLA-projecting neurons and neurons that receive DCN input (Figs. 1D, 2C). For the remainder of this study, we focused on CM and PF nuclei and sought to substantiate their role as anatomical and functional relays of DCN-BLA connectivity through super-resolution microscopy and optophysiology.

Airyscan confocal imaging of slices from dual-tracer experiments (Fig. 1) revealed fluorescently labeled DCN axons (red) in contact with neurons that were retrogradely labeled from the BLA (green) in both CM (Fig. 5A1,A2) and PF (Fig. 5A3-5) nuclei. The

existence of functional monosynaptic DCN-CM/PF connections was tested in the subset of electrophysiological experiments from Fig. 3 that targeted CM/PF neurons (Fig. 5B). Under basal conditions, CM/PF neurons received synaptic inputs from the DCN (at Vm = -70 mV; average amplitude ± SEM: -197.5 pA ± - 80.14, n = 6) (Fig. 5C1**,**C5) with short onset latency (average latency ± SEM: 2.4 ms ± 0.18) (Fig. 5C6), which is consistent with direct monosynaptic connections. Application of the sodium channel blocker tetrodotoxin (TTX) abolished the inputs (average amplitude ± SEM: -5.1 pA ± -2.03) (Fig. 5C2,C4-5), which recovered upon addition of the potassium channel blocker 4-AP (average amplitude ± SEM: -151.8 pA ± -39.52) (Fig., 5C3**-5**) (Friedman's non-parametric repeated measures ANOVA: $x^2_r = 9$, n = 6, p = 0.008; Dunn's multiple comparison test: Baseline vs TTX: p = 0.02, Baseline vs TTX+4AP: p = 0.99), confirming their monosynaptic nature.

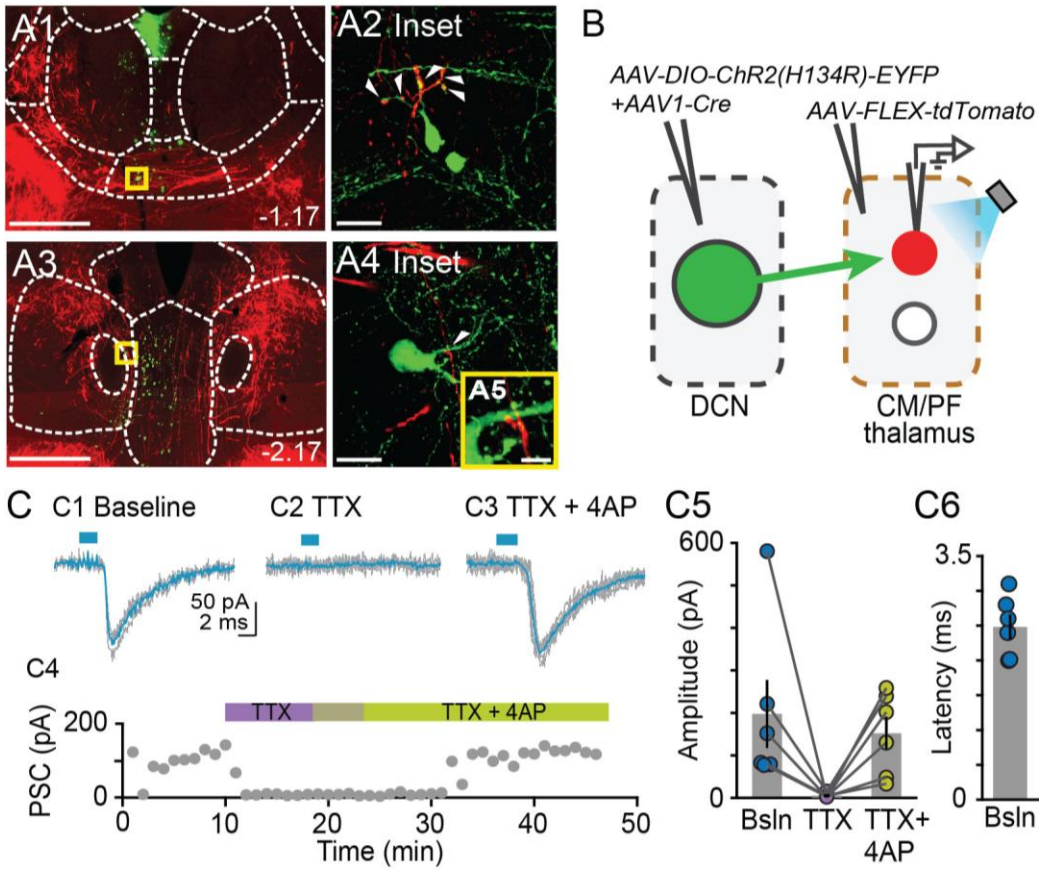

Figure 5. Centromedial and parafascicular neurons project to basolateral amygdala and receive functional monosynaptic input from the cerebellum. A1-A4, Airyscan confocal images of DCN axons (red) and BLA-projecting neurons (green) in the centromedial (CM; A**1**) and parafascicular (PF; A**3**) thalamic nuclei. **A2, A4-5,** zoomed-in areas in yellow squares from A1 and A3. Scale bars: A1,A3: 500 µm; A2,A4: 20 µm; A5: 5 µm. **B,** Schematic diagram of ex vivo optophysiology approach to test for monosynaptic connections between DCN and CM/PF thalamic n. **C1-C3,** Average ChR2-evoked synaptic current (teal), overlaid onto single trial responses (gray), at baseline (**C1**); upon addition of the action potential blocker tetrodotoxin (TTX, 1 uM) (**C2**); after further addition of the potassium channel blocker 4-aminopyridine (4AP, 100 uM) (**C3**). **C4**, Time course of wash-in experiment for the same example cell. **C5,** Summary of effects on amplitude (mean ± SEM) of ChR2-evoked synaptic responses for the indicated conditions. Bsln: baseline. **C6,** Average (± SEM) onset latency of ChR2-evoked responses at baseline.

Finally, we tested whether BLA is a target of DCN input-receiving CM/PF neurons (**Fig. 6**). We virally expressed ChR2 in DCN and stimulated cerebellar axonal projections in thalamic slices while recording from BLA-projecting CM/PF neurons (whole-cell voltage clamp mode, Vm = -70 mV), which were retrogradely labeled with CtB-CF568 in BLA (Fig. 6A). Optogenetic stimulation elicited reliable DCN-CM/PF synaptic responses

(average amplitude ± SEM: -104.1 pA ± -37.1, n = 8) (Fig. 6C,D1) with short latency (3.35 ms ± 0.25) (Fig. 6D2). Combined with the imaging findings (Fig. 5), our electrophysiological results argue strongly for a DCN-BLA disynaptic circuit that recruits CM/PF nuclei as node.

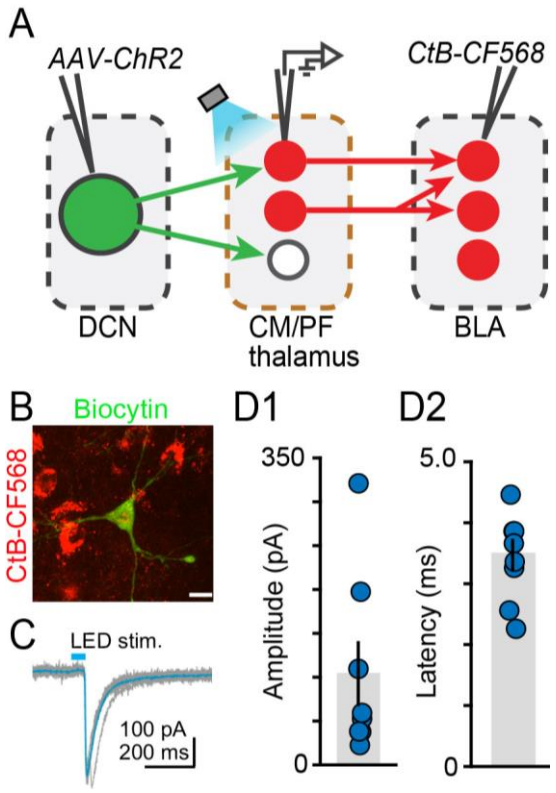

Figure 6. The centromedial and parafascicular thalamus is a functional node of the cerebello-amygdala circuit. A, Experimental approach. **B,** Example BLA-projecting neuron in centromedial (CM) thalamus retrogradely labeled with CtB CF-568 (red) is also labeled with biocytin (green) through the patch pipette. Scale bar = 10 μm. **C,** Example ChR2-evoked synaptic response. Average trace (teal) overlaid onto single trials (gray). **D1,D2,** Average (± SEM) amplitude (D1) and onset latency (D2) of ChR2-evoked synaptic currents at DCN-CM/PF synapses.

Discussion

Cerebellar connections with the amygdala have been posited previously but the neuroanatomical substrate of this connectivity has been elusive (Strick et al., 2009; D'Angelo and Casali, 2012; Adamaszek et al., 2017). Here, we obtained insight into cerebello-amygdala circuitry by combining various tracing approaches with advanced imaging and optophysiology. We established the existence of a disynaptic circuit between cerebellar nuclei and BLA, thus providing the first blueprint of cerebello-amygdala connectivity at the mesoscale level. The circuit recruits at least the centromedial and parafascicular thalamic nuclei (Figs. 5,6), and most likely also other nuclei of the limbic thalamus (Fig. 1), as relay nodes. In addition, we identified the intralaminar thalamic cluster and MD nucleus as recipients of the majority of cerebellar inputs to limbic thalamus (Fig. 2). Finally, and in addition to BLA, we identified axonal projections of DCN input-receiving thalamic neurons in limbic regions such as nucleus accumbens core and shell and anterior cingulate/prelimbic cortex (Fig. 4)

THE LIMBIC THALAMUS AS A TARGET OF CEREBELLAR INPUTS

We targeted the limbic thalamus as a conduit of cerebello-amygdala communication because several of its nuclei foster BLA-projecting neurons in close proximity to DCN axons (Fig. 1). DCN projections to limbic thalamus have been observed before (Hendry et al., 1979; Haroian et al., 1981; Ichinohe et al., 2000; Fujita et al., 2020; Judd et al., 2021) but the existence of functional synaptic terminals has only been validated for centrolateral and PF intralaminar nuclei (Gornati et al., 2018; Xiao et al., 2018), and never on amygdala-projecting neurons. Our optophysiological experiments also provided first evidence for the presence of active synaptic connections (as opposed to just passing axons) in paracentral and centromedial (part of intralaminar

group), intermediodorsal and rhomboid (part of midline group), and mediodorsal nuclei (Fig. 3), expanding the repertoire of non-motor cerebellar targets and paving the way for causal manipulations.

TECHNICAL CONSIDERATIONS

To chart cerebello-amygdala neuroanatomical connections, we used powerful circuit mapping tools including anterograde and retrograde tracer viruses and the transneuronal AAV1-Cre approach (Tervo et al., 2016; Zingg et al., 2017, 2020; Nectow and Nestler, 2020). A distinct advantage of our approach, which combined AAV1-Cre with viral injections of conditionally expressed fluorescent tracers (as opposed to reporter mouse lines), is the ability to definitively point to the thalamus as the source of the axonal projections in BLA, nucleus accumbens and prelimbic cortex- as opposed to e.g., the VTA, which also receives DCN inputs and projects to these regions (Phillipson, 1979; Kuroda et al., 1996; Beier et al., 2015; Breton et al., 2019; D'Ambra et al., 2020). Thus, our approach enabled conclusive interpretation of anatomical connectivity results. On the other hand, injection coverage/spill and viral tropism (Nectow and Nestler, 2020) need to be considered. Tropism, in particular, could skew interpretation of disynaptic inputs, as some cell groups in the limbic thalamus might be more efficiently infected by AAVs. Tropism could also explain why recent efforts to trace di- and tri-synaptic cerebellar efferent pathways with herpes simplex viruses did not identify the CM/PF pathway to BLA (Pisano et al., 2021). Lastly, one potential concern could be the propensity of AAVs to be transported in the retrograde direction at high titers (Rothermel et al., 2013; Zingg et al., 2017). To remediate these concerns, we used strict inclusion criteria for injection sites; employed a combination of viral and non-viral anterograde

and retrograde tracers; optimized viral titers to minimize retrograde transport; and confirmed circuit connections with slice optophysiology.

PROPOSED FUNCTIONS OF THE DCN-BLA CIRCUIT

Our discovery of the DCN-BLA connection through the CM/PF thalamic nuclei provides an essential map for future investigation of circuit function. The circuit, which could account for the previously observed short-latency cerebello-amygdala responses (Heath and Harper, 1974), could convey cerebellar information about prediction, salience and/or valence to BLA, shaped by the intrinsic, synaptic and integrative properties of the nodes. Indeed, the cerebellum is known to encode such information (Ohmae and Medina, 2015; Wagner et al., 2017; Hull, 2020; Ma et al., 2020; Bina et al., 2021; Shuster et al., 2021), which is also seen in BLA (Paton et al., 2006; Adolphs, 2010; Janak and Tye, 2015; Sengupta et al., 2018; Zhang and Li, 2018; Gründemann et al., 2019; Brockett et al., 2021), and which is thought to be used by CM and PF during aversive conditioning, observational learning and reward-seeking behavior (Jeon et al., 2010; Sengupta and McNally, 2014; Vertes et al., 2015; Xiao et al., 2018; Cover and Mathur, 2021; Rizzi et al., 2021).

The cellular targets of cerebello-thalamic axons in BLA remain to be determined but likely include at least BLA principle neurons, which are the major recipients of CM input (Ahmed et al., 2021). The patterns of BLA ensemble activity triggered by distinct cerebello-thalamic inputs could serve different aspects of cerebellum-dependent emotional functionality, which includes modulation of anxiety and learned fear (Sacchetti et al., 2007; Duvarci and Pare, 2014; Tovote et al., 2015; Otsuka et al., 2016; Frontera et al., 2020; Rudolph et al., 2020); processing of facial emotional expressions (Wang et al., 2017; Ferrari et al., 2018); regulation of emotional reactivity (Turner et al., 2007;

Machado et al., 2009); and even reward-driven motivated behavior (Murray, 2007; Bauer et al., 2011; Peterson et al., 2012; Carta et al., 2019).

The BLA is not the sole nucleus in the amygdala complex that receives cerebellar signals (Magal and Mintz, 2014). Similarly, it is unlikely that the CM and PF are the only nuclei to serve cerebello-amygdala communication (our findings; and (Kang et al., 2021)). Further studies are warranted to delineate the complete neuroanatomical and functional landscape of cerebello-amygdala connectivity. Our findings constitute the first step toward this goal.

Acknowledgments

We thank Dr. Brian Wiltgen of UC Davis for access to imaging equipment; and Fioravante lab members for comments on a previous version of the manuscript, which has appeared as pre-print on BioRxiv (https://doi.org/10.1101/2022.02.07.479043).

References

Adamaszek M, D'Agata F, Ferrucci R, Habas C, Keulen S, Kirkby KC, Leggio M, Mariën P, Molinari M, Moulton E, Orsi L, Van Overwalle F, Papadelis C, Priori A, Sacchetti B, Schutter DJ, Styliadis C, Verhoeven J (2017) Consensus Paper: Cerebellum and Emotion. The Cerebellum 16:552–576.

Adolphs R (2010) What does the amygdala contribute to social cognition? Annals of the New York Academy of Sciences 1191:42–61.

Ahmed N, Headley DB, Paré D (2021) Optogenetic study of central medial and paraventricular thalamic projections to the basolateral amygdala. Journal of Neurophysiology 126:1234–1247.

Ahs F, Pissiota A, Michelgård A, Frans O, Furmark T, Appel L, Fredrikson M (2009) Disentangling the web of fear: amygdala reactivity and functional connectivity in spider and snake phobia. Psychiatry Res 172:103–108.

Amir A, Paré J, Smith Y, Paré D (2018) Midline thalamic inputs to the amygdala: Ultrastructure and synaptic targets. Journal of Comparative Neurology Available at: https://onlinelibrary.wiley.com/doi/abs/10.1002/cne.24557 [Accessed May 18, 2019].

Bauer DJ, Kerr AL, Swain RA (2011) Cerebellar dentate nuclei lesions reduce motivation in appetitive operant conditioning and open field exploration. Neurobiology of Learning and Memory 95:166–175.

Beier KT, Steinberg EE, DeLoach KE, Xie S, Miyamichi K, Schwarz L, Gao XJ, Kremer EJ, Malenka RC, Luo L (2015) Circuit Architecture of VTA Dopamine Neurons Revealed by Systematic Input-Output Mapping. Cell 162:622–634.

Bina L, Romano V, Hoogland TM, Bosman LWJ, De Zeeuw CI (2021) Purkinje cells translate subjective salience into readiness to act and choice performance. Cell Reports 37:110116.

Breton JM, Charbit AR, Snyder BJ, Fong PTK, Dias EV, Himmels P, Lock H, Margolis EB (2019) Relative contributions and mapping of ventral tegmental area dopamine and GABA neurons by projection target in the rat. Journal of Comparative Neurology 527:916–941.

Brockett AT, Vázquez D, Roesch MR (2021) Prediction errors and valence: From single units to multidimensional encoding in the amygdala. Behavioural Brain Research 404:113176.

Buckner RL (2013) The cerebellum and cognitive function: 25 years of insight from anatomy and neuroimaging. Neuron 80:807–815.

Carta I, Chen CH, Schott AL, Dorizan S, Khodakhah K (2019) Cerebellar modulation of the reward circuitry and social behavior. Science 363:eaav0581.

Cover KK, Mathur BN (2021) Rostral Intralaminar Thalamus Engagement in Cognition and Behavior. Front Behav Neurosci 15:652764.

Damasio AR, Grabowski TJ, Bechara A, Damasio H, Ponto LLB, Parvizi J, Hichwa RD (2000) Subcortical and cortical brain activity during the feeling of self-generated emotions. Nat Neurosci 3:1049–1056.

D'Ambra A, Jung SJ, Ganesan S, Antzoulatos EG, Fioravante D (2020) Cerebellar Activation Bidirectionally Regulates Nucleus Accumbens Shell and Core. BioRxiv https://doi.org/10.1111/j.1460-9568.1996.tb01596.x Available at:

http://biorxiv.org/lookup/doi/10.1101/2020.09.28.283952 [Accessed January 12, 2021].
D'Angelo E, Casali S (2012) Seeking a unified framework for cerebellar function and dysfunction: from circuit operations to cognition. Front Neural Circuits 6:116.
Duvarci S, Pare D (2014) Amygdala Microcircuits Controlling Learned Fear. Neuron 82:966–980.
Ernst M (2002) Decision-making in a Risk-taking Task A PET Study. Neuropsychopharmacology 26:682–691.
Ernst TM, Brol AE, Gratz M, Ritter C, Bingel U, Schlamann M, Maderwald S, Quick HH, Merz CJ, Timmann D (2019) The cerebellum is involved in processing of predictions and prediction errors in a fear conditioning paradigm. eLife 8 Available at: https://elifesciences.org/articles/46831 [Accessed July 2, 2020].
Farley SJ, Radley JJ, Freeman JH (2016) Amygdala Modulation of Cerebellar Learning. J Neurosci 36:2190–2201.
Ferrari C, Oldrati V, Gallucci M, Vecchi T, Cattaneo Z (2018) The role of the cerebellum in explicit and incidental processing of facial emotional expressions: A study with transcranial magnetic stimulation. NeuroImage 169:256–264.
Frontera JL, Baba Aissa H, Sala RW, Mailhes-Hamon C, Georgescu IA, Léna C, Popa D (2020) Bidirectional control of fear memories by cerebellar neurons projecting to the ventrolateral periaqueductal grey. Nature Communications 11 Available at: http://www.nature.com/articles/s41467-020-18953-0 [Accessed January 12, 2021].
Fujita H, Kodama T, du Lac S (2020) Modular output circuits of the fastigial nucleus for diverse motor and nonmotor functions of the cerebellar vermis. eLife 9:e58613.
Gornati SV, Schäfer CB, Eelkman Rooda OHJ, Nigg AL, De Zeeuw CI, Hoebeek FE (2018) Differentiating Cerebellar Impact on Thalamic Nuclei. Cell Rep 23:2690–2704.
Groenewegen H, Witter M (2004) Thalamus. In: The Rat Nervous System. Oxford: Academic Press.
Gründemann J, Bitterman Y, Lu T, Krabbe S, Grewe BF, Schnitzer MJ, Lüthi A (2019) Amygdala ensembles encode behavioral states. Science 364:eaav8736.
Guell X, Gabrieli JDE, Schmahmann JD (2018) Triple representation of language, working memory, social and emotion processing in the cerebellum: convergent evidence from task and seed-based resting-state fMRI analyses in a single large cohort. NeuroImage 172:437–449.
Guo Z, Chen J, Liu S, Li Y, Sun B, Gao Z (2013) Brain areas activated by uncertain reward-based decision-making in healthy volunteers. Neural Regen Res 8:3344–3352.
Habas C, Manto M, Cabaraux P (2019) The Cerebellar Thalamus. The Cerebellum Available at: http://link.springer.com/10.1007/s12311-019-01019-3 [Accessed May 12, 2019].
Han J-K, Kwon S-H, Kim YG, Choi J, Kim J-I, Lee Y-S, Ye S-K, Kim SJ (2021) Ablation of STAT3 in Purkinje cells reorganizes cerebellar synaptic plasticity in long-term fear memory network. eLife 10:e63291.
Haroian AJ, Massopust LC, Young PA (1981) Cerebellothalamic projections in the rat:

An autoradiographic and degeneration study. The Journal of Comparative Neurology 197:217–236.
Heath RG, Dempesy CW, Fontana CJ, Myers WA (1978) Cerebellar stimulation: effects on septal region, hippocampus, and amygdala of cats and rats. Biol Psychiatry 13:501–529.
Heath RG, Harper JW (1974) Ascending projections of the cerebellar fastigial nucleus to the hippocampus, amygdala, and other temporal lobe sites: evoked potential and histological studies in monkeys and cats. Exp Neurol 45:268–287.
Hendry SHC, Jones EG, Graham J (1979) Thalamic relay nuclei for cerebellar and certain related fiber systems in the cat. The Journal of Comparative Neurology 185:679–713.
Hintiryan H et al. (2021) Connectivity characterization of the mouse basolateral amygdalar complex. Nat Commun 12:2859.
Hull C (2020) Prediction signals in the cerebellum: beyond supervised motor learning. eLife 9 Available at: https://elifesciences.org/articles/54073 [Accessed July 2, 2020].
Ichinohe N, Mori F, Shoumura K (2000) A di-synaptic projection from the lateral cerebellar nucleus to the laterodorsal part of the striatum via the central lateral nucleus of the thalamus in the rat. Brain Research 880:191–197.
Ito M (2006) Cerebellar circuitry as a neuronal machine. Prog Neurobiol 78:272–303.
Janak PH, Tye KM (2015) From circuits to behaviour in the amygdala. Nature 517:284–292.
Jeon D, Kim S, Chetana M, Jo D, Ruley HE, Lin S-Y, Rabah D, Kinet J-P, Shin H-S (2010) Observational fear learning involves affective pain system and Cav1.2 Ca2+ channels in ACC. Nat Neurosci 13:482–488.
Jhangiani-Jashanmal IT, Yamamoto R, Gungor NZ, Paré D (2016) Electroresponsive properties of rat central medial thalamic neurons. Journal of Neurophysiology 115:1533–1541.
Jones EG (2007) The thalamus, 2nd ed. Cambridge, MA: Cambridge University Press.
Judd EN, Lewis SM, Person AL (2021) Diverse inhibitory projections from the cerebellar interposed nucleus. eLife 10:e66231.
Kang S, Jun S, Baek SJ, Park H, Yamamoto Y, Tanaka-Yamamoto K (2021) Recent Advances in the Understanding of Specific Efferent Pathways Emerging From the Cerebellum. Front Neuroanat 15:759948.
Kelly E et al. (2020) Regulation of autism-relevant behaviors by cerebellar–prefrontal cortical circuits. Nature Neuroscience Available at: http://www.nature.com/articles/s41593-020-0665-z [Accessed July 13, 2020].
Kuroda M, Murakami K, Igarashi H, Okada A (1996) The Convergence of Axon Terminals from the Mediodorsal Thalamic Nucleus and Ventral Tegmental Area on Pyramidal Cells in Layer V of the Rat Prelimbic Cortex. European Journal of Neuroscience 8:1340–1349.
Kyriazi P, Headley DB, Pare D (2018) Multi-dimensional Coding by Basolateral Amygdala Neurons. Neuron 99:1315-1328.e5.
Liang KJ, Carlson ES (2019) Resistance, vulnerability and resilience: A review of the cognitive cerebellum in aging and neurodegenerative diseases. Neurobiology of Learning and Memory Available at:

https://linkinghub.elsevier.com/retrieve/pii/S107474271930005X [Accessed June 4, 2019].
Lorivel T, Roy V, Hilber P (2014) Fear-related behaviors in Lurcher mutant mice exposed to a predator. Genes Brain Behav 13:794–801.
Ma M, Futia GL, de Souza FMS, Ozbay BN, Llano I, Gibson EA, Restrepo D (2020) Molecular layer interneurons in the cerebellum encode for valence in associative learning. Nature Communications 11 Available at: http://www.nature.com/articles/s41467-020-18034-2 [Accessed September 21, 2020].
Machado CJ, Kazama AM, Bachevalier J (2009) Impact of amygdala, orbital frontal, or hippocampal lesions on threat avoidance and emotional reactivity in nonhuman primates. Emotion 9:147–163.
Magal A, Mintz M (2014) Inhibition of the amygdala central nucleus by stimulation of cerebellar output in rats: a putative mechanism for extinction of the conditioned fear response. Eur J Neurosci 40:3548–3555.
Mitchell AS (2015) The mediodorsal thalamus as a higher order thalamic relay nucleus important for learning and decision-making. Neuroscience & Biobehavioral Reviews 54:76–88.
Morgane P, Galler J, Mokler D (2005) A review of systems and networks of the limbic forebrain/limbic midbrain. Progress in Neurobiology 75:143–160.
Moulton EA, Elman I, Becerra LR, Goldstein RZ, Borsook D (2014) The cerebellum and addiction: insights gained from neuroimaging research. Addict Biol 19:317–331.
Moulton EA, Schmahmann JD, Becerra L, Borsook D (2010) The cerebellum and pain: Passive integrator or active participator? Brain Research Reviews 65:14–27.
Murray EA (2007) The amygdala, reward and emotion. Trends in Cognitive Sciences 11:489–497.
Nectow AR, Nestler EJ (2020) Viral tools for neuroscience. Nat Rev Neurosci 21:669–681.
Ohmae S, Medina JF (2015) Climbing fibers encode a temporal-difference prediction error during cerebellar learning in mice. Nature Neuroscience 18:1798–1803.
O'Neill P-K, Gore F, Salzman CD (2018) Basolateral amygdala circuitry in positive and negative valence. Current Opinion in Neurobiology 49:175–183.
Otsuka S, Konno K, Abe M, Motohashi J, Kohda K, Sakimura K, Watanabe M, Yuzaki M (2016) Roles of Cbln1 in Non-Motor Functions of Mice. J Neurosci 36:11801–11816.
Parker KL, Narayanan NS, Andreasen NC (2014) The therapeutic potential of the cerebellum in schizophrenia. Frontiers in Systems Neuroscience 8:163.
Paton JJ, Belova MA, Morrison SE, Salzman CD (2006) The primate amygdala represents the positive and negative value of visual stimuli during learning. Nature 439:865–870.
Peterson TC, Villatoro L, Arneson T, Ahuja B, Voss S, Swain RA (2012) Behavior modification after inactivation of cerebellar dentate nuclei. Behavioral Neuroscience 126:551–562.
Petreanu L, Mao T, Sternson SM, Svoboda K (2009) The subcellular organization of neocortical excitatory connections. Nature 457:1142–1145.
Phillips JR, Hewedi DH, Eissa AM, Moustafa AA (2015) The Cerebellum and Psychiatric

Disorders. Frontiers in Public Health 3.
Phillipson OT (1979) Afferent projections to the ventral tegmental area of Tsai and interfascicular nucleus: A horseradish peroxidase study in the rat. The Journal of Comparative Neurology 187:117–143.
Pisano TJ, Dhanerawala ZM, Kislin M, Bakshinskaya D, Engel EA, Hansen EJ, Hoag AT, Lee J, de Oude NL, Venkataraju KU, Verpeut JL, Hoebeek FE, Richardson BD, Boele H-J, Wang SS-H (2021) Homologous organization of cerebellar pathways to sensory, motor, and associative forebrain. Cell Reports 36:109721.
Ploghaus A, Tracey I, Gati JS, Clare S, Menon RS, Matthews PM, Rawlins JN (1999) Dissociating pain from its anticipation in the human brain. Science 284:1979–1981.
Reeber SL, Otis TS, Sillitoe RV (2013) New roles for the cerebellum in health and disease. Frontiers in Systems Neuroscience 7 Available at: http://journal.frontiersin.org/article/10.3389/fnsys.2013.00083/abstract [Accessed February 23, 2015].
Rizzi G, Li Z, Hogrefe N, Tan KR (2021) Lateral ventral tegmental area GABAergic and glutamatergic modulation of conditioned learning. Cell Reports 34:108867.
Rothermel M, Brunert D, Zabawa C, Diaz-Quesada M, Wachowiak M (2013) Transgene Expression in Target-Defined Neuron Populations Mediated by Retrograde Infection with Adeno-Associated Viral Vectors. Journal of Neuroscience 33:15195–15206.
Roy AK, Fudge JL, Kelly C, Perry JSA, Daniele T, Carlisi C, Benson B, Castellanos FX, Milham MP, Pine DS, Ernst M (2013) Intrinsic functional connectivity of amygdala-based networks in adolescent generalized anxiety disorder. J Am Acad Child Adolesc Psychiatry 52:290-299.e2.
Rudolph S, Guo C, Pashkovski SL, Osorno T, Gillis WF, Krauss JM, Nyitrai H, Flaquer I, El-Rifai M, Datta SR, Regehr WG (2020) Cerebellum-Specific Deletion of the GABAA Receptor δ Subunit Leads to Sex-Specific Disruption of Behavior. Cell Reports 33:108338.
Sacchetti B, Sacco T, Strata P (2007) Reversible inactivation of amygdala and cerebellum but not perirhinal cortex impairs reactivated fear memories. Eur J Neurosci 25:2875–2884.
Saez A, Rigotti M, Ostojic S, Fusi S, Salzman CD (2015) Abstract Context Representations in Primate Amygdala and Prefrontal Cortex. Neuron 87:869–881.
Schmahmann JD (2019) The cerebellum and cognition. Neuroscience Letters 688:62–75.
Schmahmann JD, Sherman JC (1998) The cerebellar cognitive affective syndrome. Brain 121:561–579.
Sebastiani L, La Noce A, Paton JF, Ghelarducci B (1992) Influence of the cerebellar posterior vermis on the acquisition of the classically conditioned bradycardic response in the rabbit. Exp Brain Res 88:193–198.
Sengupta A, McNally GP (2014) A role for midline and intralaminar thalamus in the associative blocking of Pavlovian fear conditioning. Front Behav Neurosci 8 Available at:

http://journal.frontiersin.org/article/10.3389/fnbeh.2014.00148/abstract [Accessed January 29, 2021].
Sengupta A, Yau JOY, Jean-Richard-Dit-Bressel P, Liu Y, Millan EZ, Power JM, McNally GP (2018) Basolateral Amygdala Neurons Maintain Aversive Emotional Salience. J Neurosci 38:3001–3012.
Shuster SA, Wagner MJ, Pan-Doh N, Ren J, Grutzner SM, Beier KT, Kim TH, Schnitzer MJ, Luo L (2021) The relationship between birth timing, circuit wiring, and physiological response properties of cerebellar granule cells. Proc Natl Acad Sci USA 118:e2101826118.
Siegel JJ, Taylor W, Gray R, Kalmbach B, Zemelman BV, Desai NS, Johnston D, Chitwood RA (2015) Trace Eyeblink Conditioning in Mice Is Dependent upon the Dorsal Medial Prefrontal Cortex, Cerebellum, and Amygdala: Behavioral Characterization and Functional Circuitry(1,2,3). eNeuro 2.
Snider RS, Maiti A (1976) Cerebellar contributions to the Papez circuit. J Neurosci Res 2:133–146.
Strata P (2015) The Emotional Cerebellum. Cerebellum.
Strick PL, Dum RP, Fiez JA (2009) Cerebellum and Nonmotor Function. Annual Review of Neuroscience 32:413–434.
Stujenske JM, Likhtik E, Topiwala MA, Gordon JA (2014) Fear and Safety Engage Competing Patterns of Theta-Gamma Coupling in the Basolateral Amygdala. Neuron 83:919–933.
Supple WF Jr, Leaton RN (1990) Cerebellar vermis: essential for classically conditioned bradycardia in the rat. Brain Res 509:17–23.
Supple WF Jr, Leaton RN, Fanselow MS (1987) Effects of cerebellar vermal lesions on species-specific fear responses, neophobia, and taste-aversion learning in rats. Physiol Behav 39:579–586.
Tervo DGR, Hwang B-Y, Viswanathan S, Gaj T, Lavzin M, Ritola KD, Lindo S, Michael S, Kuleshova E, Ojala D, Huang C-C, Gerfen CR, Schiller J, Dudman JT, Hantman AW, Looger LL, Schaffer DV, Karpova AY (2016) A Designer AAV Variant Permits Efficient Retrograde Access to Projection Neurons. Neuron Available at: http://linkinghub.elsevier.com/retrieve/pii/S0896627316305803 [Accessed October 15, 2016].
Tovote P, Fadok JP, Lüthi A (2015) Neuronal circuits for fear and anxiety. Nature Reviews Neuroscience 16:317–331.
Turner BM, Paradiso S, Marvel CL, Pierson R, Boles Ponto LL, Hichwa RD, Robinson RG (2007) The cerebellum and emotional experience. Neuropsychologia 45:1331–1341.
Van der Werf YD, Witter MP, Groenewegen HJ (2002) The intralaminar and midline nuclei of the thalamus. Anatomical and functional evidence for participation in processes of arousal and awareness. Brain Res Brain Res Rev 39:107–140.
Van Overwalle F, Baetens K, Mariën P, Vandekerckhove M (2014) Social cognition and the cerebellum: A meta-analysis of over 350 fMRI studies. NeuroImage 86:554–572.
van Vulpen EH, Verwer RW (1989) Organization of projections from the mediodorsal nucleus of the thalamus to the basolateral complex of the amygdala in the rat. Brain Res 500:389–394.

Vertes RP, Linley SB, Hoover WB (2015) Limbic circuitry of the midline thalamus. Neuroscience & Biobehavioral Reviews 54:89–107.
Wagner MJ, Kim TH, Savall J, Schnitzer MJ, Luo L (2017) Cerebellar granule cells encode the expectation of reward. Nature Available at: http://www.nature.com/doifinder/10.1038/nature21726 [Accessed March 23, 2017].
Wang S, Yu R, Tyszka JM, Zhen S, Kovach C, Sun S, Huang Y, Hurlemann R, Ross IB, Chung JM, Mamelak AN, Adolphs R, Rutishauser U (2017) The human amygdala parametrically encodes the intensity of specific facial emotions and their categorical ambiguity. Nat Commun 8:14821.
Xiao L, Bornmann C, Hatstatt-Burklé L, Scheiffele P (2018) Regulation of striatal cells and goal-directed behavior by cerebellar outputs. Nature Communications 9 Available at: http://www.nature.com/articles/s41467-018-05565-y [Accessed June 3, 2019].
Yin Y, Li L, Jin C, Hu X, Duan L, Eyler LT, Gong Q, Song M, Jiang T, Liao M, Zhang Y, Li W (2011) Abnormal baseline brain activity in posttraumatic stress disorder: a resting-state functional magnetic resonance imaging study. Neurosci Lett 498:185–189.
Yizhar O, Klavir O (2018) Reciprocal amygdala–prefrontal interactions in learning. Current Opinion in Neurobiology 52:149–155.
Zhang X, Li B (2018) Population coding of valence in the basolateral amygdala. Nat Commun 9:5195.
Zhu L, Sacco T, Strata P, Sacchetti B (2011) Basolateral Amygdala Inactivation Impairs Learning-Induced Long-Term Potentiation in the Cerebellar Cortex Izquierdo I, ed. PLoS ONE 6:e16673.
Zhu L, Scelfo B, Hartell NA, Strata P, Sacchetti B (2007) The effects of fear conditioning on cerebellar LTP and LTD: Cerebellar plasticity and learned fear. European Journal of Neuroscience 26:219–227.
Zingg B, Chou X, Zhang Z, Mesik L, Liang F, Tao HW, Zhang LI (2017) AAV-Mediated Anterograde Transsynaptic Tagging: Mapping Corticocollicular Input-Defined Neural Pathways for Defense Behaviors. Neuron 93:33–47.
Zingg B, Peng B, Huang J, Tao HW, Zhang LI (2020) Synaptic Specificity and Application of Anterograde Transsynaptic AAV for Probing Neural Circuitry. The Journal of Neuroscience 40:3250–3267.

Appendix iii: High-frequency stimulation of ventral CA1 neurons reduces amygdala activity and inhibits fear

Preface

The work presented in this appendix chapter outlines the hippocampus-amygdala connection and its association with fear conditioning. The work in its entirety has been published in the following paper: Graham J, D'Ambra AF, Jung SJ, Teratani-Ota, Y, Vishwakarma N, Venkatesh R, Parigi A, Antzoulatos EG, Fioravante D, Wiltgen BJ (2021). High-frequency stimulation of ventral CA1 neurons reduces amygdala activity and inhibits fear. Front in Beh Neuro. Doi: 10.3389/fnbeh.2021.595049. An earlier version of this manuscript was released as a pre-print on BioRxiv (Graham et al. 2020, doi: https://doi.org/10.1101/2020.07.01.183210). Author contributions is as follows: **JG**: conceptualization, animal care, investigation, data analysis and visualization, project management; **AFD**: investigation; **SJJ**: methodology, animal care, data visualization; **YTO**: methodology, resources; **NV**, **RV**, **AP**: investigation; **EGA**: data analysis and visualization; **DF**: conceptualization, methodology, investigation, data analysis and visualization, supervision, project management, project funding acquisition; **BJW**: conceptualization, data analysis and visualization, supervision, project management, project funding acquisition. Funding: **AFD** was supported by T32 GM 007377; **EGA** was supported by 2018 NARSAD Young Investigator Award BRFSG-2017-02. This work was supported by NSF1754831 and R21MH114178 to **DF**; and R21NS101694 and RO1NS088053 to **BJW**.

Abstract

The hippocampus can be divided into distinct segments that make unique contributions to learning and memory. The dorsal segment supports cognitive processes like spatial learning and navigation while the ventral hippocampus regulates emotional behaviors related to fear, anxiety and reward. In the current study, we determined how pyramidal cells in ventral CA1 respond to spatial cues and aversive stimulation during a context fear conditioning task. We also examined the effects of high and low frequency stimulation of these neurons on defensive behavior. Similar to previous work in the dorsal hippocampus, we found that cells in ventral CA1 expressed high-levels of c-Fos in response to a novel spatial environment. Surprisingly, however, the number of activated neurons did not increase when the environment was paired with footshock. This was true even in the subpopulation of ventral CA1 pyramidal cells that send direct projections to the amygdala. When these cells were stimulated at high-frequencies (20-Hz) we observed feedforward inhibition of basal amygdala neurons and impaired expression of context fear. In contrast, low-frequency stimulation (4-Hz) did not inhibit principal cells in the basal amygdala and produced an increase in fear generalization. Similar results have been reported in dorsal CA1. Therefore, despite clear differences between the dorsal and ventral hippocampus, CA1 neurons in each segment appear to make similar contributions to context fear conditioning.

Introduction

The hippocampus can be divided into distinct segments that make unique contributions to learning and memory (Fanselow and Dong 2010). The dorsal segment supports cognitive processes like spatial learning and navigation via interactions with the entorhinal, parahippocampal and retrosplenial cortices (Cenquizca and Swanson 2006, 2007; Strange et al. 2014; Moser and Moser 1998; Moser et al. 2017). The ventral hippocampus (VH), in contrast, regulates emotional behavior through its connections with the amygdala, nucleus accumbens, lateral hypothalamus, BNST and medial prefrontal cortex (Cenquizca and Swanson 2006, 2007; Jimenez et al. 2018; Hoover and Vertes 2007). Despite these differences, the dorsal and ventral hippocampus share some important properties. They have the same basic architecture and intrinsic organization (tri-synaptic loop) and neurons in both regions respond to spatial cues (e.g. place cells) (Strange et al. 2014; Kjelstrup et al. 2008; Ishizuka et al. 1990). These parallels suggest that similar computations may be carried out in the DH and VH during cognitive and emotional learning.

The integration of spatial and emotional information depends on interactions between the DH and VH. For example, during context fear conditioning, animals learn to associate a novel environment with aversive footshock. Encoding this relationship requires spatial information from the DH to be transmitted to the basal nucleus of the amygdala (BA) via the VH (Fanselow and Dong 2010; Xu et al. 2016). However, neurons in the VH do not act as passive relays; their activity is strongly modulated by emotional states like fear and anxiety, which is not typically the case in the DH (Jimenez et al. 2018; Ciocchi et al. 2015). Consistent with this fact, lesions of the VH reduce

stress hormone release and anxiety-related behaviors while damage to the DH does not (Kjelstrup et al. 2002). Place cells in the VH are also distinct; they have large, overlapping place fields that encode behaviorally-relevant contexts as opposed to precise spatial locations (Komorowski et al. 2013). Based on these findings, we hypothesized that dorsal (dCA1) and ventral (vCA1) CA1 neurons will respond to different stimuli during context fear conditioning. Specifically, we predicted that neurons in dCA1 will primarily respond to the spatial context while cells in vCA1 will be more responsive to footshock.

To examine our hypothesis, we quantified immediate-early gene expression (IEG) in vCA1 neurons after spatial exploration or emotional learning. For the former, mice were exposed to a novel environment and for the latter, mice underwent context fear conditioning. We found that vCA1 neurons were strongly activated by the novel environment but, surprisingly, c-Fos expression did not increase further when the context was paired with shock. Neurons in dCA1 have been shown to respond in the same way under similar conditions (Radulovic et al. 1998; Lovett-Barron et al. 2014). Next, we stimulated vCA1 neurons that project to the BA to determine if defensive behaviors could be induced after context fear conditioning. We found that high-frequency stimulation (20-Hz) disrupted freezing and led to feed-forward inhibition of principal cells in the BA. In contrast, low frequency stimulation (4-Hz) increased fear generalization and did not inhibit the BA. Similar results have been reported when dCA1 neurons are stimulated at low frequencies (Ryan et al. 2015). These data suggest that dorsal and ventral CA1 make similar contributions to context fear conditioning despite the functional differences between these regions.

Material and Methods

SUBJECTS

Experiments were performed in 2–5-month-old male and female F1 hybrid mice (C57BL/6NT x 129S6/SvEv) from Taconic (B6129F1) or C57BL/6J mice from Jackson Labs (Stock Number #000664). Animals were maintained on a 12-hour light/12-hour dark cycle with ad libitum access to food and water. All experiments were performed during the light portion (7am – 7pm) of the light/dark cycle. Mice were group housed until surgery, at which point they were single housed for the remainder of the experiment. All experiments were reviewed and approved by the UC Davis Institutional Animal Care and Use Committee (IACUC).

SURGERIES

Stereotaxic surgery was performed 2–3 weeks before behavioral experiments began. Mice were anesthetized with isoflurane (5% induction, 2% maintenance) and placed in a stereotaxic frame (Kopf Instruments). An incision was made in the scalp and the skull was adjusted to place bregma and lambda in the same horizontal plane. Small holes were drilled above the injection sites for each brain region and virus or tracer was injected through a glass pipette with a tip diameter between 25-40 µm using a microsyringe pump (UMP3, World Precision Instruments) at 2 nl/sec. In the tracing experiment (Figure 1), Ctb-647 was infused into the BA (50nl) at each of the following 4 sites (AP, -1.55 mm; ML, ± 2.85; DV, -5 mm and -4.8 mm from dura). In the optogenetic behavioral experiments (Figures 3, 4, 6), AAV-CaMKII ChETA-EYFP, AAV-DIO-ChETA-mCherry or a control virus (AAV-CaMKII-EYFP or AAV-FLEX-TdTomato) were infused into vCA1 (250nl) at the following 4 sites (AP, -3 mm; ML, ±3.5 mm; DV -3.9 and -3.5 mm from dura). In Figure 4, AAVrg was also infused into the BA (37nl) at the following 4

sites (AP, -1.55 mm; ML, ± 2.85; DV, -5.0 mm and -4.9 mm from dura). We waited 3-5 minutes after each infusion before withdrawing the pipette. Optic fiber cannulas (0.39 NA, 200 μm diameter, Thorlabs) were manufactured as previously described (Sparta et al. 2012) and implanted bilaterally above the virus injection sites in ventral CA1 (AP, –3 mm; ML, ±3.75 mm, length 3.4 mm). The fibers were secured to the skull using 3 screws and dental cement (Harry J. Bosworth Company). Three- to four-week-old mice were used in the electrophysiology experiments (Figures 2 and 5), so the stereotaxic coordinates were adjusted for body size. AAV-ChETA-EYFP (350 nl) was infused into the VHC at the following 2 sites (AP, -2.8 mm; ML, ±3.6 mm; DV, -2.8 mm from brain surface).

CONTEXTUAL FEAR CONDITIONING AND OPTOGENETIC STIMULATION

Stereotaxic surgery was performed on day 1. On Day 8-12, all animals were handled for 5-minutes a day (either in the vivarium or in a room adjacent to the fear conditioning chambers). Animals in optogenetic experiments had their implants attached to a 1-m split optic patch cable (0.22 NA, 200μm diameter) during handling. All mice excepting those in tagging experiments were trained 24 hours after the last handling session. Training consisted of 3-minutes of context exploration and either 2 shocks (0.3 mA, 1 min ITI, Taconic hybrids) or 3 shocks (0.6mA, 1 min ITI, C57s). Testing consisted of 5-10 minutes in the training context or a novel context (context B). Mice were sacrificed after their final testing session or training (ctb experiment) and c-Fos was quantified as described below. For optogenetic experiments, a 473 nm, 300mW DPSS laser system (OptoEngine) was coupled to the branched optic cable and implant through a rotating comutator fixed above the conditioning chamber. Laser

output was adjusted to obtain 10 mW from the optic fiber tip measured with an optical power meter (Thorlabs) before each experiment. Doric's OptG4 software was used to control laser pulse frequency and Med Associates SG-231 28V DC-TTL adapter was used to control onset and offset of laser pulses during behavioral sessions. Laser stimulation consisted of 3-minute epochs with 15 msec pulses at 20 Hz. Mice were trained and/or tested in Med Associates fear conditioning chambers (30.5 cm x 24.1 cm x 21.0 cm) that were housed in sound-attenuating boxes containing overhead LED lights and a scanning, charge-coupled video camera. Context A was lit with white light, cleaned with 70% EtOH and contained a stainless-steel grid floor. Context B was lit with infrared light, cleaned with Sani Wipes and contained a smooth plastic insert for the floor (covered with a small amount of corn cob bedding) as well as a curved plastic insert for the walls.

IMMUNOHISTOCHEMISTRY AND MICROSCOPIC IMAGING

Animals were sacrificed 90 minutes after training, testing, or final laser stimulation. Mice were deeply anesthetized using 5% isoflurane mixed with O2 and then transcardially perfused first with 0.1M Phosphate buffered saline (PBS) and fixed with 4% paraformaldehyde (PFA). Brains were extracted and left in PFA for 24-48 hours and then sliced into 40 µm coronal sections using a Leica VT-1000 vibratome. To visualize virus spread and locate injection sites and fiber optic tips, two separate series of slices were taken that spanned the anterior-posterior axis (every 5^{th} and 6^{th} slice). For Ctb injection site localization, one series was Nissl-stained and amygdala nuclei were identified using the online Allen interactive mouse reference atlas. The adjacent sections in the other series were stained with DAPI and the location of the injection site

was mapped onto the identified Amygdala nuclei. Slices 1-4 were stored for later c-Fos immunohistochemistry. 3-4 sections per area were randomly chosen for c-Fos quantification. Slices were incubated in blocking buffer (2% normal Donkey serum, 0.2% Triton-X 100 in 0.1 M PBS) for 15 minutes followed by overnight incubation in primary antibody at 1:5000 (Millipore Cat# ABE457, RRID: AB 2631318) suspended in blocking buffer. The next day, tissue was washed 3x with 0.1M PBS and then incubated with a solution containing 1:500 Biotin-SP-conjugated Donkey anti-rabbit secondary antibody (Jackson ImmunoResearch Labs Cat# 711-065-152, RRID: AB 2340593). After washing, the antibodies were detected using Streptavidin-conjugated Cy3(1:500), (Jackson ImmunoResearch Labs Cat# 016-160-084, RRID: AB 2337244) or Cy5(1:250), (Jackson ImmunoResearch Labs Cat# 016-170-084, RRID: AB 2337245). Finally, sections were counterstained with DAPI (1:10000, Life Technologies) for 15 minutes and mounted on slides (Vectashield mounting medium). Slides were imaged using an Olympus fluorescence virtual slide scanning microscope. For c-Fos quantification, 35 µm z-stacks were acquired at 20x magnification. ROIs were chosen in the vCA1 either beneath the optic fiber tip (optogenetic experiments) or that contained AMY projecting neurons (ctb experiment). Fluorescent images were imported into FIJI converted to grayscale and separated by channel. Fluorescent label was marked on each channel independently using the FIJI cell counter tool and the macro metamorph emulator (© 2005 Fabrice P. Cordelières). Overlap (as in ctb experiment) was determined by superimposing the markers from one channel onto another and counting the number of overlapping markers. For any experiments estimating the percent of cells expressing label out of the total number of cells per area,

the 3D Objects Counter tool in FIJI was used to estimate the number of DAPI stained nuclei in each area by dividing the obtained volume by the average single nucleus volume for the animal/area. For quantification of c-fos in all dorsal and ventral CA1 neurons (**Figure 1F - G**), 35 µm single-plane images were acquired at 20x magnification. Images were cropped to contain approximately 10,000 μm^2 of area CA1 in both the dorsal and ventral hippocampus. After acquisition, images were converted to grayscale and c-Fos positive cells were quantified using the FIJI cell counter tool.

VIRUS CONSTRUCTS

The following constructs (AAV2, serotype 5) were packaged by the Vector Core at the University of North Carolina: AAV5 -CaMKII-hChR2(E123T/T159C)-p2A-EYFP-WPRE had a titer of 3.6x10^12 – 4.1x10^12 viral particles/ml. AAV5- EF1a-DIO-hChR2 (E123T/T159C) p2A-mCherry had a titer of 4.10e^12 virus molecules/ml. AAV5-CAG-FLEX-tdTomato had a titer of 4.8e^12 viral particles/ml. The AAVrg-cre-EBFP plasmid was purchased from Addgene (catalog# 51507) and packaged by the UC Davis Vector Core with a titer of 7.63^12 GC/ml.

SLICE PREPARATION FOR ELECTROPHYSIOLOGICAL RECORDINGS

Mice (postnatal week 6-7; both sexes) were anesthetized through intraperitoneal injection of an anesthetic cocktail (ketamine: 10 mg/kg; xylazine: 1 mg/kg; acepromazine: 0.1 mg/kg) and transcardially perfused with ice-cold artificial CSF (aCSF; in mM: 127 NaCl, 2.5 KCl, 1.25 NaH_2PO_4, 25 $NaHCO_3$, 1 $MgCl_2$, 2 $CaCl_2$, 25 glucose; supplemented with 0.4 sodium ascorbate and 2 sodium pyruvate; ~310 mOsm). Brains were rapidly removed, blocked, and placed in choline slurry (110 choline chloride, 25 $NaHCO_3$, 25 glucose, 2.5 KCl, 1.25 NaH_2PO_4, 7 $MgCl_2$, 0.5 $CaCl_2$, 11.6

sodium ascorbate, 3.1 sodium pyruvate; ~310 mOsm). Coronal sections (250 μm) containing vCA1 or BAwere cut on a vibratome (Leica VT1200S) and transferred to an incubation chamber containing aCSF at 32°C for 25 min before moving to room temperature until used for recordings. All solutions were bubbled with 95% O_2-5% CO_2 continuously. Chemicals were from Sigma.

PATCH-CLAMP RECORDINGS

For recordings, slices were mounted onto glass coveslips coated with poly-l-lysine and placed in a submersion chamber perfused with aCSF (2 ml/min) at 30-32 ^{o}C. Loose on-cell patch-clamp recordings were made from visually identified cells in vCA1 or BAusing borosilicate glass pipettes (3–5 MΩ) filled with 150 mM NaCl. This configuration does not perturb the intracellular milieu of the recording cell. vCA1 pyramidal neurons were identified based on position and shape and were selected for ChETA-EYFP expression. BA primary neurons (PNs) were identified based on size (> 15 μm) and firing rate (< 20 Hz) (Sosulina et al., 2006; Bazelot, 2015). Recordings were performed in voltage clamp mode by setting the pipette potential to obtain 0 pA of membrane current (Perkins, 2006) and were acquired in pClamp11 using a Multiclamp 700B amplifier (Molecular Devices). Recordings were digitized at 20 kHz with a Digidata 1550 digitizer (Molecular Devices), and low-pass filtered at 8 kHz. Optical stimulation of ChETA-expressing hippocampal pyramidal neurons in vCA1 or their axons in BAwas performed under a 60x water immersion lens (1.0 N.A.) of an Olympus BX51W microscope, using an LED system (Prizmatix UHP or Excelitas X-cite; max power of 3 mW at lens tip) mounted on the microscope and driven by a Master9 stimulator (AMPI). Stimulation consisted of 5 10-ms pulses of 488 nm light delivered at various

frequencies, as indicated. Each protocol was repeated at least 5 times per stimulation frequency with an inter-trial interval of 30 s [to allow for opsin recovery (Lin, 2011)]. Pulses of increasing power were delivered until an action potential was triggered. Above threshold values (~1.5-2x threshold) were used for experiments. For vCA1 axonal stimulation in BA, higher values were also tested to examine whether more than 1 spike could be synaptically evoked in BAPNs at 20 Hz. The $GABA_A$ receptor blocker bicuculine (20 μM) was washed in during BArecordings, as indicated, for 6 min before resuming stimulation.

DATA ANALYSIS

For the behavioral experiments, group differences were analyzed with ANOVAs and Bonferroni post-hoc tests. All statistics were done using GraphPad Prism (2018).

For electrophysiology experiments, data were analyzed with custom-made tools in MATLAB (Mathworks). Spike probability was quantified as the probability of an action potential being evoked during repetitions of the same stimulation regime. For vCA1 recordings, an action potential was considered as evoked if it occurred within a time window of 10 ms from pulse onset (i.e., during the pulse). For BAPN recordings, an action potential was considered as evoked if it occurred within a time window of 15 ms from pulse onset (the longer time window was used to account for synaptic delays). Baseline spike probability was quantified as the average probability of an action potential within 500 randomly selected time windows (10 ms for vCA1; 15 ms for BA) during the 3-s pre-stimulus baseline. For peri-stimulus time histograms (PSTH), action potentials were counted in 50-ms bins, with time referenced to the start of light pulses.

Permutation tests were used for statistical comparisons of average spike probabilities between conditions (Odén and Wedel 1975). Data were randomly shuffled between conditions 1,000 times, while maintaining the original sample sizes, and the differences between the group averages of observed spike probabilities were compared against the corresponding differences between the group averages of random permutations. The reported p-values indicate the probability that a difference between average spike probabilities equal to or greater than the observed difference could have arisen by chance alone (i.e., due to random sampling).

Results

CONTEXT LEARNING ACTIVATES VCA1 NEURONS THAT PROJECT TO THE BASAL AMYGDALA

The DH responds to spatial and contextual cues while amygdala neurons respond strongly to emotional stimuli like footshock ((O'Keefe et al. 1971; O'keefe and Speakman 1987; Tanaka et al. 2018; Radulovic et al. 1998; Barot et al. 2009; Beyeler et al. 2018; Pelletier et al. 2005; Wolff et al. 2014). The current experiment determined how vCA1 neurons respond to these stimuli using c-Fos as a proxy for neural activity and plasticity. To do this, we compared changes in c-Fos expression after mice were exposed to a novel environment or underwent context fear conditioning. Expression was quantified in neurons that send direct projections to the BA and those that do not. To identify the former, the retrograde tracer ctb-647 was infused into the BA prior to conditioning **(Figure 1A)**. On the training day, control mice were left in their home cages (HC, n=7). The context group (Ctx, n=5) explored a novel environment for 5-minutes and the context + shock group underwent contextual fear conditioning (Fear, n=6) **(Figure 1B)**. Fear conditioning consisted of two footshocks (2-sec, 0.3mA, separated by

1-minute) that were delivered after a 3-minute exploration period. Ninety-minutes after training, the animals were sacrificed, and their brains fixed for c-Fos immunohistochemistry **(Figure 1C)**. Compared to the control group, there was an increase in the number of c-Fos positive vCA1 neurons in mice that explored the novel environment or underwent context fear conditioning. The size of this increase was similar for the experimental groups and observed both in vCA1 neurons that project to the BA (Ctb+ neurons) as well as those that do not (Ctb- neurons). Interestingly, a higher percentage of Ctb+ cells expressed c-Fos than Ctb- cells in all groups **(Figure 1D - E)** [Repeated Measures ANOVA, Main effect of Group, $F(2, 15) = 42.99$, $p < .0001$; Main effect of Cell type, $F(1, 15) = 22.93$, $p = .0002$; No Group x Cell type interaction $F(2, 15) = 3.115$, $p = .0739$; Bonferroni post-hoc tests, Control vs Context ($p < .0001$), Control vs Context + Shock ($p < .0001$), Context vs Context + shock ($p = .5778$)].

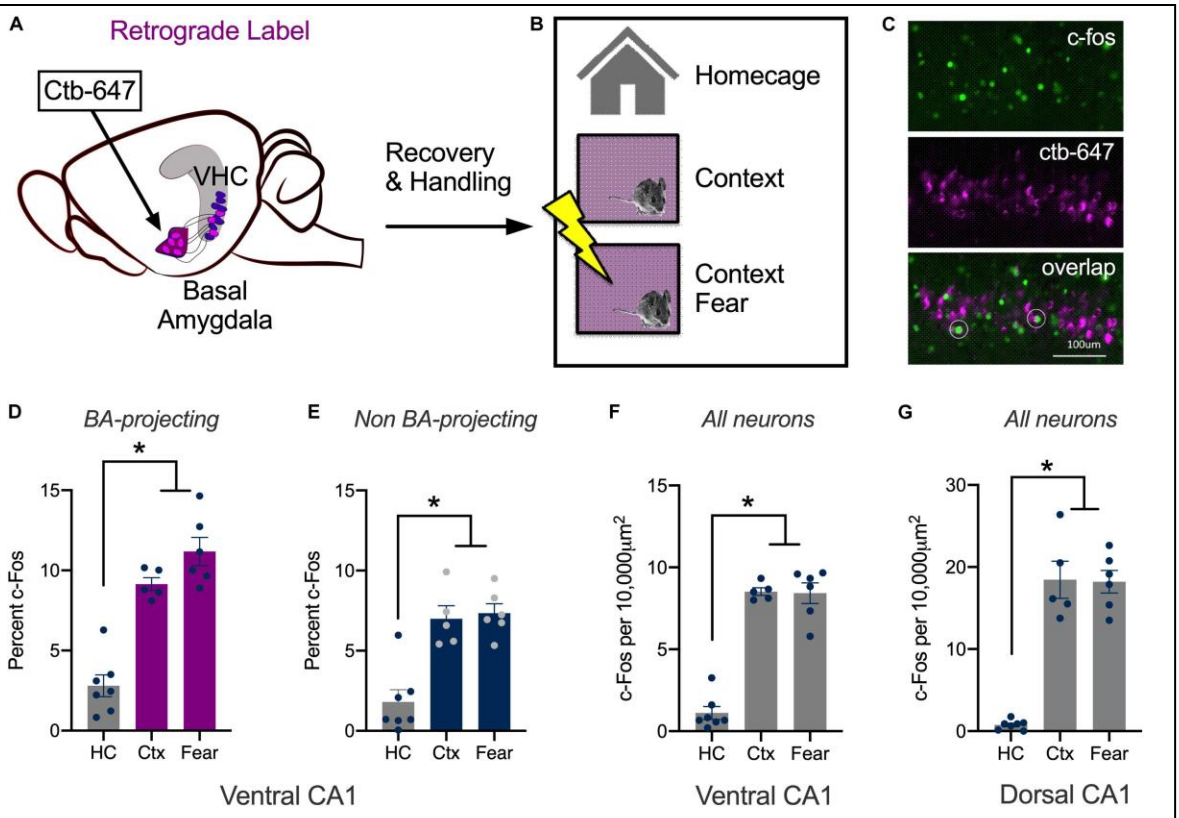

Figure 1. Context learning activates vCA1 neurons that project to the basal amygdala **A-C.** Experimental design. **A.** Ctb **(magenta)** was injected into the BA. **B.** Mice were sacrificed 90 minutes after exploring a neutral context, feared context (context + shock), or a control group that was left in the homecage. **C.** Example histology showing c-Fos staining in green, Ctb labeling in magenta and overlap in BA-projecting neurons **(right)**. **D-E**. The percentage of BA-projecting (Ctb+) and non-projecting (Ctb-) neurons that responded to homecage(HC), context(Ctx) or context + shock(Fear) conditions in F1 hybrid mice in BA-projecting(**D**) and Non-BA projecting vCA1 neurons(**E**). **F.** The percentage of BA-projecting (Ctb+) and non-projecting (Ctb-) neurons that responded to context or context + shock conditions in C57BL/6 mice. Data are presented as mean ± SEM. * = $p < .05$.

While the expression of c-Fos did not increase significantly in the fear group compared to the context group, there was a trend in this direction. The lack of a difference could be due to the fact that we used F1 hybrids (C57BL/6 x 129S6) rather than the more commonly used C57BL/6 strain. Hybrids acquire more fear than C57s and can be trained with lower shock intensities and fewer trials (Balogh and Wehner 2003; Owen et al. 1997). To determine if this difference affected our results, we fear conditioned a group of C57BL/6 mice with three, 0.75mA shocks (Fear, n=7) and

compared them to animals that only explored the context (Ctx, n = 9) Ctb was once again infused into the BA to label vCA1 neurons that project to this region. Similar to the data collected in hybrid mice, c-Fos expression was similar in fear conditioned animals and those that explored the context. This was true both in Ctb+ neurons (Ctx mean = 11.17%, SEM = .7387; Fear mean = 11.57%, SEM = .9617) and in Ctb- cells (Ctx mean = 7.932%, SEM = .9590; Fear mean = 6.113%, SEM = .5846). In addition, the overall amount of c-Fos expression was once again higher in vCA1 neurons that project to the BA (Ctb+ mean = 11.37%, SEM = .850) compared to those that do not (Ctb- mean = 7.02%, SEM = .771) [Repeated Measures ANOVA, Main effect of cell type (Ctb+/Ctb-), $F (1, 14) = 16.55$, $p < 0.0012$; No effect of group, $F (1, 14) = 1.698$, $p = 0.2135$; No group x cell type interaction $F(1, 14) = 1.077$, $p = 0.3170$] (Data not shown).

Together with previous work, these results demonstrate that novel environments strongly activate pyramidal neurons in dorsal and ventral CA1. Pairing the environment with shock does not further increase activity in either of these subregions (measured via c-Fos), as it does in subcortical areas like the amygdala (Radulovic et al. 1998; Barot et al. 2009; Milanovic et al. 1998). To ensure we could replicate the results of prior studies done in dCA1, we quantified c-Fos expression in this region and compared it to vCA1 in the same animals. For these analyses, single scan planes were taken from each area and the number of c-Fos+ neurons were counted per 10,000 um^2. The results we obtained with this methodology were similar to the vCA1 data described above; c-Fos expression increased in the context and fear conditioning groups compared to homecage controls and these conditions did not differ from one another. The same pattern was found in dCA1, although in this region, the total number of c-Fos+ cells was

higher than we observed in vCA1 **(Figure 1F-G)** [Repeated Measures ANOVA, Main effect of Group $F(2, 15) = 120.3$, $p < .0001$; Main effect of Region $F(1, 15) = 55.64$, $p < .0001$; Group x Region interaction $F(2, 15) = 16.88$, $p = .0001$; Bonferroni post-hoc tests, in both dCA1 and vCA1, HC vs Context ($p < .0001$), HC vs Fear ($p < .0001$) Context vs Fear ($p > .9999$); dCA1 vs vCA1, HC vs HC ($p > .9999$), Fear vs Fear ($p < .0001$) Context vs Context ($p > .9999$)].

We should note that vCA1 neurons activated during context exploration may also respond to footshock. If that were the case, it could be difficult to find differences in c-Fos expression between fear conditioned animals and mice that were exposed to the context. This issue could be addressed in future studies by labelling context responsive cells and footshock activated neurons with different IEGs (Barot et al. 2009). Single-unit recordings and Ca^{2+} imaging could also be used to examine the activity of individual vCA1 neurons during exploration and fear conditioning. An advantage of these tools is that precise firing patterns can be obtained and compared across different experimental conditions.

IN VITRO STIMULATION OF VCA1 NEURONS WITH CHETA

High-frequency stimulation (20-Hz) in dCA1 does not induce freezing after fear conditioning like it does in the dentate gyrus (DG) and CA3 (Ryan et al. 2015; Ramirez et al. 2013; Oishi et al. 2019). This may be the case because dCA1 does not send direct projections to the VH like DG and CA3 (Fricke and Cowan 1978; Ishizuka et al. 1990; Swanson et al. 1978). To examine this idea, we used ChETA to stimulate pyramidal neurons in vCA1 after context fear conditioning. We first identified optimal stimulation parameters in hippocampal slices by infusing AAV5-ChETA-EYFP into the VH and

recording from vCA1 neurons 2-3 weeks later. Recordings were performed using a cell-attached patch configuration (see methods for details) while stimulating with 488 nm light at 10, 20 or 50-Hz **(Figure 2)**. As observed in dCA1, pyramidal cells in vCA1 could easily follow 10-Hz and 20-Hz optogenetic stimulation across multiple trials (**Figure 2D).** At these frequencies, the spike probability for light pulses 2-5 was close to 1 and not significantly different from the spike probability for the first pulse [permutation test for pulses 2-5 compared to pulse 1: 10 Hz: $p = 0.82$, $p = 0.82$, $p = 0.82$, $p = 0.20$; 20 Hz: $p = 0.89$, $p = 0.88$, $p = 0.62$, $p = 0.43$]. In contrast, when the same neurons were stimulated at 50-Hz, they responded reliably only to the first light pulse (average spike prob. ± SEM: 1.0 ± 0.00). The firing probability to subsequent stimuli progressively decreased and was significantly reduced by pulse 4 **(Figure 2D)** [permutation test for pulses 2-5 compared to pulse 1: **50-Hz**: $p = 0.17$, $p = 0.09$, $p = 0.01$, $p = 0.001$].

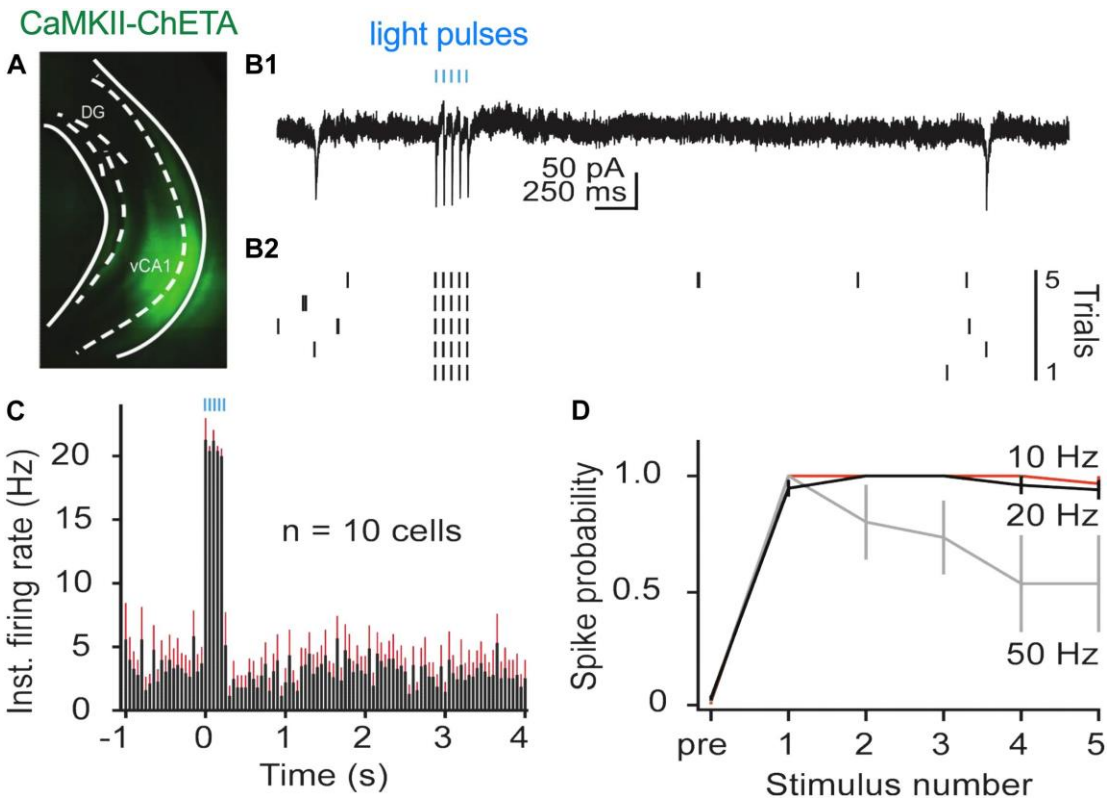

Figure 2. ***In vitro*** **stimulation of vCA1 neurons with ChETA A.** Expression of ChETA-EYFP in ventral/intermediate CA1. **B.** *Ex vivo* cell-attached recording from a representative ChETA-expressing vCA1 pyramidal neuron in response to five 10-ms light pulses at 20-Hz(blue lines). **B1.** Single example trial. **B2.** Raster plot of 5 trials. **C.** Average instantaneous firing rate (in spikes/s) for vCA1 pyramidal neurons (N = 10; bins: 50 ms, black: average firing rate, red: SEM). **D.**, Average spike probability for 3 photostimulation frequencies (10, 20 and 50 Hz). Data are presented as mean ± SEM.

IN VIVO STIMULATION OF VCA1 NEURONS WITH CHETA

Next, we confirmed that 20-Hz laser stimulation activated vCA1 pyramidal neurons *in vivo* **(Figure 3)**. Mice received infusions of CaMKII-ChETA-EYFP (n = 7) or the control virus (CaMKII-EYFP, n = 5) and 10 days later were habituated to a novel environment for 4 days (30 minutes each day) to reduce c-Fos expression (Hess et al. 1995). On Day 5, they were returned to the same context and received 3-minutes of laser stimulation after a 27-minute baseline period **(Figure 3A)**. Ninety-minutes after this session, the animals were sacrificed, and their brains fixed for c-Fos immunohistochemistry. We found a significant increase in the number of c-Fos+

neurons in the ChETA group compared to control animals, indicating that 20-Hz stimulation strongly activated vCA1 neurons (Figures 3B-C) (Two-tailed unpaired t-test, $p = 0.0066$, $t=3$ $df = 10$). While the majority of ChETA+ neurons were found in vCA1, we also observed some expression in the BA. To determine if light delivered to vCA1 could activate these cells directly, we measured the distance between each of our fiber tips and the BA **(Figure 3D)**. These data (minimum, median and maximum distances) were then plotted against the predicted decay in laser power observed when light passes through tissue **(Figure 3E)** (Stanford predicted irradiance tool), (Yizhar et al. 2011). The dashed line on this figure (0.90-0.95mm) indicates the distance at which blue light stimulation (10mW, 20-Hz) would fail to produce an action potential > 90% of the time in ChETA+ neurons (Berndt et al. 2011). We found that 94% of our fibers fell beneath this line, making it unlikely that light stimulation in vCA1 would activate BA neurons directly.

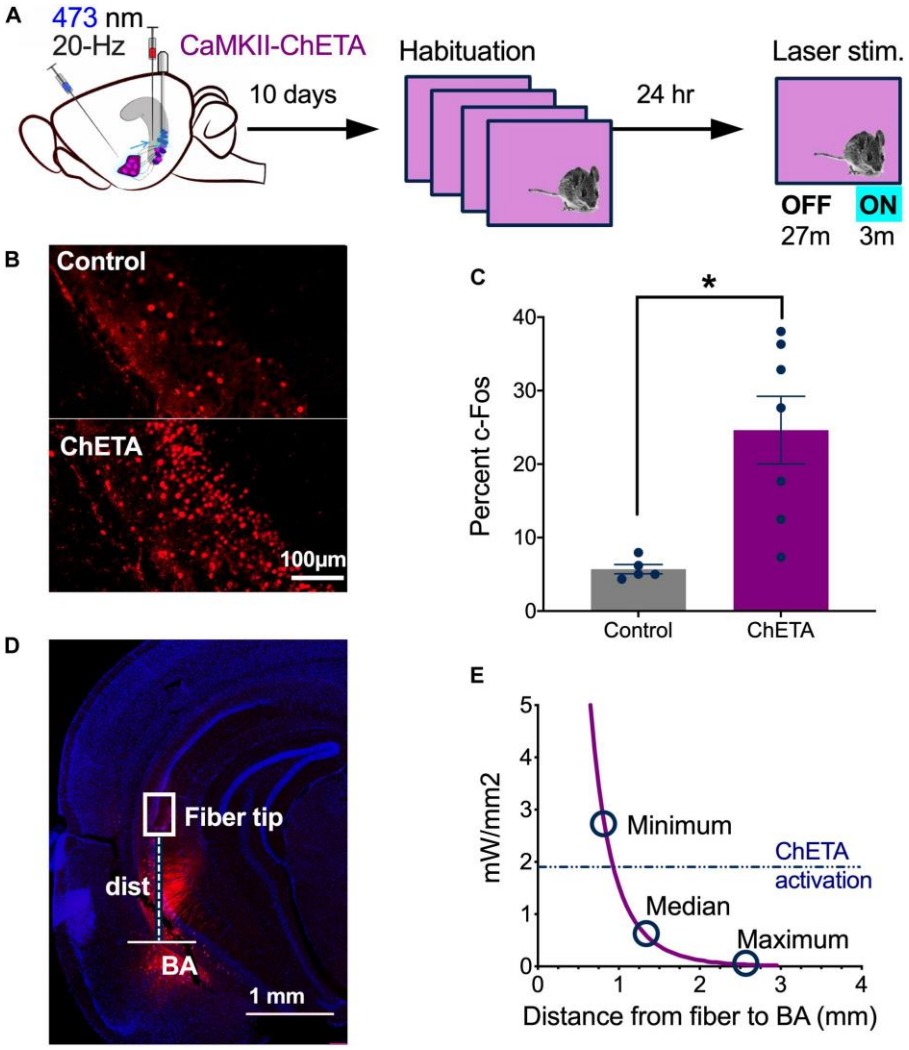

Figure 3: *In vivo* stimulation of vCA1 neurons with ChETA

A. Experiment design: details in the text. **B.** examples of c-fos from an animal injected with ChETA-EYFP (top) and the control virus(bottom). **C.** Percent of neurons expressing c-fos beneath the optic fiber tip. **D.** Image showing an example of AAVrg-ChETA-mCherry expression in vCA1 and BA and how distance was measured between the optic fiber tip and the BA. **E.** Predicted irradiance values were plotted against distance from the optic fiber tip. The minimum, median and maximum fiber tip to BA distance values are marked on the curve. The dashed line indicates the threshold at which ChETA responds to light stimulation with less than 10% fidelity (Berndt et al. 2011).

HIGH-FREQUENCY STIMULATION OF VCA1 NEURONS IMPAIRS THE EXPRESSION OF CONTEXT FEAR

Based on our recording and c-Fos results, we decided to stimulate vCA1 pyramidal neurons at 20-Hz after context fear conditioning. Our initial plan was to activate neurons that expressed c-Fos during training (i.e. engram/memory cells) using TetTag mice from

Jackson labs (stock no. 008344). However, we observed a significant amount of non-specific labeling in these mice compared to our original fos-tTA line (Tayler et al. 2011; Tanaka et al. 2014; Nakazawa et al. 2016; Crestani et al 2019; Wilmot et al. 2018). Therefore, instead of targeting c-Fos+ cells, we stimulated vCA1 neurons that project to the BA. To do this, AAVrg-EBFP-Cre was injected into the BA and FLEX-ChETA-mCherry virus was infused into the VH (BA project, n =8) (Figure 4A, left). Bilateral optic fibers were implanted directly over vCA1. Histological analyses confirmed that ChETA-mCherry was expressed in vCA1 neurons **(Figure 4B, top)** and Cre expression was restricted to cells in the BA (Figure 4B, bottom). A second group received infusions of CaMKII-ChETA-EYFP into vCA1 (All vCA1 n=8) to examine the effects of non-selective stimulation on freezing. Control groups received infusions of AAV-CaMKII-EYFP into vCA1 (n=4) or combined injections of AAVrg-EBFP-Cre into BA and FLEX-tdTomato in vCA1 (n=4).

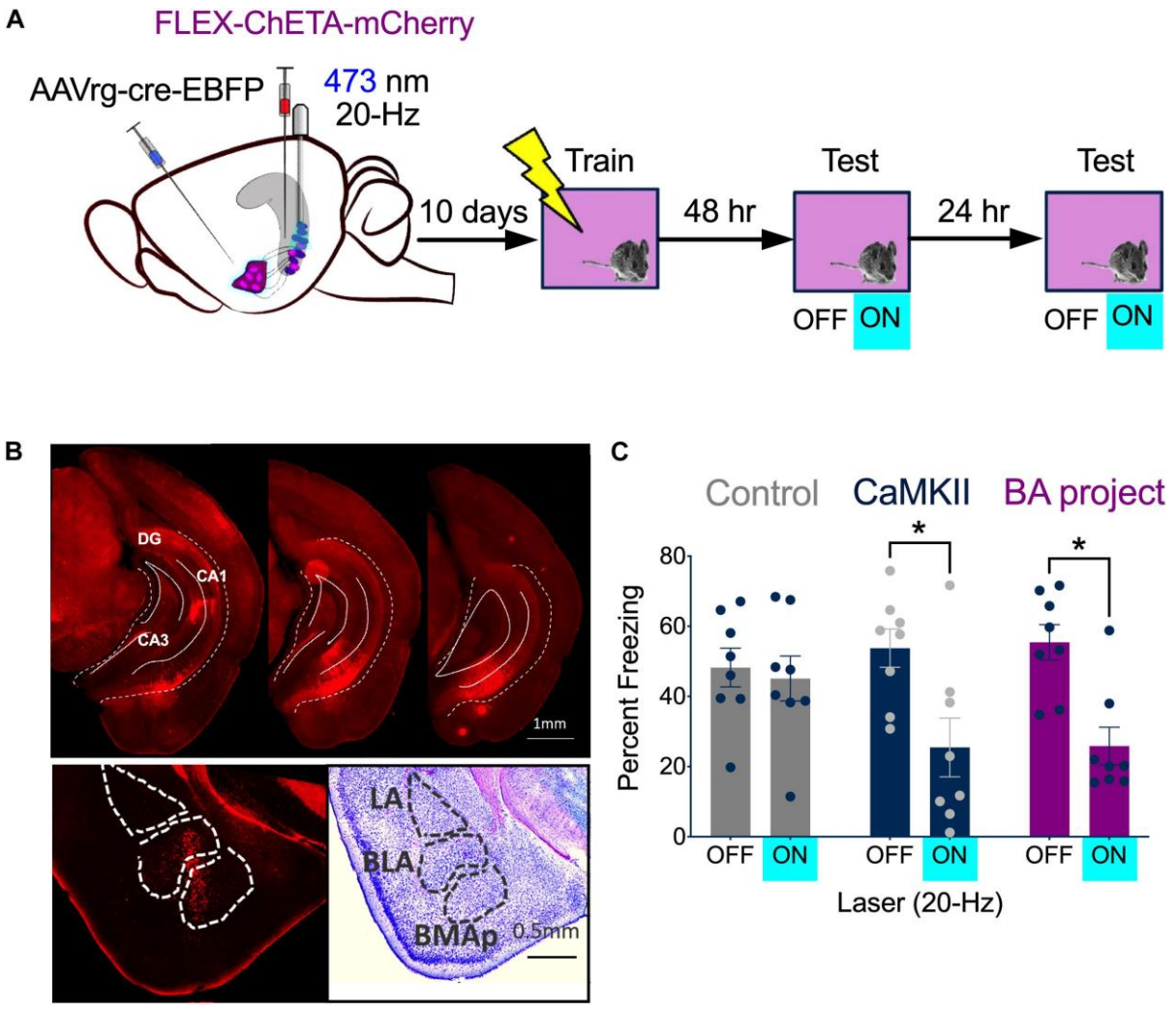

Figure 4. High-frequency stimulation of vCA1 neurons impairs the expression of context fear. **A.** Experimental design. Stimulation groups received infusions of CaMKII-ChETA-EYFP or FLEX-ChETA-EYFP into the VH. Control groups received infusions of CaMKII-EYFP or FLEX-EYFP into the VH. To target amygdala projecting vCA1 neurons, mice that received FLEX viruses also had AAVrg-Cre-EBFP infused into the BA. **B.** Expression of FLEX-ChETA-mCherry in vCA1 **(top)**; Immunostaining for Cre in the BA **(bottom left)** and an adjacent Nissl section **(bottom right)**. **C.** Average freezing during baseline (OFF) and 20-Hz stimulation epochs (ON) during the memory retrieval tests. Data are presented as mean ± SEM. * = $p < .05$.

Following recovery from surgery, animals were handled and habituated to the optic fiber cable for 5 days and then were trained on context fear conditioning. Training consisted of a 3-minute baseline period followed by 2 shocks (0.3 mA, 2 sec duration) delivered 1-minute apart. Two days later, mice were placed back in the training environment to assess context fear memory. The test began with a 3-minute baseline

period that was followed by 3-minutes of stimulation with blue light (473nm, 10 mW, 20 Hz). Mice received an identical test 24 hours later **(Figure 4A, right)**. During the baseline period, freezing was similar for all groups **(Figure 4C)**. When 20-Hz laser stimulation was delivered to vCA1, freezing decreased significantly in the ChETA groups, but not in EYFP controls [Repeated measures 2-way ANOVA, Stimulation x Group interaction ($F(2, 21) = 5.88$, $p = .0093$; Bonferroni post-hoc tests, Control On vs Off ($p > 0.9999$), All vCA1 On vs Off ($p = 0.0005$) BA- projecting vCA1 On vs Off ($p = 0.0003$)]. The size of this decrease was similar whether all vCA1 pyramidal neurons were stimulated or just those that project to the BA. No Group x laser interaction was observed [2-way ANOVA $F(1,14) = 0.01590$, $p = 0.9014$]. These results demonstrate that context fear is not enhanced by high-frequency stimulation of the vCA1-BA pathway. Therefore, the inability of 20-Hz stimulation to induce freezing in dCA1 is not due to the fact that this region lacks direct projections to the amygdala (Ramirez et al. 2013; Wilmot, Puhger, and Wiltgen 2019; Krueger and Wiltgen, 2020). To explain our results, we next examined the effects of vCA1 stimulation on the activity of principal cells in the BA.

HIGH FREQUENCY STIMULATION OF VCA1 TERMINALS INHIBITS PRINCIPAL CELLS IN THE BA

Stimulation of vCA1 neurons at high-frequencies can produce feed-forward inhibition of principal cells in the BA (Hübner et al. 2014; Bazelot et al. 2015). To examine this possibility, we recorded from BA neurons while stimulating ventral CA1 terminals at high (20-Hz) or low (4-Hz) frequencies **(Figure 5A)**. AAV5-CaMKII-ChETA was infused into the VH and coronal slices were taken from the BA 2-3 weeks later. BA neurons were excited by 4-Hz stimulation of vCA1 terminals and fired action potentials to every light

pulse in the stimulus train **(Figures 5B1-B2)** (average spike prob ± SEM: pulse 1: 0.97 ± 0.02; pulse 2: 0.88 ± 0.06, pulse 3: 0.86 ± 0.05, pulse 4: 0.86 ± 0.05, pulse 5: 0.91 ± 0.04). In contrast, 20-Hz stimulation only produced a single action potential and suppressed responding to all subsequent pulses (Figures 5C1-C2**)** (average spike prob. ± SEM: pulse 1: 0.95 ± 0.02; pulse 2: 0.06 ± 0.03, pulse 3: 0.01 ± 0.01, pulse 4: 0.05 ± 0.04, pulse 5: 0.04 ± 0.03) [permutation test, pulses 1-5, 4-Hz vs 20-Hz: p = 0.09, p = 0.00, p = 0.00, p = 0.00, p = 0.00].

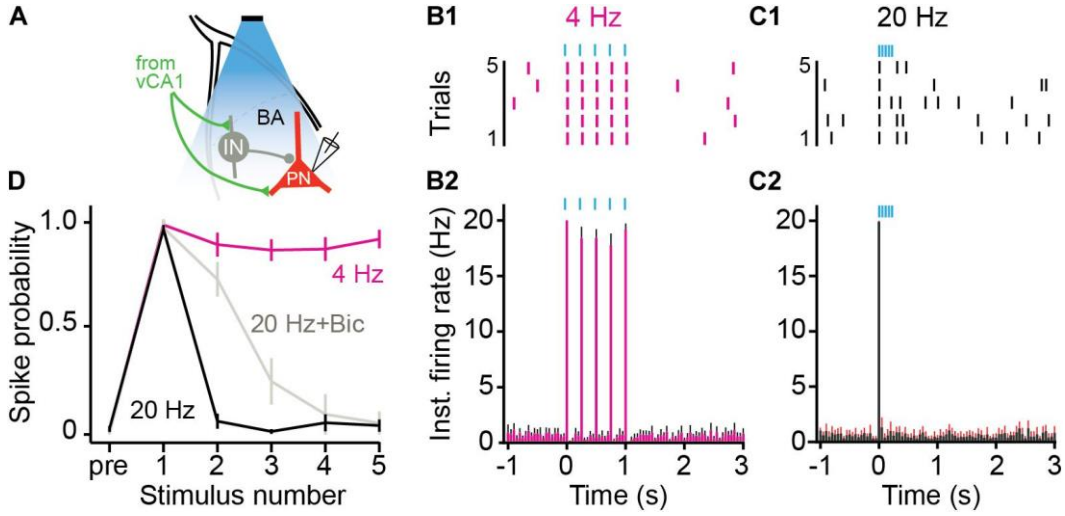

Figure 5. High frequency stimulation of vCA1 terminals inhibits principal cells in the BA
A. Schematic of the experimental configuration: vCA1 axons expressing ChETA-EYFP were optically stimulated in the BA while recording on-cell from BA PNs. IN: Interneuron. **B-C.** Example raster plots (**B1-C1**) and average instantaneous firing rates (+SEM; **B2-C2**) for BA PNs in response to 5, 10-ms light pulses at 4 (**B**) and 20 (**C**) Hz (bins: 50ms). N = 11 cells. **D.** Average spike probability for 4Hz, 20Hz, and 20Hz in the presence of the $GABA_AR$ antagonist bicuculine (Bic).

To determine if this suppression was caused by local inhibition, we stimulated vCA1 terminals at 20-Hzin the presence of the $GABA_A$ receptor antagonist bicuculine. This manipulation partially rescued the activity of BA neurons **(Figure 5D)** (average spike prob. ± SEM: pulse 1: 0.96 ± 0.04; pulse 2: 0.72 ± 0.08, pulse 3: 0.25 ± 0.11, pulse 4: 0.09 ± 0.09, pulse 5: 0.05 ± 0.05) [permutation test, pulses 1-5, 20-Hz vs 20-Hz+ Bic: p = 0.59, p = 0.001, p = 0.18, p = 0.38, p = 0.48], suggesting that feed-forward inhibition

plays a role in suppressing excitatory activity when vCA1 neurons are stimulated at high frequencies (Bazelot et al. 2015; Hübner et al. 2014). However, given that firing was not completely rescued, other factors like synaptic depression likely contribute to this effect as well.

LOW FREQUENCY STIMULATION OF VCA1 DOES NOT DISRUPT THE EXPRESSION OF CONTEXT FEAR

Activity in the hippocampus, amygdala and prefrontal cortex is synchronized around theta-frequency (4-12 Hz) during aversive learning and fear expression ((Radulovic et al. 1998; Barot et al. 2009; Milanovic et al. 1998). Given that BA neurons are able to follow 4-Hz stimulation of vCA1 terminals, we examined the impact of this manipulation on context fear. Mice received bilateral infusions of AAV-CaMKII-ChETA-EYFP (n=6) or AAV-CaMKII-EYFP (n=5) into the VH and optic fibers were implanted above vCA1. Two weeks later, they were trained on context fear conditioning as described above. Memory was tested 48 hours after training and vCA1 neurons were stimulated at 4-Hz (473nm, 10 mW, 15 msec pulses) during the last 3 minutes of the session (Figure 6A, left). Unlike high-frequency stimulation, this manipulation did not disrupt the expression of context fear **(Figure 6B)** [2-way ANOVA, no laser x virus interaction $F = 0.05282$, $p = 0.824$, no main effect of laser $F(1,9) = 0.005282$, $p = 0.8234$].

FEAR GENERALIZATION INCREASES AFTER LOW-FREQUENCY STIMULATION OF VCA1 NEURONS

We next determined if 4-Hz stimulation could induce freezing in a novel environment. To do this, mice from the previous experiment were first exposed to context B for 2 days to reduce generalized fear **(Figure 6A, right)**. On day 3, the animals were put back in context B and, after a baseline period, vCA1 neurons were stimulated at 4-Hz. This

manipulation did not produce an increase in freezing in ChETA mice relative to controls **(Figure 6C)** [2-way repeated measures ANOVA, no Group x Laser interaction, $F(1,9) = .001$, $p = 0.968$]. However, ChETA mice did exhibit an overall increase in freezing in context B, which suggests that prior stimulation altered their behavior [Main effect of Group, $F(1,9) = 5.50$, $p = .043$]. To determine if vCA1 stimulation increased fear generalization, we compared freezing levels during the first exposure session in context B to that observed during the test in context A **(Figure 5D).** Both ChETA mice and controls froze more in the training context (A) than the novel environment (B), which indicates they could discriminate between these places [Two-way ANOVA main effect of context $F(1, 9) = 76.30$, $p < 0.0001$]. Nonetheless, ChETA mice showed significantly more fear in context B than control animals (Bonferroni post-hoc test, $p < .05$), suggesting that vCA1 stimulation increased generalization. However, additional studies are needed to confirm the selectivity of this effect, as the group x context interaction did not quite reach statistical significance [Two-way repeated measures ANOVA, No group x context interaction $F(1,9) = 4.04$, $p = .075$; no effect of group $F(1,9) = 1.94$, $p = .19$].

Finally, to determine if vCA1 stimulation altered the extinction of generalized fear, we analyzed freezing during the 3 sessions in context B **(Figure 6E)**. Analyses were restricted to the first 3-minutes of each session so we could include the data from day 3. We found that freezing levels decreased slightly across days in both groups, but this change did not reach statistical significance. This suggests that our exposure sessions were not long enough to induce robust extinction [2-way repeated measures ANOVA, No Group x Session interaction $F(2,18) = 1.38$, $p = 0.27$; No effect of Group $F(1,9) = 3.31$, $p = 0.1$; No effect of session, $F(2, 18) = 1.81$, $p = .19$]. However, it should be

noted that our experiments were not designed to detect small/moderate differences in fear generalization or extinction. Future work will need to use behavioral protocols that are optimized to study these processes to determine how they are affected by low-frequency stimulation in vCA1.

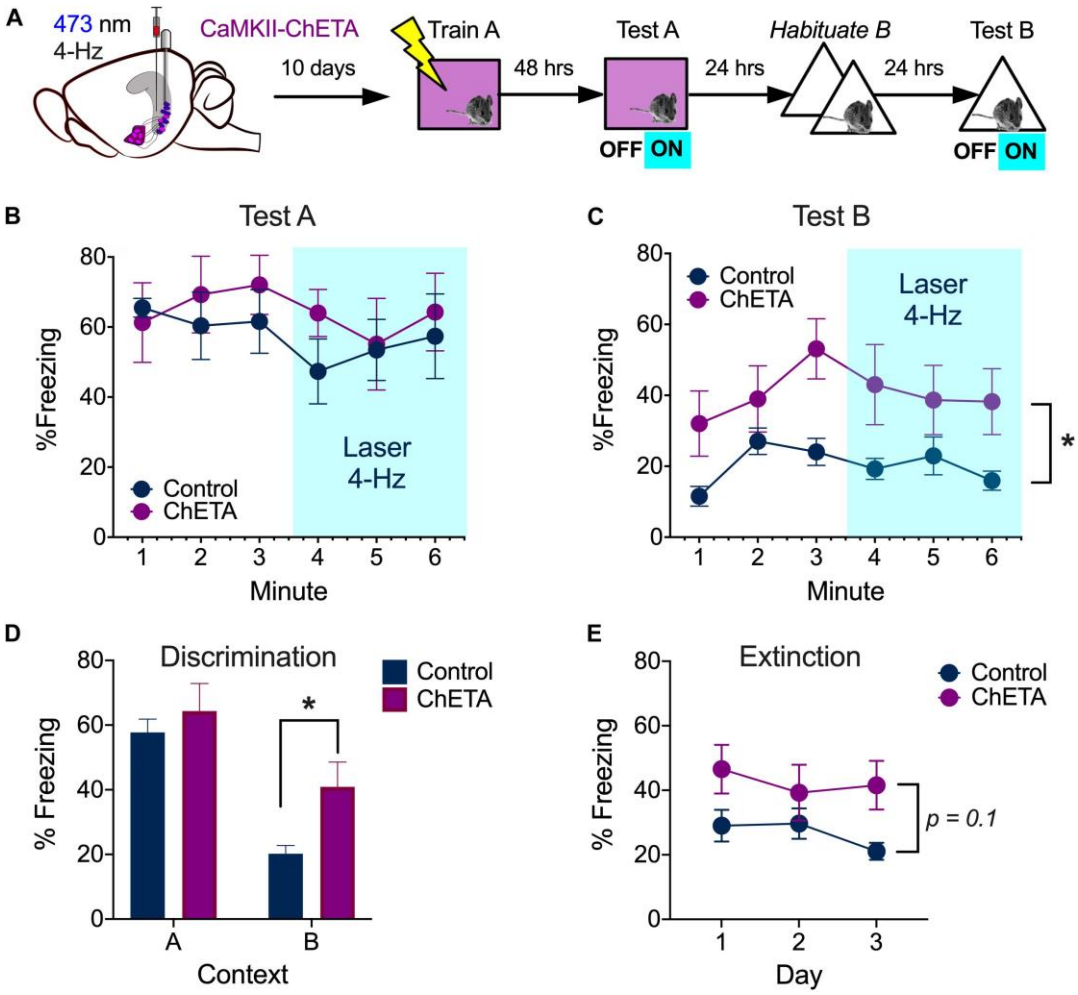

Figure 6. Low frequency stimulation of vCA1 does not disrupt the expression of context fear and enhances generalization. A. Experimental design. **B**. Percent freezing over time (minutes) during baseline and laser stimulation in the training context (Test A). **C**. Percent freezing over time (minutes) during baseline and laser stimulation in a novel environment (Test B). **D**. Percent freezing during the first 3-minutes of the test in context A and the exposure session in context B 24-hours later. **E**. Percent freezing in control and ChETA groups during the first 3-minutes of the context B exposure days. All data are presented as the mean ± SEM. * = $p < 0.05$. Blue = Control virus, Magenta = CaMKII-ChETA.

Discussion

During context fear conditioning, spatial information is thought to be transmitted from the dorsal hippocampus to the ventral hippocampus where it can be relayed to the amygdala and associated with shock (Wiltgen et al. 2006; Sutherland et al. 2008; Maren and Fanselow 1995; Xu et al. 2016; Jimenez et al. 2018; Kim and Cho 2020). The current study examined the role of the vCA1-basal amygdala pathway in the acquisition and expression of context fear. Similar to previous results obtained in the DH, we found that c-Fos expression increased in vCA1 neurons after exposure to a novel environment (Radulovic et al. 1998). However, the addition of shock did not further increase the number of labelled cells as it does in subcortical structures like the amygdala (Barot et al. 2009; Milanovic et al., 1998; Radulovic et al. 1998). This result was surprising given the role of the VH in learned fear and anxiety and the fact that it communicates with subcortical regions involved in emotion (Jimenez et al. 2018; Hoover and Vertes 2007; Cenquizca and Swanson 2006, 2007). Nonetheless, it remains possible that footshock activated many of the same cells that responded to the context, making it difficult for us to find a difference between these groups. Consistent with this idea, a recent study showed that vCA1 neurons activated during exploration (c-Fos+) are the same cells that strengthen their connections with BA neurons after the environment is paired with shock (Kim and Cho 2020).

High-frequency stimulation (20-Hz) of engram cells (c-Fos+) in dorsal DG and CA3 has been shown to increase freezing after context fear conditioning (Ryan et al. 2015; Ramirez et al. 2013; Oishi et al. 2019). However, the same manipulation does not drive freezing when performed in dorsal CA1 (Ryan et al. 2015). We hypothesized that

this may be the case because dCA1 neurons do not project to the VH like cells in dDG and dCA3 (Fricke and Cowan 1978; Swanson et al. 1978; Ishizuka et al. 1990). Inconsistent with this idea, we found that 20-Hz stimulation of BA-projecting vCA1 neurons impaired freezing rather than enhancing it. A similar effect was observed when vCA1 terminals in the BA were stimulated at 10-Hz (Jimenez et al. 2018). To determine why high-frequency stimulation produced impairments in freezing, we recorded from principal cells in the BA while activating terminals from vCA1. We found that 20-Hz stimulation inhibited excitatory responses in the BA while 4-Hz did not. The inhibitory effect of 20-Hz stimulation could be reduced with a $GABA_A$-receptor antagonist, indicating that it was due, in part, to feed-forward inhibition. Interestingly, the medial prefrontal cortex (mPFC) has been shown to disinhibit principal cells in the BA and allow them to respond to strong input from vCA1 (Hübner et al. 2014). A circuit like this could function to rapidly select adaptive responses in different situations. For example, when animals come across a novel environment place cell activity in vCA1 could inhibit BA neurons and promote exploration. If a threat was subsequently encountered in this same place, input from the mPFC could quickly disinhibit BA neurons and allow vCA1 to drive defensive behaviors like freezing. We plan to examine these ideas in future experiments by simultaneously manipulating inputs from vCA1 and the mPFC to the BA after fear conditioning.

Unlike 20-Hz, stimulation of vCA1 neurons at 4-Hz did not inhibit principal cells in the BA. Given that the hippocampus, amygdala and mPFC oscillate at theta-frequency during fear expression, we hypothesized that low-frequency stimulation may enhance freezing rather than impair it (Seidenbecher et al. 2003; Padilla-Coreano et al. 2016;

Narayanan et al. 2007; Lesting et al. 2011; Courtin et al. 2014; Karalis et al. 2016). Consistent with this idea, 4-Hz stimulation produced an increase in fear generalization and did not disrupt freezing in the training context. However, freezing did not increase during laser stimulation itself, as has been observed when dCA1 engram cells are stimulated at this frequency (Ryan et al. 2015). It is possible that our behavioral effects would have been larger if we were able to selectively stimulate engram/memory cells in vCA1. In addition, high-frequency stimulation of BA-projecting vCA1 neurons may be able induce freezing if it co-occurs with a disinhibitory input from the mPFC (Hübner et al. 2014; Karalis et al. 2016).

To summarize, our results suggest that dorsal and ventral CA1 neurons respond similarly to context exploration and fear conditioning. Many cells in each region express c-Fos when mice are exposed to a novel environment, and the number of activated neurons does not increase further if the context is paired with shock. In addition, the expression of fear is impaired when neurons in dorsal or ventral CA1 are stimulated at 20-Hz. Low-frequency stimulation, in contrast, increases freezing and enhances fear generalization in dorsal and ventral CA1, respectively. Additional research will be required to determine if more robust changes in defensive behavior can be induced when firing patterns are coordinated in the mPFC, BA and vCA1.

References

Balogh, S.A., and Wehner, J.A., (2003). Inbred mouse strain differences in the establishment of long-term fear memory. *Behav Brain Res* 140 (1–2): 97–106. https://doi.org/ 10.1016/s0166-4328(02)00279-6.

Barot, S.K., Chung, A., Kim, J.J. and Bernstein, I.L. (2009). Functional imaging of stimulus convergence in amygdalar neurons during pavlovian fear conditioning. *PLoS ONE* 4 (7): 1–8. https://doi.org/10.1371/journal.pone.0006156.

Bazelot, M., Bocchio, M., Kasugai, Y., Fischer, D., Dodson, P.D., Ferraguti, F., and Capogna, M. (2015). Hippocampal theta input to the amygdala shapes feedforward inhibition to gate heterosynaptic plasticity. *Neuron* 87 (6): 1290–1303. https://doi.org/10.1016/j.neuron.2015.08.024.

Berndt, A., Schoenenberger, P., Mattis, J., Tye, K.M., Deisseroth, K., Hegemann, P., Oertner, T.G. (2011). High-efficiency channelrhodopsins for fast neuronal stimulation at low light levels. *PNAS* 108 (18): 7595-7600.

Beyeler, A., Chang, C., Silvestre, M., Leveque, C., Namburi, P., Wildes, C.P., and Tye, K.M. (2018). Organization of valence-encoding and projection-defined neurons in the basolateral amygdala. *Cell Reports* 22 (4): 905–18. https://doi.org/10.1016/j.celrep.2017.12.097.

Cenquizca, L.A. and Swanson, L.W. (2006). Analysis of direct hippocampal cortical field ca1 axonal projections to diencephalon in the rat. *The Journal of Comparative Neurology* 497 (1): 101–14. https://doi.org/10.1002/cne.20985.

Cenquizca, L.A. and Swanson, L.W. (2007). Spatial organization of direct hippocampal field CA1 axonal projections to the rest of the cerebral cortex. *Brain Res Rev* 56 (1): 1–26. https://doi.org/10.1016/j.brainresrev.2007.05.002.

Ciocchi, S. Passecker, J., Malagon-Vina, H., Mikus, N. and Klausberger, T. (2015). Selective information routing by ventral hippocampal ca1 projection neurons. *Science (New York, N.Y.)* 348 (6234): 560–63. https://doi.org/10.1126/science.aaa3245.

Courtin, J., Chaudun, F., R. Rozeske, R.R., Karalis, N., Gonzalez-Campo, C., Wurtz, H., Abdi, A., Baufreton, J., Bienvenu, T.C.M., and Herry, C. (2014). Prefrontal parvalbumin interneurons shape neuronal activity to drive fear expression. *Nature* 505 (7481): 92–96. https://doi.org/10.1038/nature12755.

Fanselow, M.S., and Dong, H.W. (2010). Are the dorsal and ventral hippocampus functionally distinct structures? *Neuron* 65. https://doi.org/10.1016/j.conb.2013.11.010.

Fricke, R., and Cowan, W.M. (1978). An autoradiographic study of the commissural and ipsilateral hippocampo-dentate projections in the adult rat. *Journal of Comparative Neurology* 181 (2): 253–69. https://doi.org/10.1002/cne.901810204.

Graham, J., D'Ambra, A., Jung, S.J., Vishwakarma, N., Venkatesh, R., Parigi, A.,

Antzoulatos, E.G., Fioravante, D., and Wiltgen, B.J. (2020). High Frequency stimulation of ventral CA1 neurons reduces amygdala activity and inhibits fear. *BioRxiv* 2020.07.01.183210; doi: https://doi.org/10.1101/2020.07.01.183210

Hess, Ursula S., Gary Lynch, and Christine M. Gall. 1995. “Regional Patterns of C-Fos MRNA Expression in Rat Hippocampus Following Exploration of a Novel Environment versus Performance of a Well-Learned Discrimination.” *Journal of Neuroscience* 15 (12): 7796–7809. https://doi.org/10.1523/jneurosci.15-12-07796.1995.

Hoover, W.B. and Vertes, R.P. (2007). Anatomical analysis of afferent projections to the medial prefrontal cortex in the rat. *Brain Structure and Function* 212 (2): 149–79. https://doi.org/10.1007/s00429-007-0150-4.

Hübner, C., Bosch, D., Gall, A., Lüthi, A. and Ehrlich, I. (2014). Ex vivo dissection of optogenetically activated mPFC and hippocampal inputs to neurons in the basolateral amygdala: implications for fear and emotional memory. *Frontiers in Behavioral Neuroscience* 8 (March): 64. https://doi.org/10.3389/fnbeh.2014.00064.

Ishizuka, N., Weber, J. and Amaral, D.G. (1990). Organization of intrahippocampal projections originating from CA3 pyramidal cells in the rat. *Journal of Comparative Neurology* 295 (4): 580–623. https://doi.org/10.1002/cne.902950407.

Jimenez, J.C., Su, K., Goldberg, A.R., Luna, V.M., Biane, J.S., Ordek, G. et al. (2018). Anxiety cells in a hippocampal-hypothalamic circuit. *Neuron* 97 (3): 670–83. https://doi.org/10.1016/j.neuron.2018.01.016

Karalis, N., Dejean, C., Chaudun, F., Khoder, S., R Rozeske, Wurtz, H., et al. (2016). 4 Hz oscillations synchronize prefrontal-amygdala circuits during fear behaviour 19 (4): 605–12. https://doi.org/10.1038/nn.4251.4.

Kim, W.B., and Cho, J.H. (2020). Encoding of contextual fear memory in hippocampal–amygdala circuit. *Nature Communications* 11 (1): 1–22. https://doi.org/10.1038/s41467-020-15121-2.

Kjelstrup, K.B., Solstad, T., Brun, V.H., Hafting, T., Leutgeb, S., Witter, M.P., et al. (2008). Finite scale of spatial representation in the hippocampus. *Science* 321 (5885): 140–43. https://doi.org/10.1126/science.1157086.

Kjelstrup, K.G., Tuvnes, F.A., Steffenach, H., Murison, R., Moser, E.I., and Moser, M-B. (2002). Reduced fear expression after lesions of the ventral hippocampus. *Proceedings of the National Academy of Sciences of the United States of America* 99 (16): 10825–30. https://doi.org/10.1073/pnas.152112399.

Komorowski, R.W., Garcia, C.G., Wilson, A., Hattori, S., Howard, M.W., and Eichenbaum, H. (2013). Ventral hippocampal neurons are shaped by experience to represent behaviorally relevant contexts. *The Journal of Neuroscience : The Official Journal of the Society for Neuroscience* 33 (18): 8079–87. https://doi.org/10.1523/JNEUROSCI.5458-12.2013.

Krueger, J.N., Wilmot, J.H., Teratani-Ota, Y., Puhger, K.R., Nemes, S.E., Crestani,

A.P., Lafreniere, M.M., and Wiltgen, B.J. (2020) Amnesia for context fear is caused by widespread disruption of hippocampal activity. *Neurobiology of Learning & Memory* Volume 175. https://doi.org/10.1016/j.nlm.2020.107295

Lesting, J., Narayanan, R.T., Kluge, C., Sangha, S., Seidenbecher, T., and Pape, H.C. (2011). Patterns of coupled theta activity in amygdala-hippocampal-prefrontal cortical circuits during fear extinction. *PLoS ONE* 6 (6). https://doi.org/10.1371/journal.pone.0021714.

Lovett-Barron, M., Kaifosh, P., Kheirbek, M.A., Danielson, N., Zaremba, J.D., Reardon, T.R. et al. (2014). Dendritic inhibition in the hippocampus suports fear learning. *Science* 343 (February): 857–64. https://doi.org/10.1126/science.1247485.

Maren, S. and Fanselow, M.S. (1995). Synaptic plasticity in the basolateral amygdala induced by hippocampal formation stimulation in vivo. *J Neurosci* 15 (11): 7548–64. http://www.ncbi.nlm.nih.gov/pubmed/7472506.

Milanovic, S., Radulovic, J., Laban, O., Stiedl, O., Henn, F., and Spiess, J. (1998). Production of the fos protein after contextual fear conditioning of C57BL/6N mice. *Brain Res* 784 (1–2): 37–47. http://www.ncbi.nlm.nih.gov/pubmed/9518543.

Moser, E.I., Moser, M-B. and McNaughton, B.L. (2017). Spatial representation in the hippocampal formation: a history. *Nature Neuroscience* 20 (11): 1448–64. https://doi.org/10.1038/nn.4653.

Moser, M-B. and Moser, E.I. (1998). Functional differentiation in the hippocampus. *Hippocampus* 8 (6): 608–19. https://doi.org/10.1002/(SICI)1098-1063(1998)8:6<608::AID-HIPO3>3.0.CO;2-7.

Nalloor, R., Bunting, K.M. and Vazdarjanova, A. (2012). Encoding of emotion-paired spatial stimuli in the rodent hippocampus. *Frontiers in Behavioral Neuroscience* 6 (June): 1–11. https://doi.org/10.3389/fnbeh.2012.00027.

Narayanan, R.T., Seidenbecher, T., Kluge, C., Bergado, J., Stork, O., and Pape, H-C. (2007). Dissociated theta phase synchronization in amygdalo-hippocampal circuits during various stages of fear memory. *European Journal of Neuroscience* 25 (6): 1823–31. https://doi.org/10.1111/j.1460-9568.2007.05437.x.

Odén, A., & Wedel, H. (1975). Arguments for Fisher's permutation test. *The Annals of Statistics*, *3*(2), 518-520

Oishi, N., Nomoto, M., Ohkawa, N., Saitoh, Y., Sano, Y., Tsujimura, S. et al. (2019). Artificial association of memory events by optogenetic stimulation of hippocampal CA3 cell ensembles. *Mol Brain* 12(2). https://doi.org/10.1186/s13041-018-0424-1

O'Keefe, J. and Dostrovsky, J. (1971). The hippocampus as a spatial map . Preliminary evidence from unit activity in the freely-moving rat. *Brain Research* 34 (1): 171–75. http://www.ncbi.nlm.nih.gov/pubmed/5124915.

O'keefe, J, and Speakman, A. (1987). Single unit activity in the rat hippocampus during a spatial memory task. *Exp Brain Res* 68: 1–27. https://link.springer.com/content/pdf/10.1007%2FBF00255230.pdf.

Owen, E. H., Logue, S.F., Rasmussen, D.L. and Wehner, J.M. (1997). Assessment of learning by the morris water task and fear conditioning in inbred mouse strains and F1 hybrids: implications of genetic background for single gene mutations and quantitative trait loci Analyses. *Neuroscience* 80 (4): 1087–99. https://doi.org/10.1016/S0306-4522(97)00165-6.

Padilla-Coreano, N., Bolkan, S.S., Pierce, G.M., Dakota R., Blackman, W.D. Hardin, A.Garcia-Garcia, A.L. et al. (2016). Direct ventral hippocampal-prefrontal input is required for anxiety-related neural activity and behavior. *Neuron* 89 (4): 857–66. https://doi.org/10.1016/j.neuron.2016.01.011.

Pelletier, J.G., Likhtik, E., Filali, M., and Paré, D. (2005). Lasting increases in basolateral amygdala activity after emotional arousal: implications for facilitated consolidation of emotional memories. *Learning & Memory (Cold Spring Harbor, N.Y.)* 12 (2): 96–102. https://doi.org/10.1101/lm.88605.2.

Radulovic, J., Kammermeier, J. and Joachim Spiess. (1998). Relationship between fos production and classical fear conditioning : effects of novelty , latent inhibition , and unconditioned stimulus preexposure. 18 (18): 7452–61.

Ramirez, S., Liu ,X., Lin, P.A., Suh J., Pignatelli M., Redondo, R.L. et al. (2013). Creating a false memory in the hippocampus. *Science (New York, N.Y.)* 341 (6144): 387–91. https://doi.org/10.1126/science.1239073.

Ryan, T.J., Roy, D.S., Pignatelli, M., Arons, A., Tonegawa, S. (2015). Engram cells retain memory under retrograde amnesia. *Science* 348 (6238): 1007–14. https://science.sciencemag.org/content/348/6238/1007.

Seidenbecher, T., Laxmi, R.T., Stork, O., and Pape, H-C. (2003). Amygdalar and hippocampal theta rhythm synchronization. *Science* 846 (2003): 846–51. https://doi.org/10.1126/science.1085818.

Sparta, D.R., Stamatakis, A.M., Phillips, J.L., Hovelsø, N., van Zessen, R., Stuber, G.D. (2012) Construction of implantable optical fibers for long-term optogenetic manipulation of neural circuits. *Nature Protocols* 7: 12-23. https://doi.org/10.1038/nprot.2011.413.

Strange, B.A., Witter, M.P., Lein, E.S., and Moser, E.I. (2014). Functional organization of the hippocampal longitudinal axis. *Nature Publishing Group* 15 (10): 655–69. https://doi.org/10.1038/nrn3785.

Sutherland, R.J., O'Brien, J. and Lehmann, H. (2008). Absence of systems consolidation of fear memories after dorsal, ventral, or complete hippocampal damage. *Hippocampus* 18 (7): 710–18. https://doi.org/10.1002/hipo.20431.

Swanson, L.W., Wyss, J.M. and Cowan, W.M. (1978). An autoradiographic study of the organization of intrahippocampal association pathways in the rat. *The Journal of*

Comparative Neurology 181 (4): 681–715. https://doi.org/10.1002/cne.901810402.

Tanaka, K.Z., He, H., Anupratap,T., Niisato, K., Huang, A.J.Y. and McHugh, T.J. (2018). The hippocampal engram maps experience but not place. *Science* 361 (6400): 392–97. https://doi.org/10.1126/science.aat5397.

Wilmot, J.H, Graham, J.A., LaFreniere, M.M., Puhger, K. and Wiltgen, B.J. (2018) Altered immediate early gene expression in fos-tTA transgenic mice. Society for Neuroscience Poster, 331.26.

Wilmot, J.H., Puhger, K. and Wiltgen, B.J. (2019). Acute disruption of the dorsal hippocampus impairs the encoding and retrieval of trace fear memories. *Frontiers in Behavioral Neuroscience* 13 (May): 1–9. https://doi.org/10.3389/fnbeh.2019.00116.

Wiltgen, B.J., Sanders, M.J., Anagnostaras, S.G., Sage, J.R. and Fanselow, M.S. (2006). Context fear learning in the absence of the hippocampus. *J Neurosci* 26 (20): 5484–91. https://doi.org/ 10.1523/JNEUROSCI.2685-05.2006

Wolff, S.B.E., Gründemann, J., Tovote, P., Krabbe, S., Jacobson, G.A., Müller, C., et al. (2014). Amygdala interneuron subtypes control fear learning through disinhibition. *Nature* 509 (7501): 453–58. https://doi.org/10.1038/nature13258.

Xu, C., Krabbe, S., Gründemann, J., Botta, P., Fadok, J.P., Osakada, F., et al. (2016). Distinct hippocampal pathways mediate dissociable roles of context in memory retrieval. *Cell*, 1–12. https://doi.org/10.1016/j.cell.2016.09.051.

Yizhar, O., Fenno, L.E., Davidson, T.J., Mogri, M., Deisseroth., K., (2011). Optogenetics in neural systems. *Neuron*, 71 (1): 9-34. https://doi.org/10.1016/j.neuron.2011.06.004